

Regenerative Dampers for FSAE Race Car

LIM HONG WEE

NATIONAL UNIVERSITY OF SINGAPORE

2013

Regenerative Dampers for FSAE Race Car

LIM HONG WEE

(B.Eng.(Hons.), NUS)

A THESIS SUBMITTED

FOR THE DEGREE OF MASTER OF ENGINEERING

DEPARTMENT OF MECHANICAL ENGINEERING

NATIONAL UNIVERSITY OF SINGAPORE

2013

Declaration

I hereby declare that this thesis is my original work and effort and it has been written by me in its entirety. I have duly acknowledged all the sources of information which have been used in the thesis.

This thesis has also not been submitted for any degree in any university previously

Name: Lim Hong Wee

Signature:  _____

Acknowledgements

The author would like to express his most sincere appreciation to the following individuals without whom the thesis could not have been successfully completed:

1. Associate Professor Lu Wen Feng, my supervisor, for his technical guidance, kind understanding, dedication and encouragement throughout the duration of this thesis.
2. Professor Seah Kar Heng, for his technical guidance, kind understanding, dedication and encouragement throughout the duration of this thesis.

Summary

The feasibility of a regenerative damper for use in a single seater race vehicle will be investigated in this thesis. The single seater race vehicle will be based on the Formula SAE platform and damper data from the vehicle will be used to calculate the power dissipation from the damper.

The velocity data of the dampers is also used to calculate the theoretical power generated for different regenerative damper design for the selection of the most suitable design. The chosen regenerative damper design will be fabricated and tested in a damper dynamometer for verification of the calculated data.

This thesis will end off with design improvement for Formula SAE regenerative damper and an upscale design of regenerative damper for road car application.

Table of Contents

Declaration	i
Acknowledgements	ii
Summary	iii
Table of Contents	iv
List of Tables	vii
List of Figures	viii
List of Symbols	x
1 Introduction	1
1.1 Formula SAE Electric.....	1
1.2 Energy Recovery in Electric Vehicle.....	2
1.3 Motivation of the Thesis.....	3
1.4 Objectives and Scope of the Thesis.....	4
1.5 Organisation of Thesis.....	5
2 Power Dissipation and Energy Harvesting Method	6
2.1 Power Dissipation.....	6
2.1.1 Suspension Movement.....	7
2.1.2 Power Calculation.....	7
2.1.3 Damping Curve.....	9
2.2 Energy Harvesting Methods.....	14
2.2.1 Rotary Motion of Components.....	16
2.2.2 Linear Motion of Dampers.....	19
2.3 Advantages and Disadvantages of Different Systems.....	25
3 Electromagnetic Damper Design	28
3.1 Linear Actuator.....	28
3.2 Neodymium Magnets.....	30
3.2.1 Ansys Magnetostatic Simulation.....	33
3.3 Laminated Copper Wires.....	42
3.3.1 Ansys Magnetostatic Analysis on No Wire Housing.....	43
3.3.2 Wire Coil Orientation.....	45
3.4 Damper Design.....	48
3.5 Electromagnetic Damper Power Calculation.....	52
3.5.1 Induced Voltage.....	53
3.5.2 Current.....	56
3.5.3 Power.....	56

4	Electromagnetic Damper Manufacturing.....	58
4.1	Manufacturing.....	58
4.2	Assembly.....	58
4.2.1	Magnet Assembly	58
4.2.2	Wire Coils	62
5	Testing Method	64
5.1	Damper Dynamometer	64
5.2	Current Direction	65
5.3	Data Logging.....	66
5.4	Problems Encountered	69
6	Design Change and Improvement.....	72
6.1	Design Change (Without Inner Magnet).....	74
6.2	Ansys Magnetostatic Analysis	75
6.2.1	Voltage and Current Calculation.....	76
6.3	Testing and Results Evaluation.....	77
6.3.1	Theoretical Calculations.....	77
6.3.2	Results Table.....	79
6.4	Design Improvement.....	80
6.4.1	Additional Coils	80
6.4.2	Larger Inner Magnets.....	83
6.4.3	Thicker Magnets	85
7	Results Evaluation on Road Vehicle.....	87
7.1	Road Profile	87
7.2	Damper Design	87
7.2.1	Laminated Wire.....	88
7.2.2	Magnet Setup and Analysis.....	89
7.2.3	Damper CAD	93
7.2.4	Voltage and current calculation	94
8	Conclusion	97
	Appendix	100
	Appendix 1: Rocker Rotation Frequency.....	100
	Appendix 2: Low Torque Motor Specification Sheet	101
	Appendix 3: Damper Velocity Frequency	102
	Appendix 4: American Wire Gauge Table.....	103
	Appendix 5: Misumi South East Asia Gear Catalogue	104
	Appendix 6: Ring Magnet Sources	106

Appendix 7: Ansys Magnetostatic Analysis Linear Plot Data (Ebay.com Magnet).....	107
Appendix 8: Ansys Magnetostatic Analysis Linear Plot Data (Ebay.com Magnet).....	108
Appendix 9: Ansys Magnetostatic Analysis Linear Plot Data (No Wire Coil Housing).....	109
Appendix 10: Bill of Materials for Electromagnetic Damper.....	110
Appendix 12: LTS 25-NP Datasheet.....	116
Appendix 13: Bill of Materials for Electromagnetic Damper 2nd Design.....	118
Appendix 14: Ansys Magnetostatic Analysis Linear Plot Data (Without Inner Magnet).....	121
Appendix 15: Test Data	122
Appendix 16: Magnetic Field Plot for Outside Coils.....	125
Appendix 17: Ansys Magnetostatic Analysis for Varying Diameter Inner Magnet	126
Appendix 18: Ansys Magnetostatic Analysis for Varying Thickness Magnet	127

List of Tables

Table 1: Portion of the logged data during Endurance event.....	8
Table 2: Velocity-Force Data Points.....	10
Table 3: Sample Logged Data.....	13
Table 4: Assumptions for Electromagnetic Induction Calculation.....	20
Table 5: Advantages and Disadvantages of Different Regenerating Systems.....	26
Table 6: Magnet Comparison from Suppliers.....	33
Table 7: Coil Drop Velocity and Voltage Induced.....	48
Table 8: Electromagnetic Damper Specifications.....	53
Table 9: Design change table.....	73
Table 10: New Data for Calculation.....	78
Table 11: Comparison of Calculated and Test Voltage and Current.....	79
Table 12: Comparison of Calculated and Tested Power.....	80
Table 13: Specifications of Wire Coils on the Outside.....	82
Table 14: Magnet Diameter Size Iterations.....	83
Table 15: Magnet and Spacer Thickness Configuration.....	85
Table 16:3- Magnet and 4-Magnet Iterations.....	91
Table 17: Road Car Electromagnetic Damper Power Generation.....	95

List of Figures

Figure 1: Linear Potentiometer on NUS Formula SAE 2012 Race Car Damper.....	6
Figure 2: Front View Formula SAE Vehicle	7
Figure 3: Damper Curve of Penske Dampers	9
Figure 4: Force Vs Velocity Plot for Penske Damper Curve.....	10
Figure 5: Low Speed and High Speed Bound and Rebound Plot	12
Figure 6: Part of Suspension System that Moves.....	15
Figure 7: Rocker Rotation.....	16
Figure 8: Rocker Rotation Frequency Plot.....	17
Figure 9: Low RPM High Torque DC Motor	18
Figure 10: Suspension Arms Rotation	19
Figure 11: Damper Linear Motion.....	20
Figure 12: Damper Velocity Frequency Plot	21
Figure 13: Crank, Scotch Yoke and Rack and Pinion System	23
Figure 14: Damper Stroke Frequency	23
Figure 15: Crank Rotation 2D Sketch.....	24
Figure 16: Electric Field Induction when Crossing a Magnetic Field	28
Figure 17: Linear Actuator.....	29
Figure 18: Magnet and Wire Location in a Damper	30
Figure 19: Magnetic Fields Produced by a Ring Magnet.....	31
Figure 20: Magnet and Ferrous Spacer Layout.....	32
Figure 21: 3 Magnets CAD.....	33
Figure 22: Ansys Workbench	34
Figure 23: Ansys Magnetostatic Setup	35
Figure 24: Magnetic Flux Lines (Top) and Zoom in of Analysis (Bottom) for Ebay.com Magnet	35
Figure 25: Magnetic Field Intensity Plot for Ebay.com Magnet.....	36
Figure 26: Magnetic Flux Lines (Top) and Zoom in of Analysis (Bottom) for Lifton Magnet	37
Figure 27: Magnetic Field Intensity Plot for Lifton Magnet.....	38
Figure 28: Various Ferrous Spacer Analysis, No Spacer, Quarter Spacer Height, 34 Spacer Height and Same Magnet Height, Left to Right	39
Figure 29: Magnetic Field Intensity Plot of Various Ferrous Spacer Thicknesses	39
Figure 30: FEMM Setup	40
Figure 31: FEMM Plot.....	41
Figure 32: Magnetic Field Intensity Plot Along Wire Coil.....	42
Figure 33: Magnetic Flux Lines (Top) and Zoom in of Analysis (Bottom) for Magnet with no Wire Housing	44
Figure 34: Magnetic Field Intensity Plot for Magnet With No Coil Housing	45
Figure 35: Magnetic Field Direction on 3 magnet spacer layout.....	46
Figure 36: CAD of Wire Coils Changing Direction	46
Figure 37: Simple Experiment on Wire Coil Orientation	47
Figure 38: 10 Turns Clockwise (Left), 20 Turns Clockwise (Middle) and 10 Turns Clockwise and 10 Turns Anticlockwise Wire Coils (Right).....	47
Figure 39: Damper Design (Left) and Sectional View (Right).....	49
Figure 40: Section View of Electromagnetic Damper	50
Figure 41: Upper Half of Electromagnetic Damper.....	51
Figure 42: Lower Half of Electromagnetic Damper	52

Figure 43: Fully Extended (Left) and Fully Compressed (Right) Damper	54
Figure 44: Zoom In View of Wire Coil Interaction with Magnets	55
Figure 45: Magnet Stacks (Top) and Method of Extracting Magnets (Bottom).....	59
Figure 46: Wedge Made of Wood to Ease the Magnet to the Spacer	60
Figure 47: Using the Wedge to Ease the Magnet to the Spacer.....	60
Figure 48: Bench Drill Used to Press the Magnet-Spacer into the Outer Casing	61
Figure 49: Inner Magnet Assembly with Lower Bearing Mount.....	61
Figure 50: AWG 18 Wire Coil on Wire Coil Housing	62
Figure 51: Electromagnetic Damper Fully Assembled.....	63
Figure 52: Damper Dynamometer (Left) and Cathode Ray Oscilloscope (Right).....	64
Figure 53: Schematics for a Full Bridge Rectifier	66
Figure 54: Full Bridge Rectifier.....	66
Figure 55: Race Technology DL1 Data Logger.....	67
Figure 56: LTS 25-NP Current Transducer (Top) and Current Transducer Being Wired Up (Bottom).....	67
Figure 57: Electromagnetic Damper and Measuring Equipments Setup in Damper Dynamometer.....	68
Figure 58: CRO Output.....	69
Figure 59: Enamel Wires Being Scrapped (Top), Zoom In of the Damage (Bottom)	70
Figure 60: Lower Bearing Mount (Left) with Arrow Showing Tapped Hole Location, Bolt Inserted into Lower Bearing Mount Badly Slanted	70
Figure 61: Design Change for Electromagnetic Damper	72
Figure 62: Section View of Electromagnetic Damper 2nd Design.....	74
Figure 63: Magnetic Flux Lines (Top) and Zoom in of Analysis (Bottom) for No Inner Magnet	75
Figure 64: Magnetic Field Intensity Plot for No Inner Magnet	76
Figure 65: Electromagnetic Damper with Coils on the Outside (Left) and Section View (Right)	81
Figure 66: Ansys Magnetostatic Analysis on Original Design.....	81
Figure 67: Section View of 3 Magnet Setup.....	82
Figure 68: Ansys Magnetostatic Analysis for Coils on the Outside	82
Figure 69: Magnet Diameter Size Iterations	84
Figure 70: Magnetic Field Plot for Varying Inner Magnet Diameter	84
Figure 71: Magnet and Spacer Thickness Configuration.....	85
Figure 72: Magnet Field Plot for Varying Thickness Magnet	86
Figure 73: Road Profile Data	87
Figure 74: 4-Magnet Setup	88
Figure 75: Wire Coil Cross Section	89
Figure 76: 3-Magnet Layout	89
Figure 77: Multiple Step Wire coil Housing.....	90
Figure 78: Ferrous Spacer and Cross Section View.....	90
Figure 79: Ansys Magnetostatic Analysis of 3- Magnet Setup Set 12.....	92
Figure 80: Magnetic Field Intensity Plot for 3-Magnet Setup	92
Figure 81: Road Car Electromagnetic Damper (Left) and Section View (Right).....	93
Figure 82: Close up Section View of Road Car Electromagnetic Damper.....	94
Figure 83: Power Vs Velocity Plot for Road Car Electromagnetic Damper.....	96

List of Symbols

a	Acceleration
A	Wire Cross Sectional Area
B	Magnetic Field
d	Diameter of Damper Dynamometer Wheel
d_a	Average Diameter of Wire Coil
F	Force
F_{1-2}	Force from position 1 to 2
F_{2-3}	Force from position 2 to 3
I	Current
l	Length of Wire
m	Mass
N	Number of Wire Coils
P	Power
P_{1-2}	Power from position 1 to 2
P_{2-3}	Power from position 2 to 3
R	Resistance of Resistor
r	Internal Resistance of Wire
v	Velocity
V	Voltage
v_{1-2}	Velocity from position 1 to 2
v_{2-3}	Velocity from position 2 to 3
σ	Conductivity

1 Introduction

1.1 Formula SAE Electric

Formula SAE (<http://students.sae.org/competitions/formulaseries/>) is a student design competition organized by SAE International. The first competition started back in 1978 and was originally called the Mini Indy.

The concept behind Formula SAE is that a fictional manufacturing company has contracted a design team to develop a small Formula-style race car. The prototype race car is to be evaluated for its potential as a production item. The target marketing group for the race car is the non-professional weekend autocross racer. Each student team designs, builds and tests a prototype based on a series of rules whose purpose is both to ensure onsite event operations and promote clever problem solving.

Formula SAE requires the participants to conduct research, design, manufacturing, testing, developing, marketing, management and financing the production of a race car. Formula SAE takes students out of the classroom and allows them to apply textbook theories to real work experiences.

Currently, there are 8 recognised Formula SAE competitions held worldwide:

1. Formula SAE Michigan
2. Formula SAE Lincoln
3. Formula Hybrid (New Hampshire)
4. Formula SAE Australasia
5. Formula SAE Brazil
6. Formula SAE Italy
7. Formula SAE Student
8. Formula Student Germany

In view of the vast development of electric saloon vehicles by major automotive companies, Formula SAE has also taken steps to allow participants to design and build pure electric race vehicles so that the knowledge can be used in the industry when the participants graduate.

In 2013, there will be Formula SAE Electric event in the Formula SAE Lincoln and Formula Student Germany. Formula Hybrid also has an essence of electric vehicle coupled with an internal combustion engine. The Formula SAE organisers are also taking steps to make all events worldwide to allow electric race cars to participate with a unified rule.

1.2 Energy Recovery in Electric Vehicle

The power source like battery or super capacitor for electrical vehicles can be recharged using any method as long as the right amount of electricity is available; it is therefore worthwhile to harness electricity from any suitable source available. Currently the only technology that is widely used in the automotive industry is regenerative braking [1] as a large amount of energy is required during braking.

Other forms of energy recovery can be incorporated in the vehicle to further improve its overall energy efficiency. These recovery devices must not be too heavy such that more energy is instead required to propel the vehicle.

However, lightweight energy recovery add-on such as piezoelectric generator [2] only produces low energy; and it is more worthwhile to have vibration energy generators on roads than on vehicles [3].

The challenge is to develop a energy recovery device that can replace an existing component in the vehicle so that the overall weight of the vehicle will not be increased by a significant amount.

The suspension system in a vehicle experiences one of the largest force and movement to support the vehicle's sprung mass. It is a good platform to tap energy from as there are a few active suspension system [4], [5] being developed where the damping performance of the

dampers can be adjusted through electromagnets. The whole damper will not be the traditional hydraulic damper but instead more resembles an electromagnet linear actuator.

Harnessing energy from other sources is cumulative to the efficiency an electric vehicle and thus leads to lower energy consumption. The electric vehicle will thus be able to achieve a higher range with the same amount of batteries.

1.3 Motivation of the Thesis

The Formula SAE race vehicle for the Formula SAE Electric event will be equipped with electric motor instead of internal combustion engine. The fuel will be battery or super capacitor instead of petrol. Other rules that are out of the power train, drive train and electronics rules but pertaining to the car remains almost similar.

With an increase in popularity in electric Formula SAE race vehicle, there is a new opportunity for NUS to participate in as NUS has built a vast knowledge to design and manufacture Formula SAE race vehicle. The Formula SAE competition encourages efficiency in the midst of performance through innovation and the regenerative damper has not been design and implemented by any teams in the competition.

This is also in tune with the electric vehicle projects that are ongoing in NUS and the regenerative dampers can be up-scaled to electric road vehicle uses. In addition, the regenerative dampers can be further developed into active suspension for road vehicles through varying the charging rate of the regenerative dampers.

In addition, there are vast amount of data collected on the suspension system and various design of the suspension system over the years of competition. These data can be used to conduct calculations for the current dampers so that the regenerative dampers can be design and verified.

1.4 Objectives and Scope of the Thesis

The scope of the thesis involves in looking at energy recovery or regeneration of a Formula SAE race vehicle. The energy recovered can be used to charge the power plant on the Formula SAE race vehicle. This will eliminate the use of a larger number of batteries to last the 22 km Endurance race and translate to a lighter race vehicle with higher power to weight ratio. As the author is involved in the suspension department of the previous Formula SAE race vehicle, he will attempt to look at energy recovery from suspension movements.

When a vehicle moves on the road, the suspension components move with respect to the chassis to compensate for the irregularities on the road. These suspension components or unsprung mass (mass not supported by springs) can experience from 2 to 3 Hz for Formula SAE race vehicle or 1 to 2 Hz for road vehicles [6]. Formula SAE race vehicle have a minimum suspension travel of 2 inches (by rules).

With the high frequency of the suspension components coupled with the sufficient travel, there is an advantage to capture the movement and harness it as energy. There are several types of energy regenerative suspension design done using different methods, such as hydraulic storage suspension [7], battery coil induction suspension [8], rack and pinion suspension [9], ball screw suspension [10] and linear motion suspension [11].

With such, various locations of the suspension will be investigated and suitable energy harnessing methods employed to find out the most beneficial way of tapping the energy from the suspension movement. Damper stroke data from the Formula SAE race vehicle from the race in America will be used to calculate and evaluate the power dissipation.

The objectives of the thesis are thus as follows:

- Calculate power dissipated from suspension movements through logged data
- Determine the location of the suspension assembly to capture energy from
- Determine the method to capture the energy
- Calculate how much energy can be harness and design the system

- Test and verify results

1.5 Organisation of Thesis

In this thesis, Chapter 1 covers the introduction of and the objectives of the thesis. Chapter 2 calculates the power dissipated by the damper from the logged data and conducted calculations to compare the different methods of damper power generation. With the electromagnetic damper chosen as the more suitable method of energy recovery, Chapter 3 went on to specify the magnet through analysis and laminated wires through calculations. The design of the electromagnetic damper is also presented and the total power generated by the electromagnetic damper is computed using the logged data. When the design of the electromagnetic damper is completed, the components are manufactured and assembled in Chapter 4. Difficulties and challenges were presented for the electromagnetic damper. After the electromagnetic damper is assembled, it is tested in Chapter 5. The wire coils were damaged and the damaged is investigated with design improvement in Chapter 6. The improved electromagnetic damper is tested again and results are computed and compared with the power dissipation of the original hydraulic dampers. Chapter 7 ends off with further design improvement (not manufactured and tested) for future reference. Taking the results obtained from Chapter 7, a whole new electromagnetic damper is redesigned for road car usage. The size of the electromagnetic damper is increased such that it will be able to fit into a road car. The design is analysed and power is calculated based on the test data in Chapter 7. The thesis ends off with the conclusion in Chapter 8 on the feasibility of electromagnetic damper on a Formula SAE race vehicle and on a road vehicle.

2 Power Dissipation and Energy Harvesting Method

2.1 Power Dissipation

The power dissipated from the suspension system can be calculated through data obtained from sensors. Common sensors that measure the movement or the acceleration of the suspension system include linear potentiometer placed alongside the dampers and accelerometer placed on the unsprung mass of the suspension system.

The linear potentiometer shown in Figure 1 measures the absolute position of the dampers and logs it against time. With these two data, the velocity of the damper can be found. Accelerometer is able to measure the vertical acceleration of the unsprung mass. This acceleration can be resolved to find the acceleration of the damper. The equation $F=ma$ can be used to calculate the force due to the acceleration value. With both force and velocity, power can be found using the formula $P=Fv$.



Figure 1: Linear Potentiometer on NUS Formula SAE 2012 Race Car Damper

Unfortunately, for the 2012 Formula SAE vehicle, there are only linear potentiometers installed on the 4 dampers of the vehicle; the only accelerometer is mounted near to the centre of gravity of the car to measure the acceleration and lateral G-forces of the car. Thus, the power dissipation of the suspension system during operation can only be calculated with the data available through the spring and dampers. The unsprung mass acceleration cannot be used.

2.1.1 Suspension Movement

Error! Reference source not found. Figure 2 shows the front view of the front suspension assembly of the Formula SAE vehicle. As the wheel moves up and down due to the irregularities on the road (red arrows), it moves the push rod, which pushes or pull on the rocker. The rocker rotates about its pivot and compresses or extends the dampers (blue arrows). This system is employed to be able to vary the motion ratio of the suspension system which is the vertical displacement of the wheel due to irregularities in the road to the stroke of the dampers.

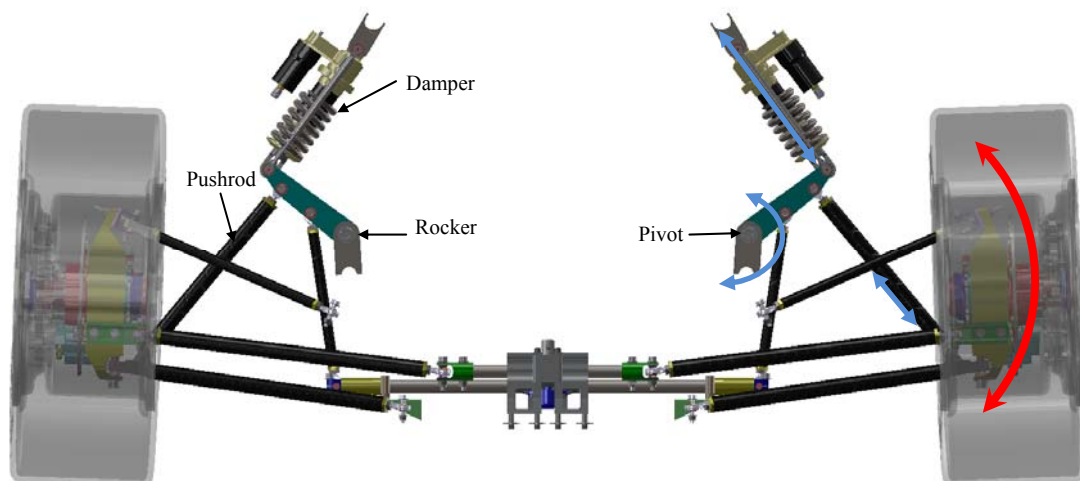


Figure 2: Front View Formula SAE Vehicle

2.1.2 Power Calculation

With velocity data of the dampers, the power that is dissipated due to the movement can be calculated using the damping curve to determine the force due to the velocity. The data is

logged at 500 Hz and this gives a data point every 0.002 sec. Over a 280 sec endurance run, there are over 140,000 data points.

Table 1 shows the logged data from a practice run for a particular driver in the endurance event over a period of 0.04 sec. From Table 1, the front left suspension position fluctuates from 45.01 mm to 45.03 mm over the period which is too small to be significant. This could be mostly due to the vibration of the engine.

Time (s)	Engine RPM (rpm)	Throttle Pos	G Force Lat (G)	G Force Long (G)	Susp Pos FL (mm)	Susp Pos FR (mm)	Susp Pos RL (mm)	Susp Pos RR (mm)	Gyro Yaw Velocity (deg/s)	Gyro Roll Velocity (deg/s)
0.000	222	6	-0.88	1.14	45.01	47.08	51.55	50.96	7.6	-39.2
0.002	229	6	-0.88	1.14	45.03	47.08	51.55	50.98	7.7	-39
0.004	237	6	-0.88	1.14	45.01	47.08	51.55	50.98	7.8	-38.7
0.006	244	6	-0.88	1.14	45.03	47.08	51.57	50.98	7.9	-38.5
0.008	252	6	-0.88	1.14	45.03	47.08	51.57	50.98	8.1	-38.2
0.010	259	6	-0.88	1.14	45.03	47.06	51.53	50.96	8.2	-38
0.012	267	6	-0.88	1.14	45.03	47.06	51.53	50.94	8.3	-37.7
0.014	274	6	-0.88	1.14	45.03	47.08	51.57	50.98	8.4	-37.5
0.016	282	6	-0.88	1.14	45.01	47.08	51.57	50.96	8.6	-37.2
0.018	289	6	-0.88	1.14	45.03	47.06	51.55	50.96	8.7	-37
0.020	296	6	-0.88	1.14	45.03	47.08	51.57	50.98	8.8	-36.7
0.022	304	6	-0.87	1.13	45.01	47.08	51.55	50.96	8.9	-36.5
0.024	311	6	-0.87	1.13	45.03	47.08	51.55	50.96	9.1	-36.2
0.026	319	6	-0.87	1.13	45.03	47.08	51.55	50.96	9.2	-36
0.028	326	6	-0.87	1.13	45.03	47.06	51.53	50.96	9.3	-35.7
0.030	334	6	-0.87	1.13	45.03	47.08	51.57	50.98	9.4	-35.5
0.032	341	6	-0.87	1.13	45.03	47.08	51.57	50.96	9.6	-35.2
0.034	348	6	-0.87	1.13	45.03	47.06	51.55	50.96	9.7	-35
0.036	356	6	-0.87	1.13	45.03	47.08	51.57	50.98	9.8	-34.7
0.038	363	6	-0.87	1.13	45.03	47.08	51.57	50.98	10	-34.5
0.040	371	6	-0.87	1.13	45.03	47.08	51.55	50.98	10.1	-34.2

Table 1: Portion of the logged data during Endurance event

The time interval for the data collection can be determined by the operating frequency of the suspension system itself. Since a Formula SAE vehicle can achieve up to 20.0 Hz at the unsprung mass, 0.05 sec interval is used to find out the maximum velocity of the unsprung mass and thus power. When the data point is increased to 0.05 sec this will reduce the data points to 41,943 points which is more manageable.

The mode of the suspension positions is taken for every 0.002 sec as the new data points within each 0.05 sec interval. Using mode to determine the new suspension position is a reasonable way as the data will not be much affected by random vibrations; rather the most frequent suspension position will be taken.

2.1.3 Damping Curve

The damping curve is a force versus velocity curve that shows the characteristics of the damper. The different shapes of the damping curve shows whether the damper is linear, progressive or digressive. The damping curve for the current Penske dampers are obtained from the manufacturer as shown in Figure 3.

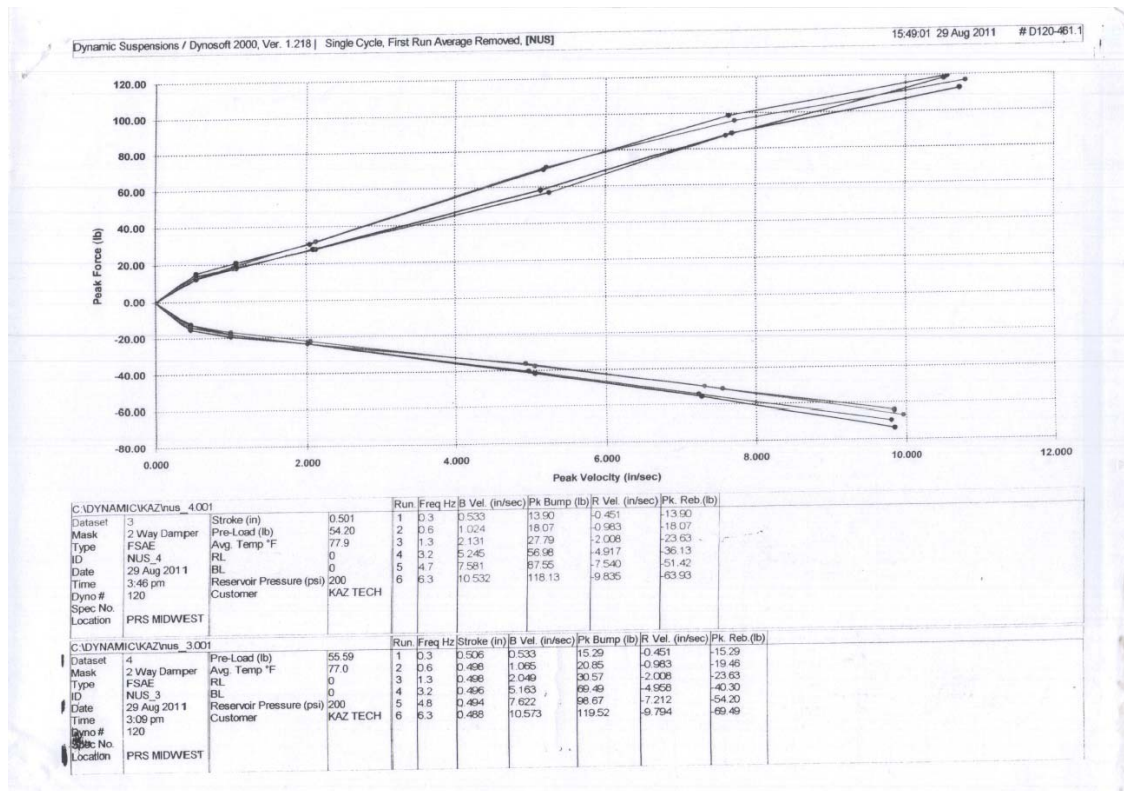


Figure 3: Damper Curve of Penske Dampers

Force from the dampers can be obtained from the graph using the velocity of the dampers from the logged data. The few curves for both bound and rebound are different damper settings from the adjustable knobs. The force per each velocity is averaged for each setting for bound and rebound. From the graph in Figure 3, there is a kink in almost all the curve at around 0.5 in/sec. This kink defines the low speed and high speed damping. Velocity below 0.5 in/sec is for

Formula SAE race vehicle is low speed damping while velocity above that is high speed damping.

Low speed damping occurs mostly during corner entry and high speed damping is when a vehicle travel over a hump or sudden irregularities on the road. As the Formula SAE vehicle focuses mostly on taking corners and travels on relatively flat roads, the dampers should be operating in low speed damping region. Table 2 shows the data points from the damping curve.

Bound		Rebound	
Velocity	Force	Velocity	Force
m/s	N	m/s	N
0.000	0.00	0.000	0.00
0.014	61.85	0.011	61.85
0.026	80.41	0.025	80.41
0.054	123.66	0.051	105.15
0.133	253.55	0.125	160.77
0.193	389.57	0.192	228.81
0.268	525.65	0.250	284.47

Table 2: Velocity-Force Data Points

Figure 4 shows the averaged bound and rebound curve for the damper. The rebound curve is shifted above the x axis as the negative y-values in Figure 3 are meant to show the direction of the force.

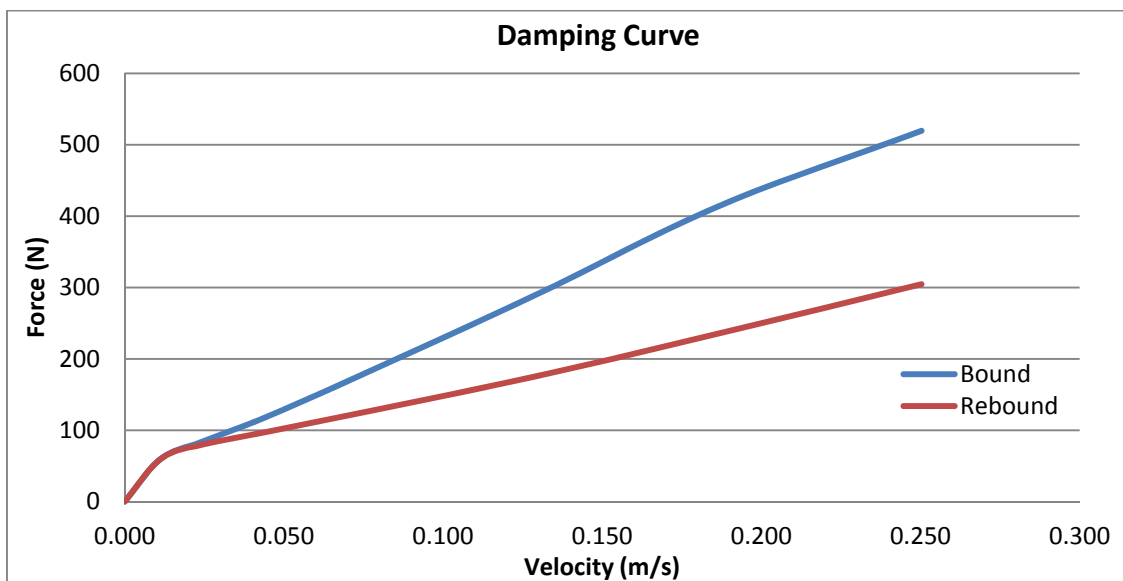
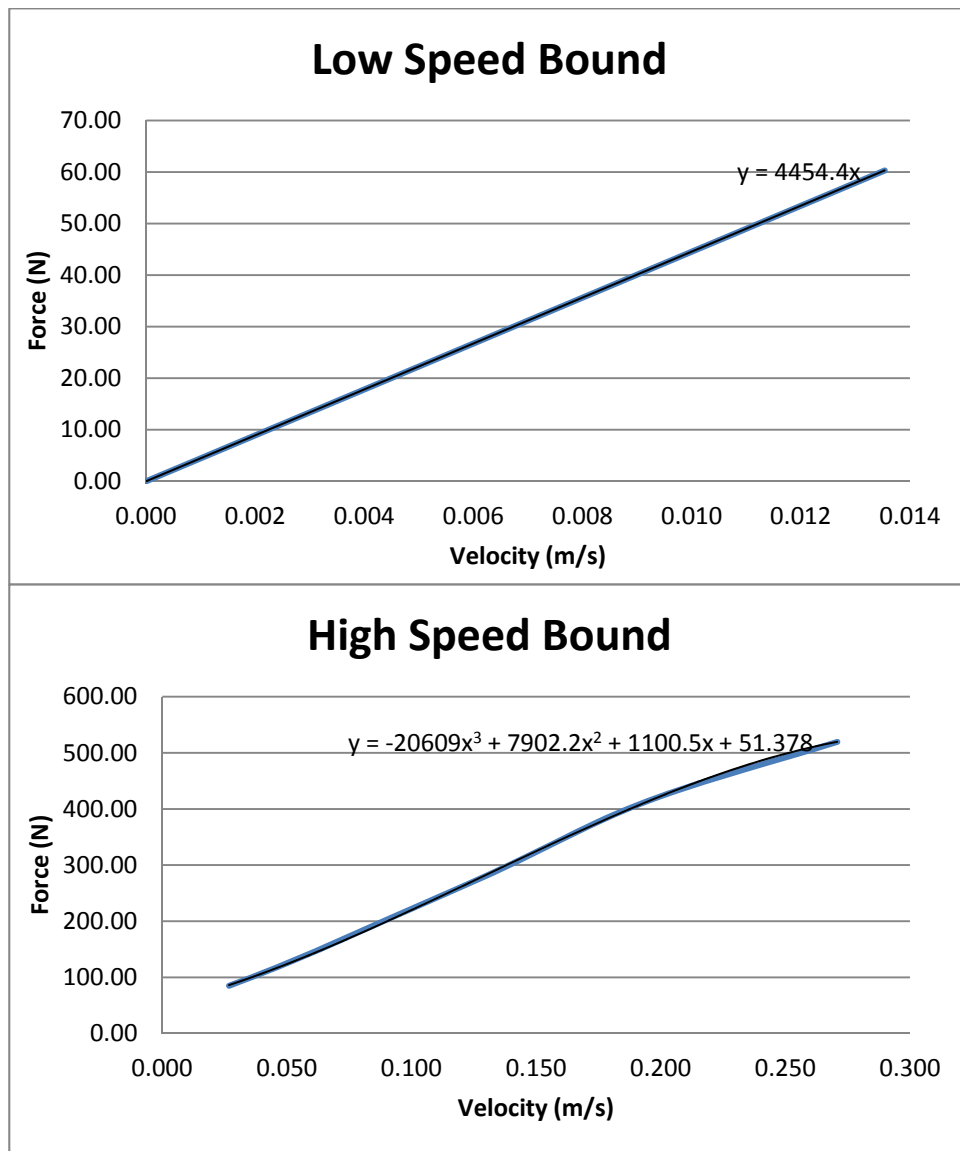


Figure 4: Force Vs Velocity Plot for Penske Damper Curve

Since there is both low speed and high speed within each damping curve, each curve has to be further split into 2 individual graphs. The curve will be split at around 0.5 in/ sec which is around 0.013 m/s. The graph is split as the equation of the curve is required to calculate the force due to the velocity of the damper. If the graph in Figure 4 above is used to generate the equation, it might not be accurate to obtain a best fit curve to give the equation.

Microsoft excel spreadsheet is used to obtain the equation of the line using trend line. Figure 5 shows the low speed bound, low speed rebound, high speed bound and high speed rebound curves as 4 separate curves.



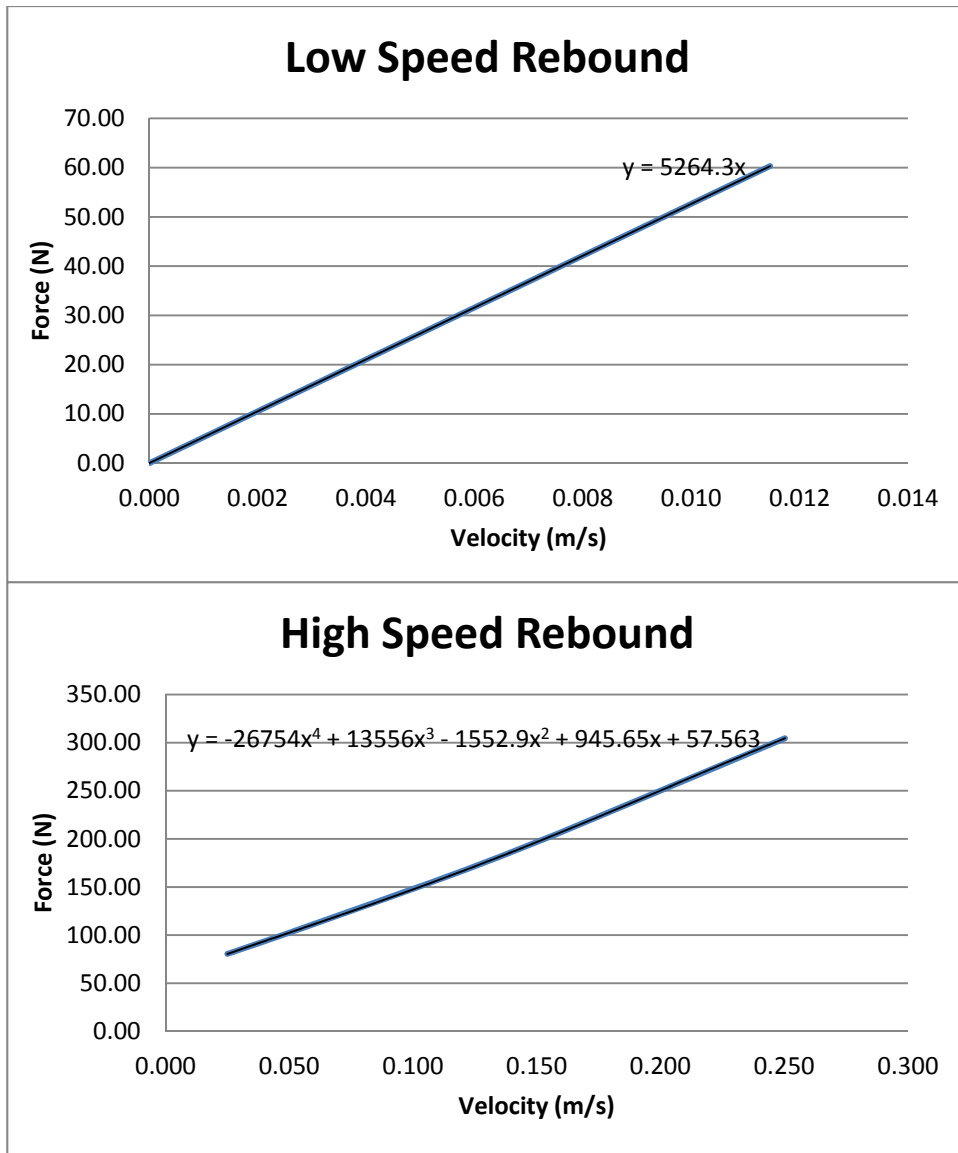


Figure 5: Low Speed and High Speed Bound and Rebound Plot

The trend line equation is used to obtain the force the damper is resisting at a particular velocity. With that, the power can be calculated using the formula $P=Fv$. The velocity is obtained by An Excel Spreadsheet is used to automate the calculation of the force by examining if the travel is in compression or rebound. It also examine if the speed is high or low speed From there, it will conduct the necessary calculation by using the correct equation for the calculation. A sample of the logged data is shown in Table 3.

Position	Time (s)	Damper Position (mm)
1	2085.00	44.17
2	2085.50	39.40

3	2086.00	53.21
---	---------	-------

Table 3: Sample Logged Data

Velocity can be found by taking change in position per unit time.

For position 1:

$$v_{1-2} = \frac{39.40 - 44.17}{2085.50 - 2085.00} \times \frac{1}{1000}$$

$$= -0.00954 \text{ m/s}$$

Since from positions 1 to 2 the damper has a reduction in length, it means that the damper is under compression and thus has a negative velocity. The negative value will be ignored in this calculation as it is meant to show the direction. As the velocity is lower than 0.013 m/s, the equation used will be under the table Low Speed Bound curve with the equation as $F_{1-2} = 4454x$, where x is the velocity.

$$F_{1-2} = 4454 \times 0.00954$$

$$= 42.49N$$

$$P_{1-2} = F_{1-2}V_{1-2}$$

$$= 42.49 \times 0.00954$$

$$= 0.405W$$

For position 2:

$$v_{2-3} = \frac{53.21 - 39.40}{2086.00 - 2085.50} \times \frac{1}{1000}$$

$$= 0.0276 \text{ m/s}$$

Since from positions 2 to 3 the damper has an increase in length, it means that the damper is being extended. As the velocity is higher than 0.013 m/s, the equation used will be under Figure 5: High Speed Rebound curve with the equation as

$$F_{2-3} = -26754x^4 + 13556x^3 - 1552.9x^2 + 945.65x + 57.563, \text{ where } x \text{ is the velocity}$$

$$\begin{aligned}
F_{2-3} &= -26754(0.0276)^4 + 13556(0.0276)^3 - 1552.9(0.0276)^2 + 945.65(0.0276) \\
&\quad + 57.563 \\
&= 82.78N
\end{aligned}$$

$$\begin{aligned}
P_{2-3} &= F_{2-3}V_{2-3} \\
&= 82.78 \times 0.0276 \\
&= 2.286W
\end{aligned}$$

From the calculations it can be observed that the power dissipated by the dampers can reach up to 2 Watts. From the logged data, the highest power dissipated is calculated to be 81 Watts. However, the occurrence is very low as it might be due to the vehicle going over a pothole during the race.

Taking logged data for an endurance race that lasts 1,758 seconds or 29.3 minutes, the total power dissipated is around 18,800 Watts, which is a still a significant amount of power to be harness even if only 20% of the power can be harnessed.

2.2 Energy Harvesting Methods

With reference to Figure 6, energy can be harvested through rotational means from the suspension arm joining points, rocker rotation or anti roll bar. Energy can also be harvested through linear motion from the dampers or the anti roll bar.

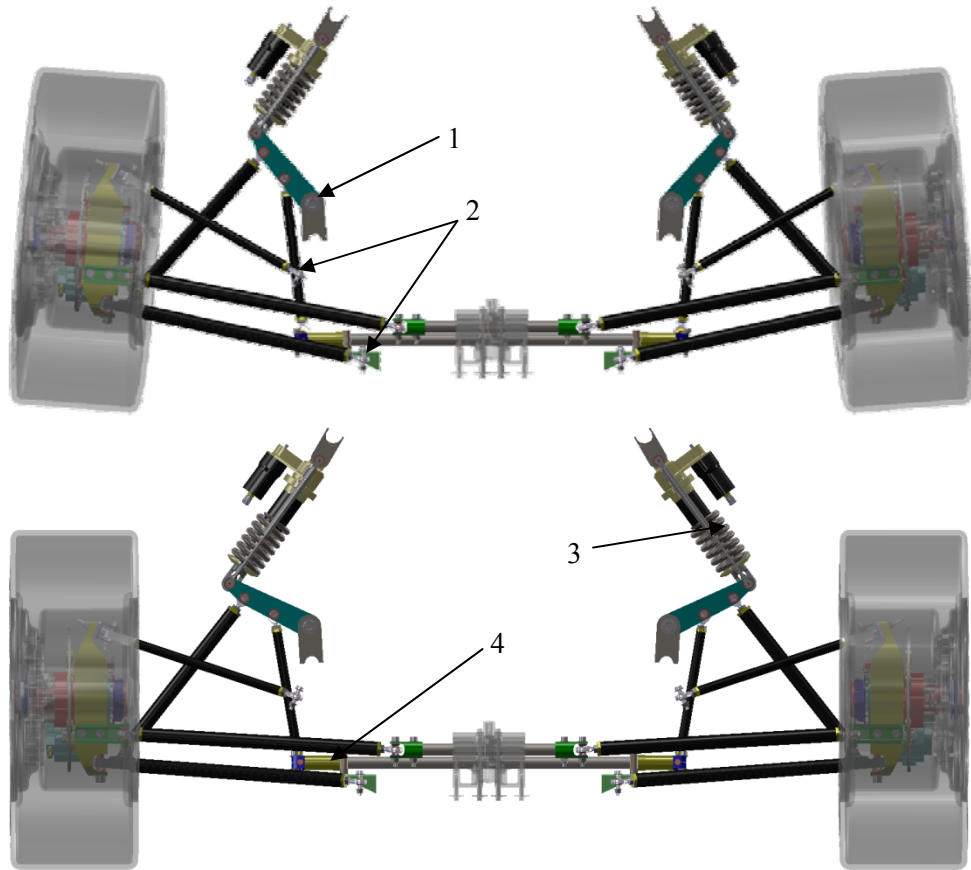


Figure 6: Part of Suspension System that Moves

Figure 6 shows the suspension in full bump position (Top) and full droop position (Bottom). From the figure, there is relative movement of the suspension points between the droop to bump position.

1. Rotation of the rocker due to the actuation from the wheels to the push rod and the compression of the dampers
2. Rotation of the suspension arms about the pickup points due to the movement of the wheels
3. Linear motion of the dampers due to compression and extension of the springs
4. Rotational twisting of the anti roll bar and the rotation of the linkage linking the anti roll bar and the rocker.

These motions will be examined in the following chapters to evaluate the ease of implementation to harvest energy from the movement.

2.2.1 Rotary Motion of Components

Energy harvesting from rotation motion makes use of electric motor with speed multiplier to amplify the motion of the movement so that significant rotation can be achieved at the motor.

2.2.1.1 Rocker Rotation

Figure 7 shows the rocker motion when the car experiences bump and droop. From CAD calculations, a motion of 2 inches travel from the wheel translates to 23.6° of rocker rotation from the rocker.

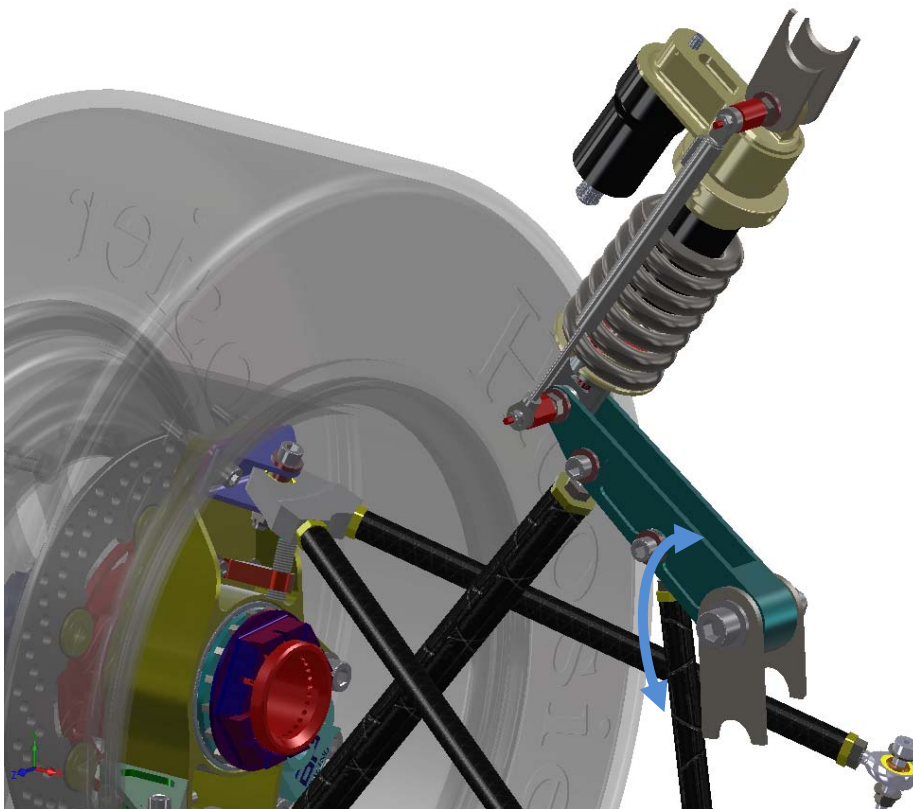


Figure 7: Rocker Rotation

The degree per travel is calculated as below:

$$\begin{aligned} \text{Degree Per mm Travel} &= \frac{23.6}{2 \times 25.4} \\ &= 0.468^\circ/\text{mm} \end{aligned}$$

Taking the highest damper travel in the logged data for calculation at 54.0 mm within half a second,

$$\begin{aligned} \text{Angle rotated at maximum travel} &= 54.0 \times 0.468 \\ &= 25.27^\circ \end{aligned}$$

The RPM of the rocker at that instant is thus:

$$\begin{aligned} \text{RPM of Rocker} &= \frac{25.27}{360} \times \frac{1}{0.5} \times 60 \\ &= 8.42 \text{ RPM} \end{aligned}$$

That is the maximum RPM for the entire Endurance run. Figure 8 shows the frequency of the rocker RPM during an Endurance run. Appendix 1 shows the frequency table of the rocker rotation. As seen from Appendix 1, there are only a few single occurrences for 10.0 mm and larger travel.

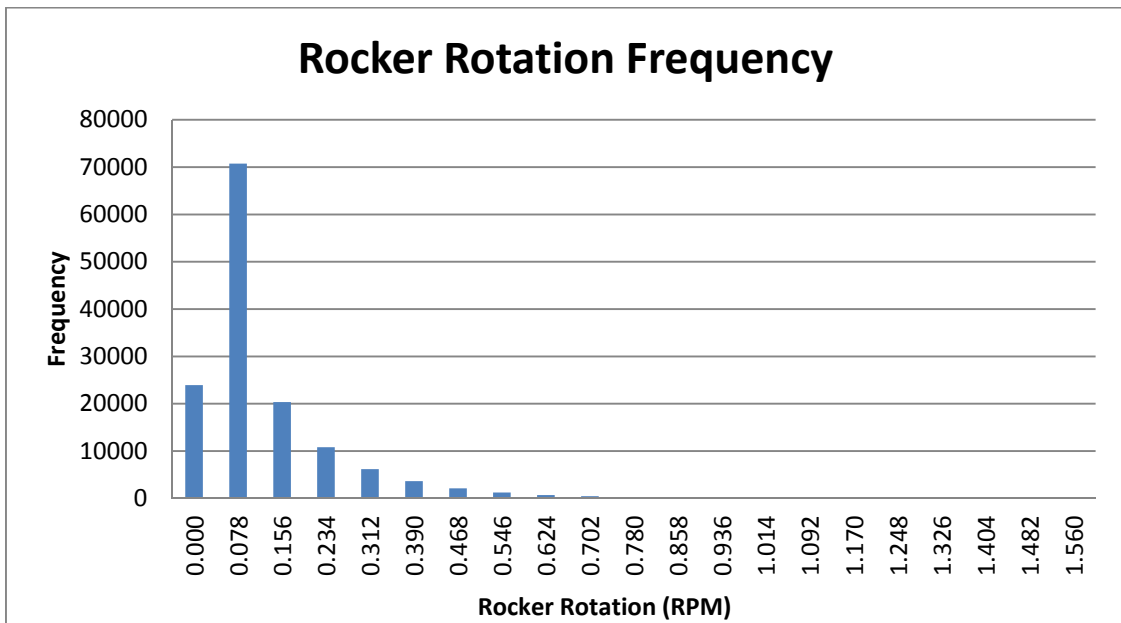


Figure 8: Rocker Rotation Frequency Plot

The RPM for the rocker occurs more frequently below 1.56 RPM. Therefore, the maximum voltage is set to be produced at 1.56 RPM. In order to provide sufficient voltage to charge a 12 V battery in a car, the charging system will generally need to produce around 14.4 V. The voltage per RPM for the generator motor will thus need to be:

$$\begin{aligned} \text{Motor Voltage per RPM} &= \frac{14.4}{1.56} \\ &= 9.23 \text{ Volt per RPM} \end{aligned}$$

With such high voltage per RPM, a very low RPM gearbox with high reduction is required. Searching through the World Wide Web for low rpm 12 V motor, the lowest found at RS Components is a 1.1 – 64.0 RPM 12 V motor with worm and spur gear combination with a price of SGD 682.00 (Figure 9). The specifications are attached in Appendix 2. There is different wattage available depending on the power input from the suspension travel.

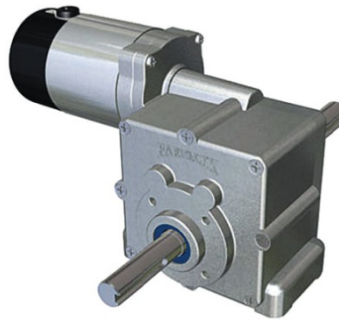


Figure 9: Low RPM High Torque DC Motor

From the specifications, the motor fits the 1.56 RPM limit set for the suspension travel. A step-up DC-DC converter can be used to convert the lower voltage due to the lower travel to maintain the voltage output at a constant 14.4 V. The above is just an initial calculation for the feasibility of harvesting energy from the movement. More detailed calculation will be conducted if this method is chosen.

2.2.1.2 Suspension Arms and Anti-Roll Bar Rotation

Figure 10 shows the suspension motion when the car experiences bump and droop. From CAD calculations, a motion of 2 inch travel from the wheel translates to 8.34°, 11.65° and 0.7° for the lower arm, upper arm and anti-roll bar rotation respectively.

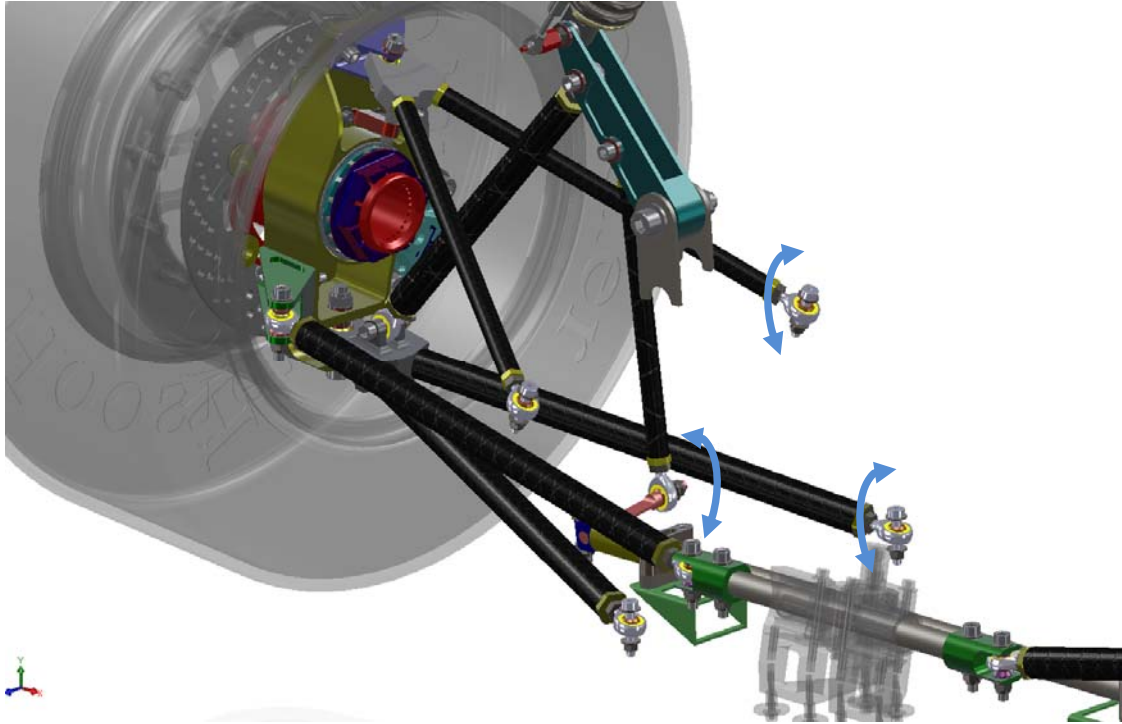


Figure 10: Suspension Arms Rotation

The anti-roll bar angle is to be neglected as the travel is too low. The energy harvested can be obtained by summing the total angle that the 4 inboard suspension arms move, which is around 40°.

The method of calculation and energy harvesting method will be the same as the rocker movement, with the generator motor mounted to individual pickups. The generator motor can be connected in parallel or in series with different specification motors.

2.2.2 Linear Motion of Dampers

Figure 11 shows the suspension motion when the car experiences bump and droop. As the motion ratio of the suspension components is 1.0, therefore when the wheel moves 2 inches, the damper stroke also changes 2 inches. The linear motion can be tapped directly using electromagnetic induction or converting it to rotational motion and tapped using electric motor.

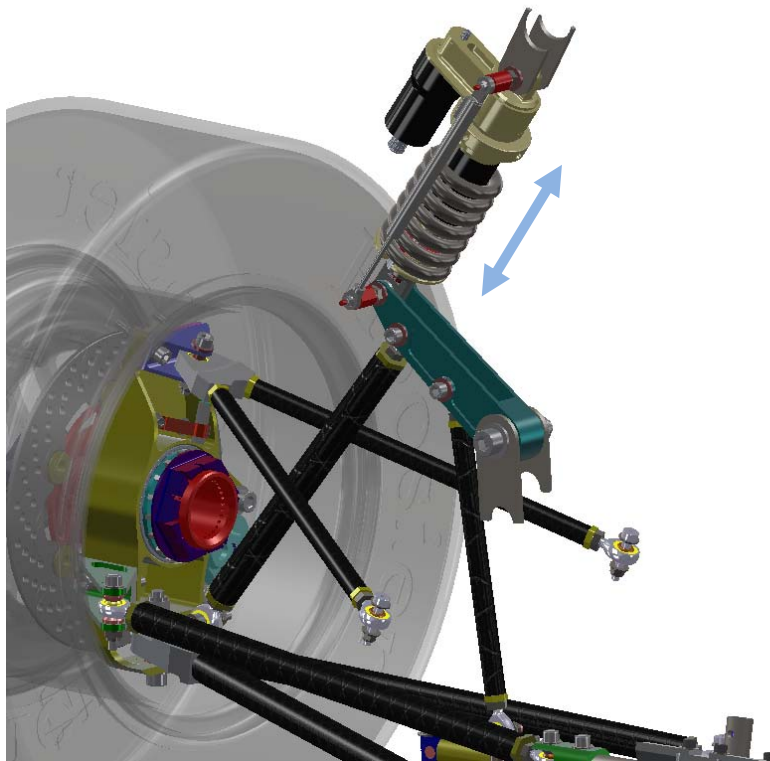


Figure 11: Damper Linear Motion

2.2.2.1 Electromagnetic Induction

Electromagnetic induction relies on the speed of the movement and the magnetic field that the wire coils cut through. Some assumptions (Table 4) will be used to calculate the voltage and current induced to do a quick calculation of the number of coils. The maximum velocity of the damper from the logged data is 1.081 m/s.

Assumption	Value
Damper length	170 mm
Diameter of coil	40 mm
Diameter of wire	1 mm
Magnetic field (N52)	2 T
Voltage to be induced	14.4 V

Table 4: Assumptions for Electromagnetic Induction Calculation

The voltage induced is calculated by the formula

$$V = Blv$$

$$V = B(\pi N d_a)v$$

$$14.4 = 2 \times \left(\pi \times N \times \frac{40}{1000} \right) \times 1.081$$

$$N = 53 \text{ turns}$$

Taking a damper length of 170 mm and wire diameter of 1.0 mm, there is sufficient space to fill up 53 coils of wires. More coil sets can be added to provide more current by wiring the coil sets in parallel.

Due to the above layout, the damper will have to be replaced by the magnets and wire coils. The Lorentz force due to the electromagnetic force will be calculated and check if it matches the damping force. If the force matches, then the dampers can be completely replaced.

The frequency of velocity for the damper for the endurance run is shown in Figure 12. Tabulated data for the velocity frequency is shown in Appendix 3. The velocity of the dampers occurs more frequently below 0.068 m/s. Therefore, the velocity at maximum voltage (14.4 V) will be set at 0.068 m/s.

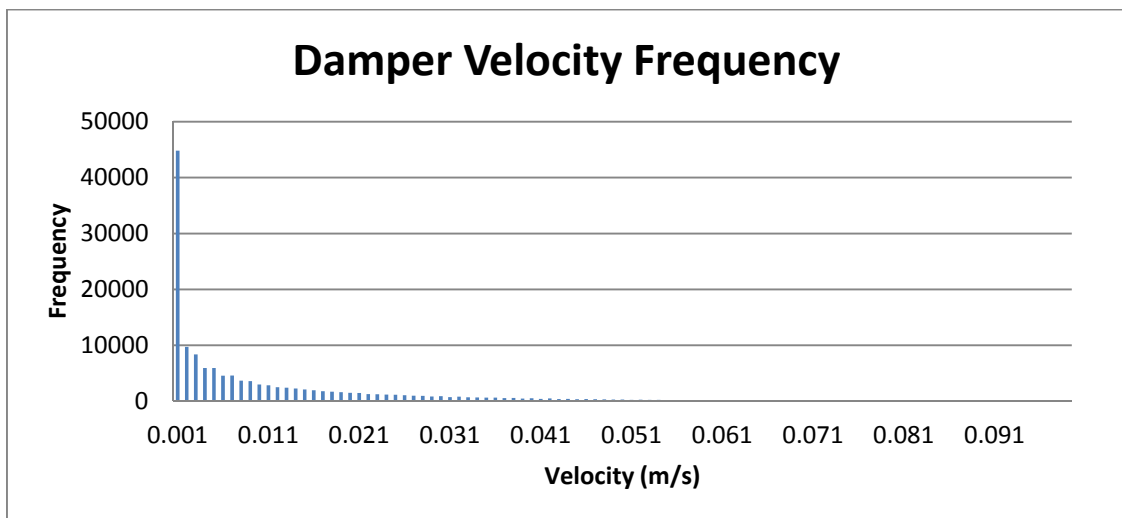


Figure 12: Damper Velocity Frequency Plot

At 0.068 m/s, the number of turns for the wire coils will need to be:

$$V = Blv$$

$$V = B(\pi N d_a)v$$

$$14.4 = 2 \times \left(\pi \times N \times \frac{40}{1000} \right) \times 0.068$$

$$N = 843 \text{ turns}$$

Taking the damper length of 170 mm and wire diameter of 1.0 mm, the wires have to be coiled around 5 times along the length of the damper. That will occupy around 5.0 mm of space for all the wires with a nominal coil diameter of 40 mm. The induced current is calculated by the formula below:

$$I = B\sigma Av$$

The electrical conductivity of copper (σ) is obtained from the website http://www.powerstream.com/Wire_Size.htm. From the website, the diameter of the copper laminated wire and the resistance per length is given. The resistivity of the wire can be found by multiplying the area of the wire with the resistance per length. From there, the conductivity can be found by taking the reciprocal of the resistivity and it is found to be 5.78×10^7 S/m.

The short circuit induced current at 0.035 m/s can be calculated as below:

$$\begin{aligned} I &= B\sigma Av \\ &= 2.0 \times 5.78 \times 10^7 \times \pi \times \left(\frac{1.0}{2 \times 1000}\right)^2 \times 0.068 \\ &= 6.17 \text{ A} \end{aligned}$$

Appendix 4 shows the American Wire Gauge (AWG) table. The 1.0 mm wire falls in the category of AWG 18 and the maximum current is at 16.0 A. If a higher gauge wire is used, more coils can be added in the same amount of confined space.

2.2.2.2 Electric Motor

Displacement of the dampers can be converted to rotational motion through the use of crank, scotch yoke or rack and pinion methods as shown in Figure 13 to convert linear motion to rotational motion.

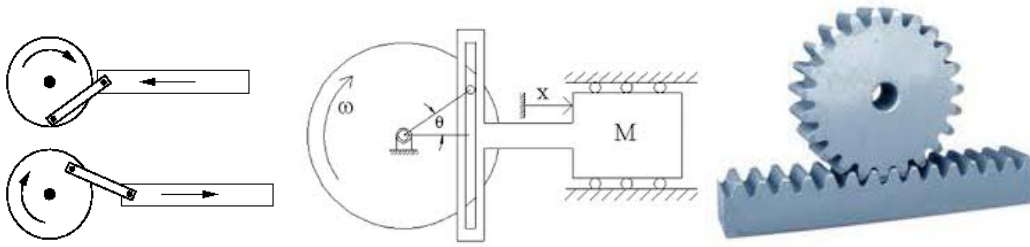


Figure 13: Crank, Scotch Yoke and Rack and Pinion System

2.2.2.2.1 Crank and Scotch Yoke

Crank and scotch yoke is almost the same and the rotation is affected by the diameter of the wheel. The diameter of the wheel have to be matched with the stroke of the travel otherwise the system will get jammed or the system might be damaged. It is therefore necessary to specify the diameter of the travel such that it can travel through the damper maximum travel of 2 inches.

Figure 14 shows the damper stroke frequency and the more frequently occurred stroke is around 10.0 mm. Taking 10.0 mm of travel from the neutral point (25.0 mm stroke at ride height), and the crank level arm as 50.0 mm, the crank will rotate through an angle of 22.7° as shown in Figure 15.

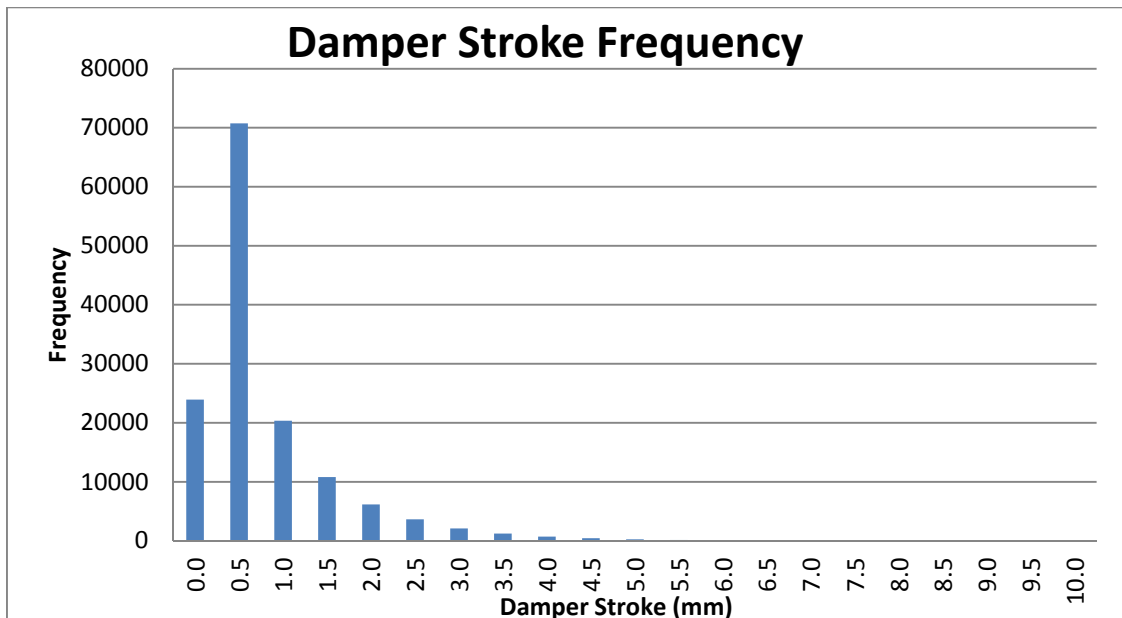


Figure 14: Damper Stroke Frequency

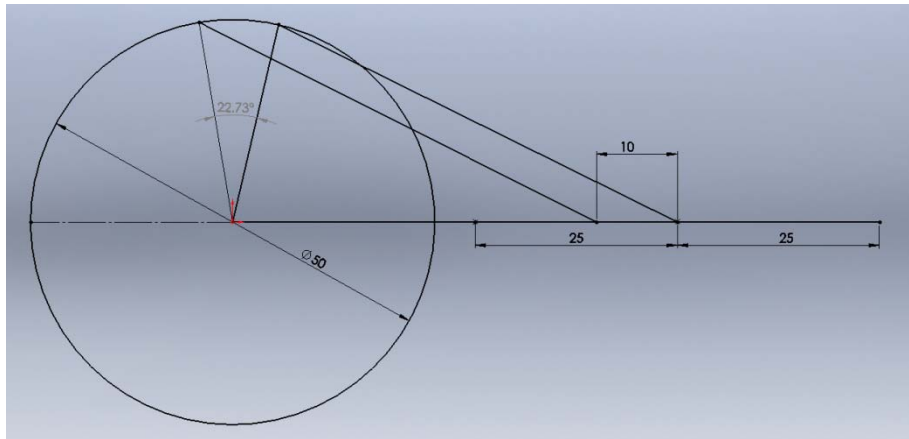


Figure 15: Crank Rotation 2D Sketch

As per in chapter 2.2.1.1, the angle displaced will be used to calculate the RPM of the crank at the instant through the formula:

$$\begin{aligned} RPM \text{ of Crank} &= \frac{22.7}{360} \times \frac{1}{0.5} \times 60 \\ &= 7.57 \text{ RPM} \end{aligned}$$

The voltage per RPM for the generator motor will thus need to be:

$$\begin{aligned} Motor \text{ Voltage per RPM} &= \frac{14.4}{7.57} \\ &= 1.9 \text{ Volt per RPM} \end{aligned}$$

With a lower voltage per RPM, a gearbox with a lower reduction as compared to chapter 2.2.1.1 can be used.

2.2.2.2.2 Rack and Pinion

For a rack and pinion system, the angle of rotation per stroke is dependent on the radius of the pinion gear and also the module of the gear. The smaller the pinion, the more rotation it will go through when the rack moves linearly.

The smallest commercially available module gears will be used to maximise rotation, coupled with the lowest teeth for the pinion gear. From Misumi South East Asia Website (<http://sg.misumi-ec.com/>), the smallest module for rack gears is 0.5. The lowest number of teeth for the pinion with 0.5 module is 15 teeth. Appendix 5 shows the catalogue for the gears.

The pitch circle diameter for the 0.5 module 15 teeth pinion gear is 7.5 mm. This gives a linear travel of $\pi \times 7.5 = 23.56 \text{ mm}$ linear travel for the rack for 1 revolution.

Taking the frequently occurred stroke of 16 mm from chapter 2.2.2.2.1, the angle the pinion rotate through is

$$\begin{aligned} \text{Angle Pinion rotate} &= \frac{10.0}{23.56} \times 360 \\ &= 152.8^\circ \end{aligned}$$

As per in chapter 2.2.1.1, the angle displaced will be used to calculate the RPM of the pinion at the instant through the formula:

$$\begin{aligned} \text{RPM of Pinion} &= \frac{152.8}{360} \times \frac{1}{0.5} \times 60 \\ &= 50.9 \text{ RPM} \end{aligned}$$

The voltage per RPM for the generator motor will thus need to be:

$$\begin{aligned} \text{Motor Voltage per RPM} &= \frac{14.4}{50.9} \\ &= 0.283 \text{ Volt per RPM} \end{aligned}$$

With an even lower voltage per RPM, a normal gearbox with low reduction as compared to chapter 2.2.1.1 can be used.

2.3 Advantages and Disadvantages of Different Systems

Table 5 shows the pros and cons of each system and restrictions involved. It will be used to decide which system will be used to test the output power from the suspension system.

System	Advantages	Disadvantages	Restrictions
Rotary Motion of Rocker	<ul style="list-style-type: none"> • Easy to implement 	<ul style="list-style-type: none"> • Space required for motor mounting • Required to test with car moving • Introduce new force at the rocker 	Availability of low RPM electric motor
Rotary Motion of Suspension Arms	<ul style="list-style-type: none"> • Easy to implement • Able to tap 16 points in suspension pickup points 	<ul style="list-style-type: none"> • Even more space required for motor mounting • Required to test with car moving • Introduce new force at the joints • Control arms in bending 	Availability of low RPM electric motor
Electromagnetic Induction of Dampers	<ul style="list-style-type: none"> • Least mechanical mechanism • Replaces damper which does not take up more space • Able to test damper independently using damper dynamometer 	<ul style="list-style-type: none"> • Damping ratio might not match original damper • Difficulty in installation due to strong magnetic field 	Availability of high strength magnets
Linear to Rotational Motion of Dampers	<ul style="list-style-type: none"> • Replaces damper which does not take up more space • Able to test damper independently using damper dynamometer 	<ul style="list-style-type: none"> • Damping ratio might not match original damper • Crank and Scotch Yoke method could get damaged if over travel • Unable to predict Crank and Scotch Yoke rotation direction • At each extreme points of the Crank and Scotch Yoke system, a tangential force is required to turn the system, but damper force is perpendicular 	Availability of low RPM electric motor

Table 5: Advantages and Disadvantages of Different Regenerating Systems

One of the major restrictions is the non availability of the low RPM motor from RS Components. Another restriction is the requirement of testing the Formula SAE vehicle. As there is only one testing ground available to the Formula SAE team currently and it is not near

NUS, the whole team has to go down to the testing ground to support the test run. Therefore it is time and resource intensive to conduct tests that require the actual vehicle to be tested. In addition, after the Formula SAE vehicle is back from the competition, team members will be taking apart certain components of the vehicle to conduct independent testing to improve the design for the next vehicle. Therefore the Formula SAE vehicle is usually not complete to conduct road testing.

The biggest restriction is that at the point of time when a decision is to be made, there is an accident involving the Formula SAE vehicle which the safety committee in NUS put a halt to Formula SAE vehicle testing. Therefore, the decision was made to proceed with the electromagnetic induction of dampers as the tests will be independent of the Formula SAE vehicle availability.

For all the calculations, it is also assumed that the voltage generated is the open circuit voltage and the current is the short circuit current. When the actual load (the charging of the battery) is being applied, the power generated might be lower.

3 Electromagnetic Damper Design

The electromagnetic damper makes use of high performance Neodymium magnets that has high magnetic flux density. Laminated copper wires will be used to induce the electricity when the copper wire cuts through the magnetic field. For a wire cutting through a magnetic field, a current is induced as shown in Figure 16.

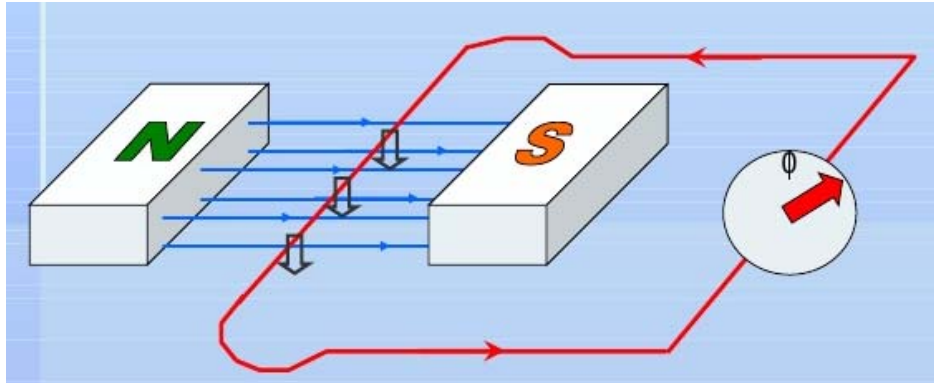


Figure 16: Electric Field Induction when Crossing a Magnetic Field

The current will flow in the opposite direction when the wire is moved in the opposite direction. Using Faraday's law of electromagnetic induction, the induced voltage generated in the magnetic field due to the moving wire is given by the formula:

$$V = Blv$$

And the current induced is given by:

$$I = B\sigma Av$$

From the 2 formula above, the magnetic field, the velocity of the coil and the density of copper coils directly affect how high the voltage and current is induced.

3.1 Linear Actuator

The design of the electromagnetic damper will be almost similar to that of a linear actuator as shown in Figure 17.

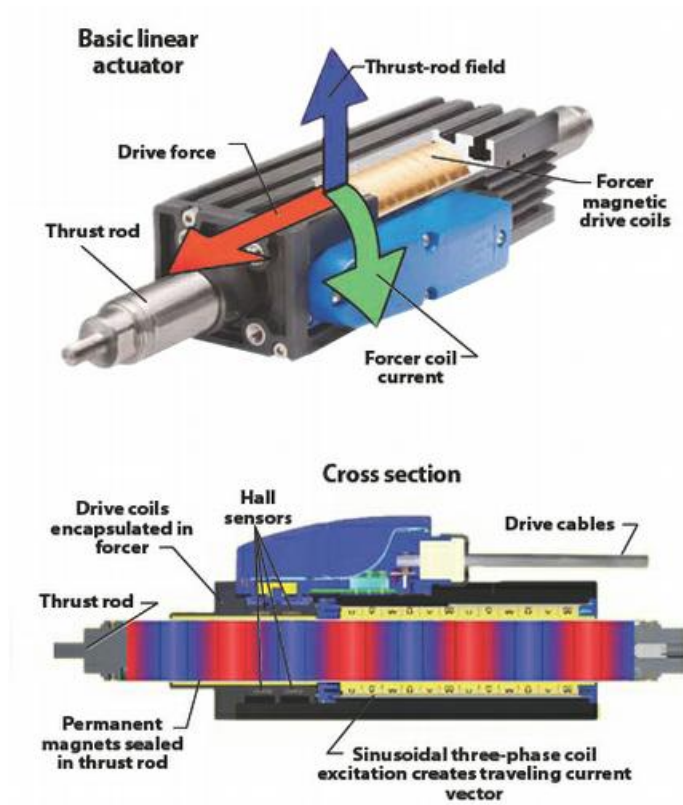


Figure 17: Linear Actuator

For the linear actuator above, a current is applied to the wires on the fixed casing. The magnet is mounted on the actuator. When sinusoidal current is applied to the wire coil, it will interact with the magnetic field and causes a force to be produced to move the actuator using Fleming's Left Hand Rule. For electromagnetic damper, the process is reversed where the road forces cause the coils to move in the magnetic field and this produces voltage and current.

The use of magnets inside the wire coil housing is such that manufacturing of the coils is difficult for a prototype electromagnetic damper since the wire coils are hand wound rather than machine wound. It is easier to externally wind than internally wind to make sure that the wire windings are tight.

The design of the electromagnetic damper will thus be a series of ring magnets as the upper portion of the damper with wire coil in the inside connected to the lower portion of the damper as illustrated in Figure 18.

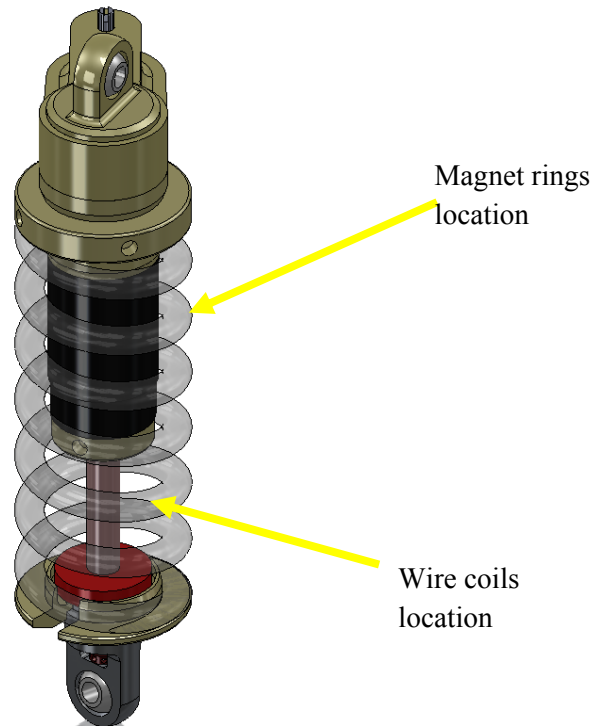


Figure 18: Magnet and Wire Location in a Damper

3.2 Neodymium Magnets

The strongest magnet with the highest magnetic flux density currently available in the market is N52 magnet. The area of focus for the electromagnetic damper design is the magnetic field of the magnet as it crosses the copper wires. The higher the magnetic flux density as the wire crosses the area, the higher the voltage and current induced in the wire.

The shape of the magnet will be matched to the shape of the damper which is a round cylinder. This is to accommodate the spring and also to prevent interference with other components by keeping the electromagnetic damper as close to the original damper as possible.

Figure 19 shows the magnetic field produced by a ring magnet which is magnetized through its thickness. At the centre of the ring magnet, the magnetic field is moving in the direction that is similar along the axis of the movement of the damper. The moving wire coils will not cut through the magnetic field in this manner and no current will be induced. This can also explain the location of the magnet inside the wire coils for the linear actuator in Figure 17 above. The

magnetic fields are travelling perpendicular to the movement of the current and thus a force induced in the direction along the axis of the magnet.

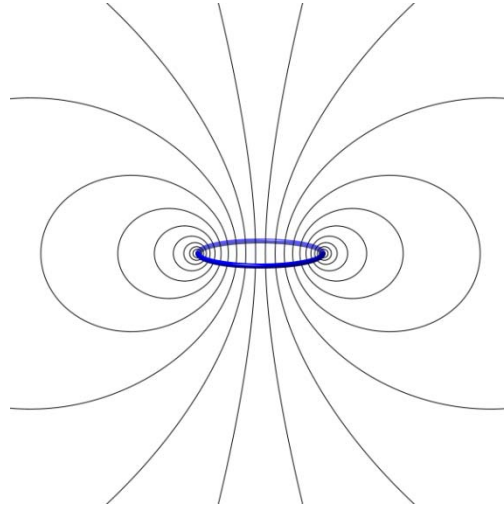


Figure 19: Magnetic Fields Produced by a Ring Magnet

Since there are a series of ring magnets stacked on top of each other, a solution is to place the magnets in opposite poles to each other and introduce a ferrous material between each magnet. The placing of poles opposite to each other allows the repelling magnetic fields to travel into the central axis of the ring magnet and perpendicular to the direction of travel. The ferrous material between each magnet serves to direct the magnetic field towards the centre of the cylinder. If the 2 magnets of opposite poles were to be stacked on top of each other without the ferrous material, the magnetic flux lines would have no place to bend to be pointing towards the centre of the cylinder. Analysis on the different layout of the magnet will be carried out in the next chapter.

In order to saturate a higher magnetic flux, an inner ring of magnet will be introduced with its ferrous spacers. It will be placed in concentricity with the outer ring magnet, in opposing poles.

Figure 20 shows the cross section view of a 3 set magnet-spacer layout. The opposing poles on the outer and inner magnet will be able to force the magnetic flux to travel along the ferrous spacer and concentrate its magnetic strength in the circled areas as shown in Figure 20.

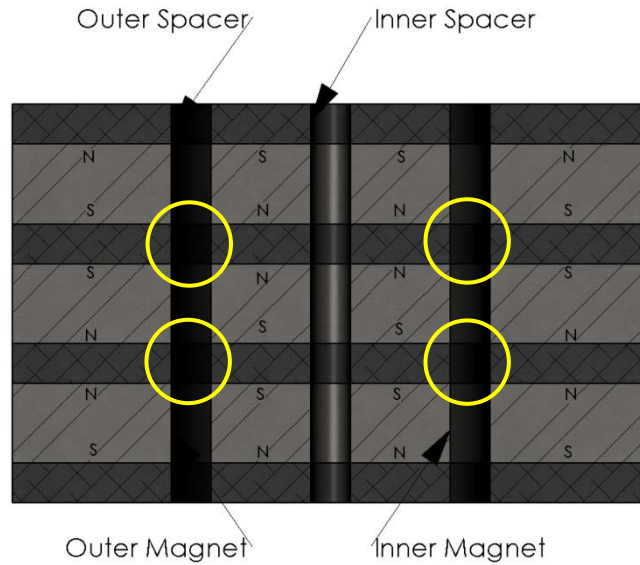


Figure 20: Magnet and Ferrous Spacer Layout

In addition, the smaller ring magnet has to be able to fit into the internal diameter of the larger magnet with allowances for the laminated wires and its holder to pass through. The thickness of the 2 ring magnets must be the same as well. Searching through the World Wide Web, there is not much suppliers locally that sell high strength magnet.

It happened that the author was going to USA for the Formula SAE competition. Therefore USA sources were also taken into consideration. Appendix 6 lists the different sources of ring magnets from the World Wide Web. Magnets with similar colour bands are similar thickness magnets with the outer diameter of the inner magnet able to fit within the inner diameter of the outer magnet.

Eventually, the more cost effective magnet sets are from Ebay.com and Lifton Magnets. The dimension for both sets of magnet is almost similar as shown in Table 6. One is in imperial and the other in metric dimensions. For a total of 12 inner and outer magnets, the total cost for Ebay.com and Lifton magnets are \$504.24 and \$347.88 respectively. Analysis will be conducted in the next chapter for comparison.

ID (mm)	OD (mm)	T (mm)	Price (SGD)	Type	Source
19.0500	3.1750	6.3500	2.69	N48	Ebay
50.8000	25.4000	6.3500	39.33	N48	Ebay
20.0000	6.0000	6.0000	5.90	N50	Lifton magnets
50.0000	25.0000	6.0000	23.09	N50	Lifton magnets

Table 6: Magnet Comparison from Suppliers

The analysis of the magnetic field due to the interaction of the inner magnet, outer magnet and the ferrous core will be conducted using two software. A set of 3 magnets and core will be used to conduct the analysis for simplicity. Ansys Magnetostatic analysis will be used to directly import the 3D CAD and conduct 3D analysis. The analysis is resource intensive and thus another software FEMM is used to conduct a 2D analysis on the cross sectional view of the setup. Using a 2D analysis allows iterations to be done and also provide a check with Ansys Magnetostatic analysis.

3.2.1 Ansys Magnetostatic Simulation

The 3-Magnet simulation is first modelled in Solidworks CAD software.

Figure 21 shows the CAD and the section view of the magnet. It consists of 3 sets of magnets and 4 sets of ferrous spacer layout similar to Figure 20. There is a cylinder in the centre which is the wire coil housing. The ferrous spacer is assumed to be half the thickness of the magnet and the wire coil housing having a diameter which allows 2 rows of AWG 18 wire to be wound without interference with the magnet.

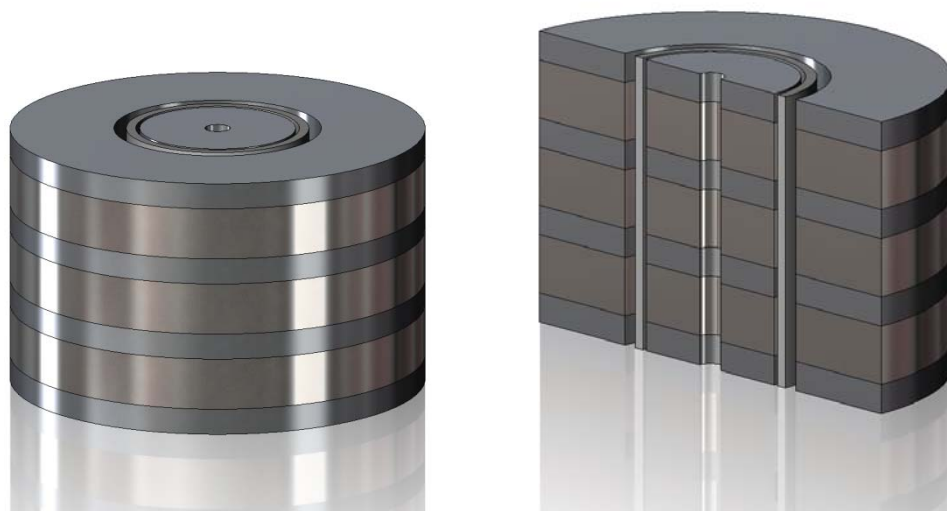


Figure 21: 3 Magnets CAD

The CAD file is exported to Ansys Workbench in Figure 22 where engineering data (material properties) can be added and multiple simulations can be linked on the same model, engineering data or simulation setup.

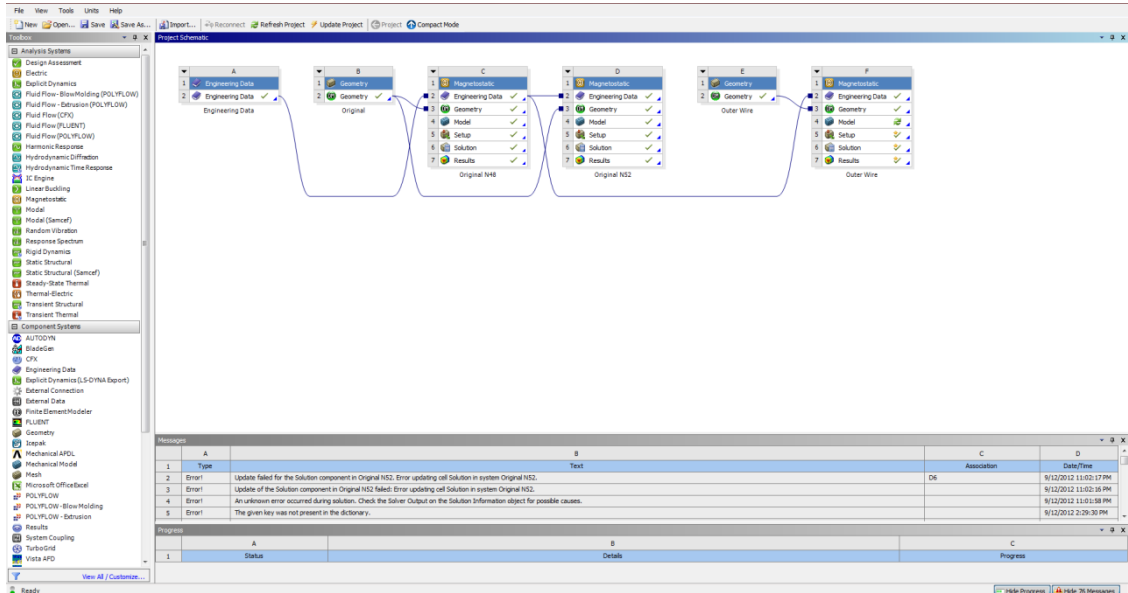


Figure 22: Ansys Workbench

Ansys Workbench eases simulation setup when there are multiple iterations of simulation to be conducted. After Ansys Workbench is set up, the simulation is pre-processed by enclosing a box around the magnets to be simulated. The box will be used to confine the region of magnetic flux through setting a parallel magnetic flux at each faces of the box.

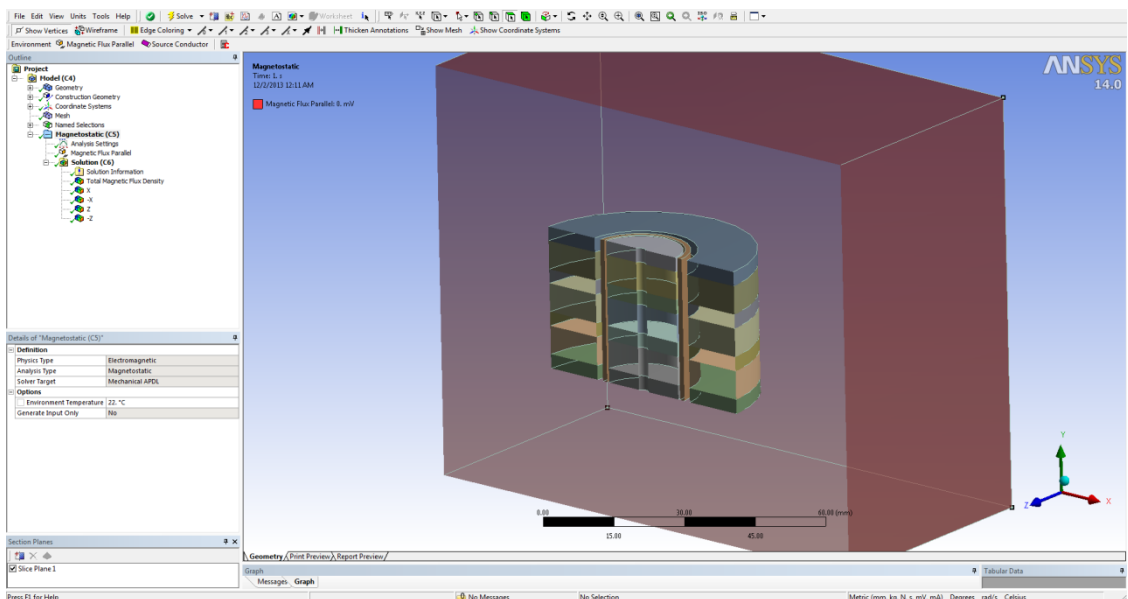


Figure 23: Ansys Magnetostatic Setup

The material can also be assigned to the CAD with magnetic polarity. Mesh can be controlled to balance between simulation time and accuracy of results. Post processing of data includes setting of linear plot of magnetic field fluctuation and directional colour plot with local maxima.

3.2.1.1 *Ebay.com Magnets Ansys Magnetostatic Plot*

Figure 24 shows the magnetic flux density plot with arrow colour plot in section view. The diagram shows that the magnetic flux is concentrated mostly at the ferrous spacer region. The maximum magnetic flux for the plot is 2.33 T.

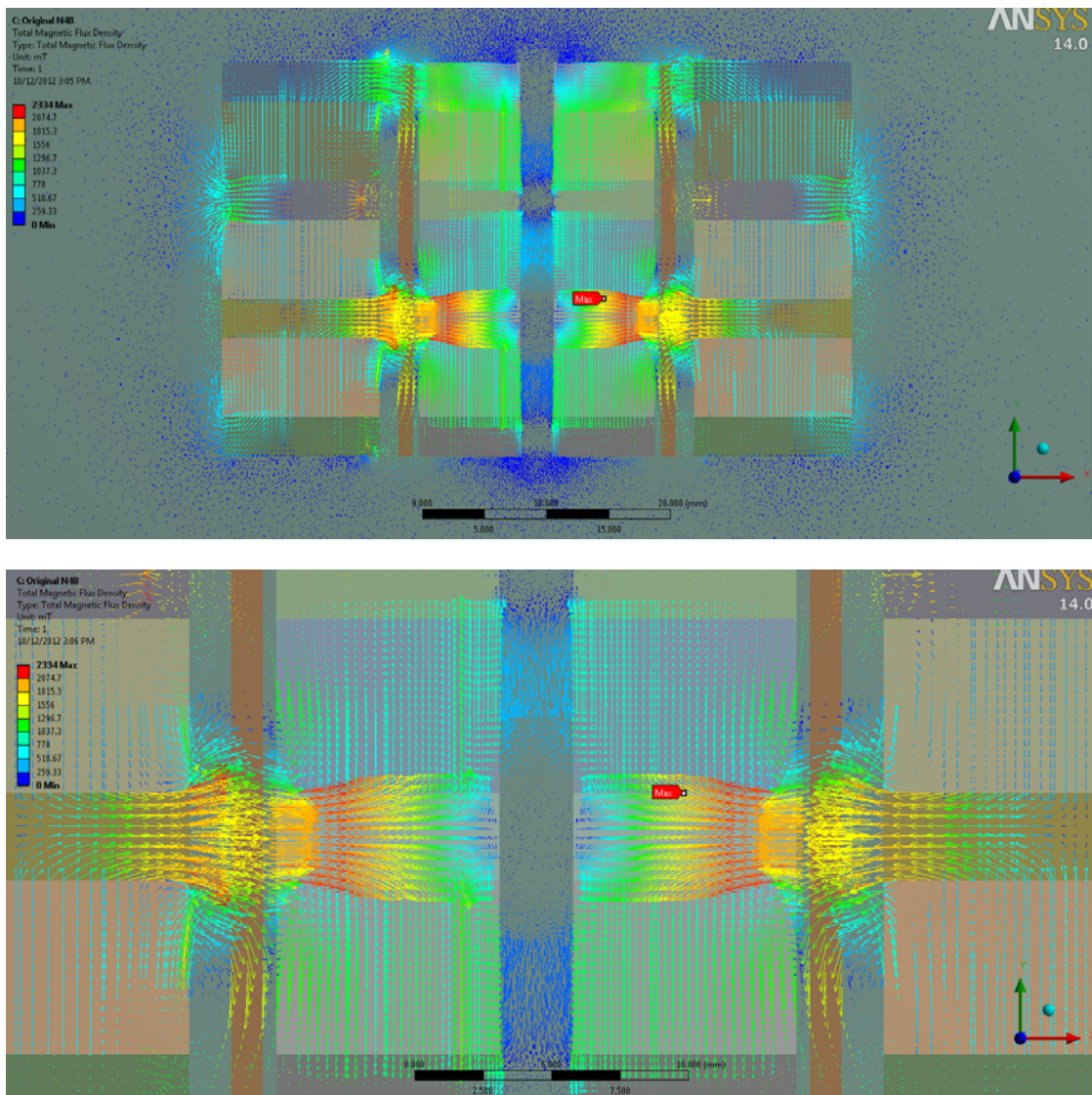


Figure 24: Magnetic Flux Lines (Top) and Zoom in of Analysis (Bottom) for Ebay.com Magnet

A line plot is also conducted to know the magnetic flux at the region where the copper coils will pass through. Figure 25 shows the maximum for the air region; the maximum intensity might be at the small air gaps between the wire coil housing and the inner magnets. However, the area of interest is the air gap where the wire will pass through. Therefore, the line plot along the area where the wire coil will move around should be considered and be used for calculation.

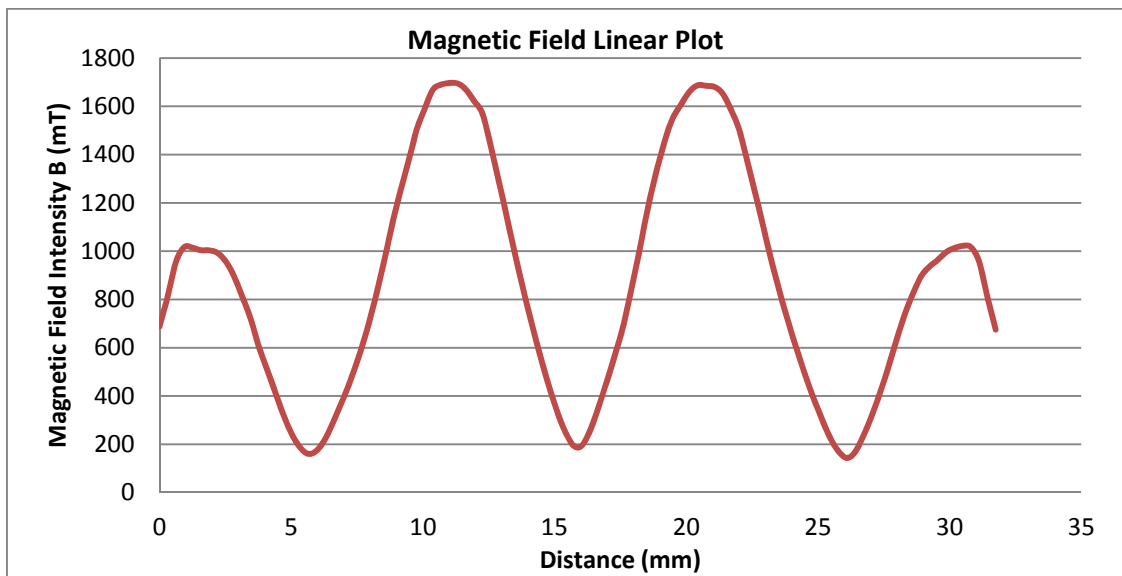


Figure 25: Magnetic Field Intensity Plot for Ebay.com Magnet

From the line plot in Figure 25, the maximum magnetic field intensity is 1.70 T. The coils will experience the peak magnetic field within 3.175 mm of the maximum magnetic field intensity as it travel pass the spacer. Thus, the average magnetic field intensity will be taken within the region.

Appendix 7 shows the tabular form of Figure 25. The average magnetic field intensity is calculated to be 1.56 T within the region.

3.2.1.2 *Lifton Magnets Ansys Magnetostatic Plot*

Figure 26 shows the magnetic flux density plot with arrow colour plot in section view. The diagram shows that the magnetic flux is concentrated mostly at the ferrous spacer region. The maximum magnetic flux for the plot is 2.77 T.

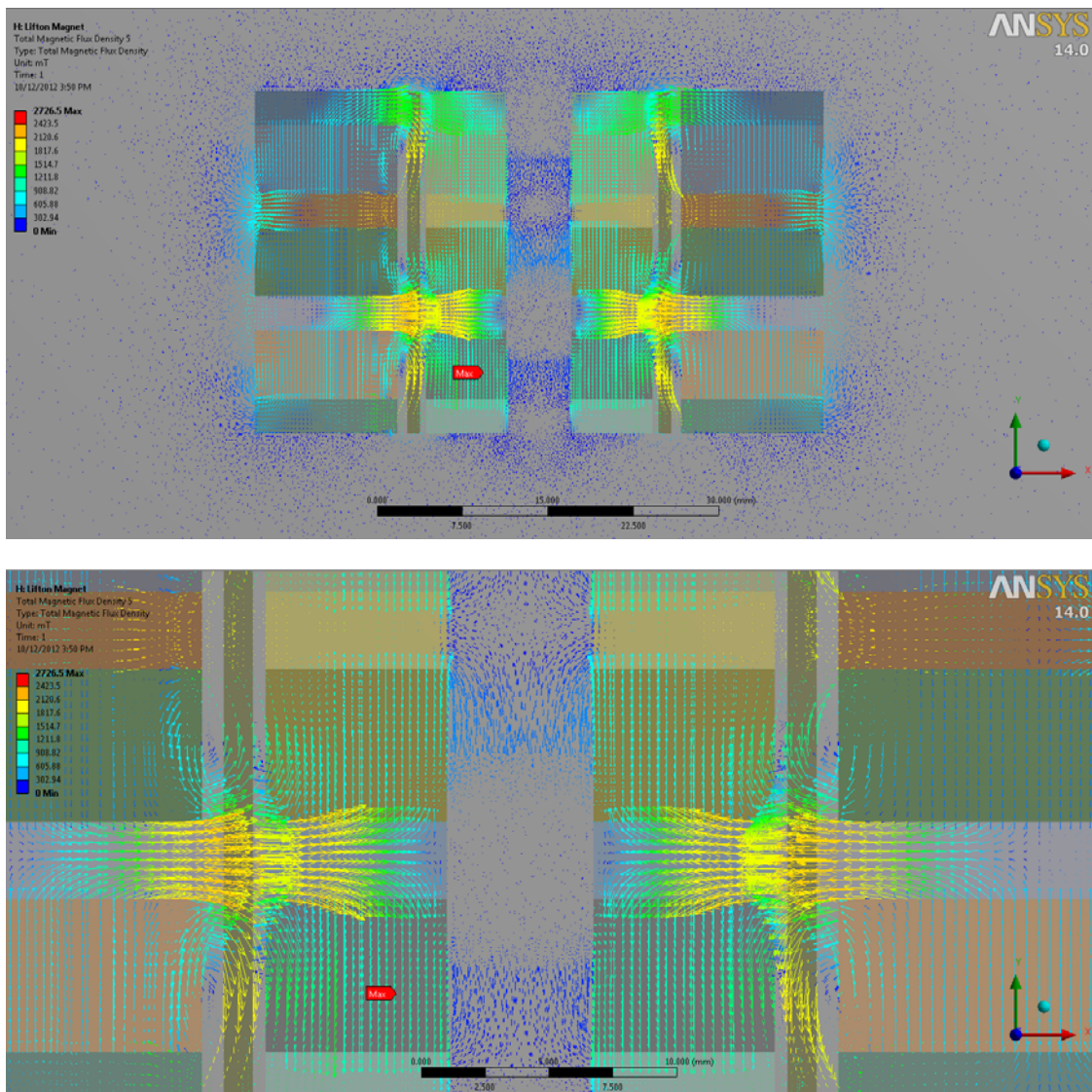


Figure 26: Magnetic Flux Lines (Top) and Zoom in of Analysis (Bottom) for Lifton Magnet

A line plot is also conducted to know the magnetic flux at the region where the copper coils will pass through. Figure 27 shows the maximum for the air region; the maximum intensity might be at the small air gaps between the wire coil housing and the inner magnets. However,

the area of interest is the air gap where the wire will pass through. Therefore, the line plot along the area where the wire coil will move around should be considered and be used for calculation.

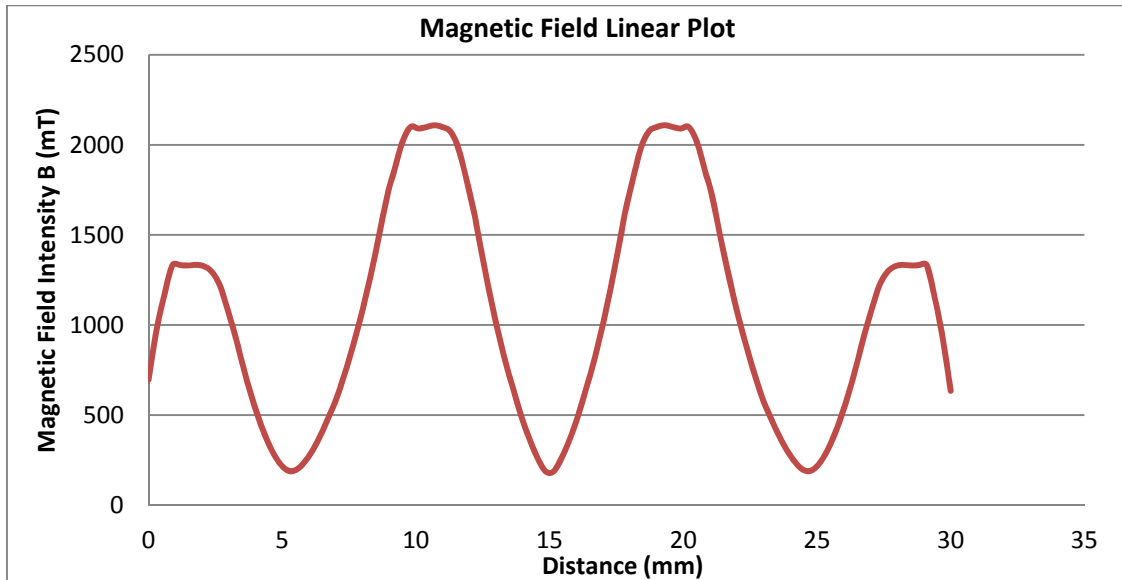


Figure 27: Magnetic Field Intensity Plot for Lifton Magnet

From the line plot in Figure 26, the maximum magnetic field intensity is 2.11 T. The coils will experience the peak magnetic field within 3.175 mm of the maximum magnetic field intensity as it travel pass the spacer. Thus, the average magnetic field intensity will be taken within the region. It is calculated to be 1.97 T within the region.

Lifton magnets have higher magnetic field intensity at a much lower price. However, the supplier at the point of purchase does not have stock for 12 pieces of each ring magnet (1 extra for fabrication fitting). Thus, the only way is to purchase it when the author is in America for the Formula SAE competition and purchase it from Ebay.com to save shipping cost. Due to the purchase of magnets only during the Formula SAE competition, it causes a delay in the fabrication of the electromagnetic damper.

3.2.1.3 Ferrous Spacer Thickness

Ansys Magnetostatic analysis will be used to determine the thickness of the ferrous spacer. As shown in Figure 28, 4 configuration of ferrous spacer thickness will be analysed, from no ferrous spacer to ferrous spacer with the same thickness as the magnet (1 configuration of half

height ferrous spacer is conducted in Chapter 3.2.1.1). The maximum height analysed is a same height as the magnets. Anything thicker is not considered as making the ferrous spacer thicker means having lesser magnets in the whole system.



Figure 28: Various Ferrous Spacer Analysis, No Spacer, Quarter Spacer Height, $\frac{3}{4}$ Spacer Height and Same Magnet Height, Left to Right

Figure 29 shows the plot for the different configuration of ferrous spacer. 1018 steel is used as it is more commonly found steel with ferrous properties. From the plot, the half height spacer has one of the highest magnetic fields induced at its peak at around 1.70 T.

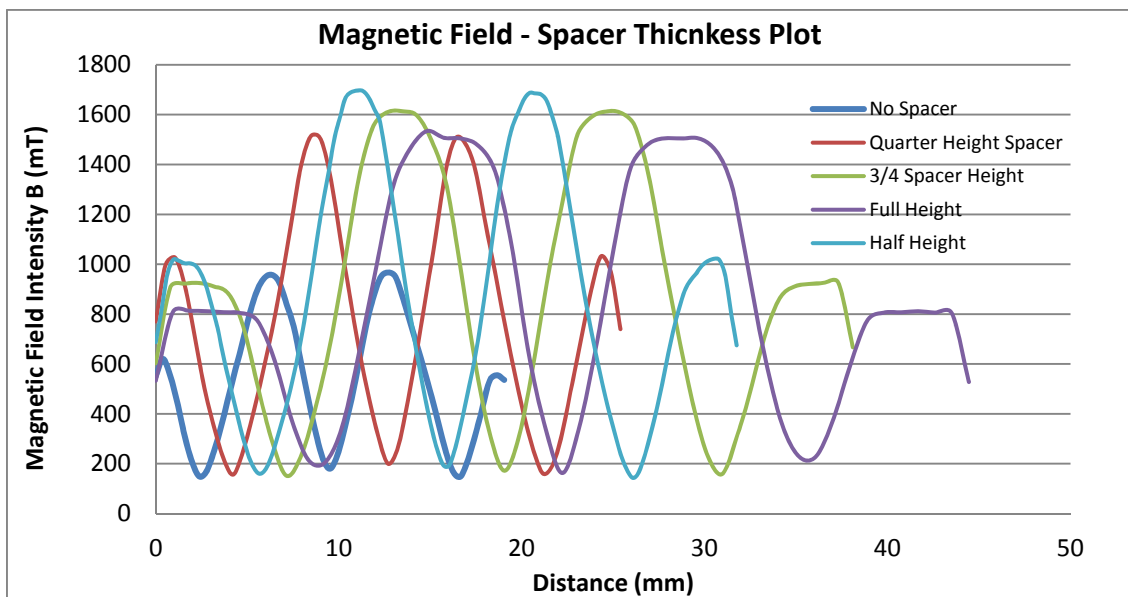


Figure 29: Magnetic Field Intensity Plot of Various Ferrous Spacer Thicknesses

3.2.1.4 Finite Element Method Magnetics (FEMM)

Finite Element Method Magnetics (FEMM) is the software to compute magnetic field intensity in 2D. It is used to compare with the results from Ansys Magnetostatic analysis. Since ring magnet is axis symmetry, it can be computed using 2D analysis on a half model. The computational time is much shorter as compared to Ansys Magnetostatic analysis. It also

accepts .dwg drawing files from Solidworks CAD. Figure 30 shows the setup of the FEMM software. It involves inputting nodes and lines to define the boundary of the materials.

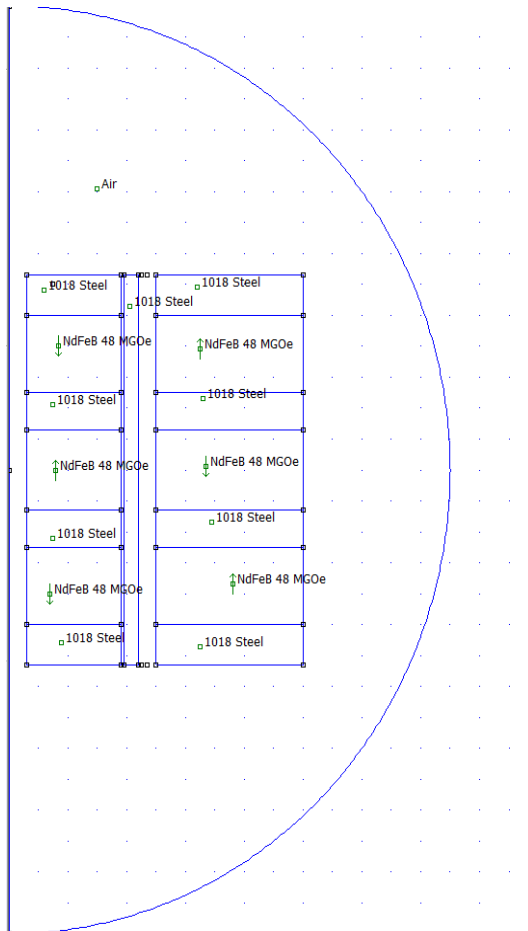


Figure 30: FEMM Setup

Figure 31 shows the magnetic field density plot. Similar to Figure 24, the highest magnetic field is saturated in the region of the ferrous spacer. The highest magnetic field in the region is at 2.35 T, which is pretty close to 2.33 T from Ansys Magnetostatic analysis.

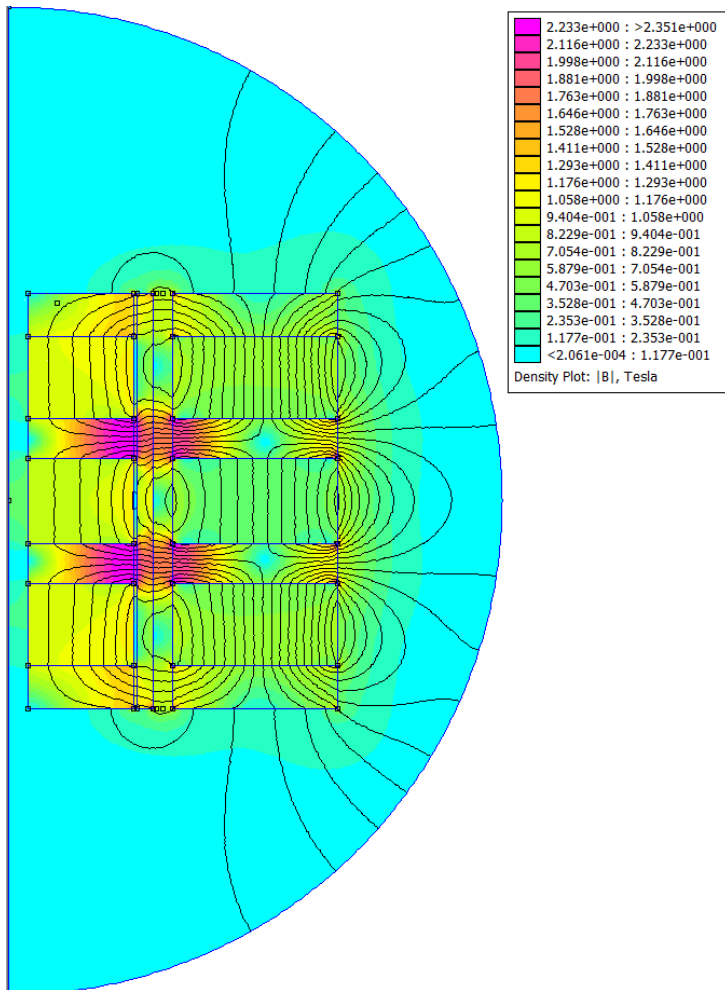


Figure 31: FEMM Plot

Figure 32 is the line plot of the magnetic field at the region similar to the line plot in Figure 25. Through scaled measurement from the plot, the magnetic field is around 1.83 T, which is very close to the magnetic field of 1.70 T from the Ansys Magnetostatic analysis.

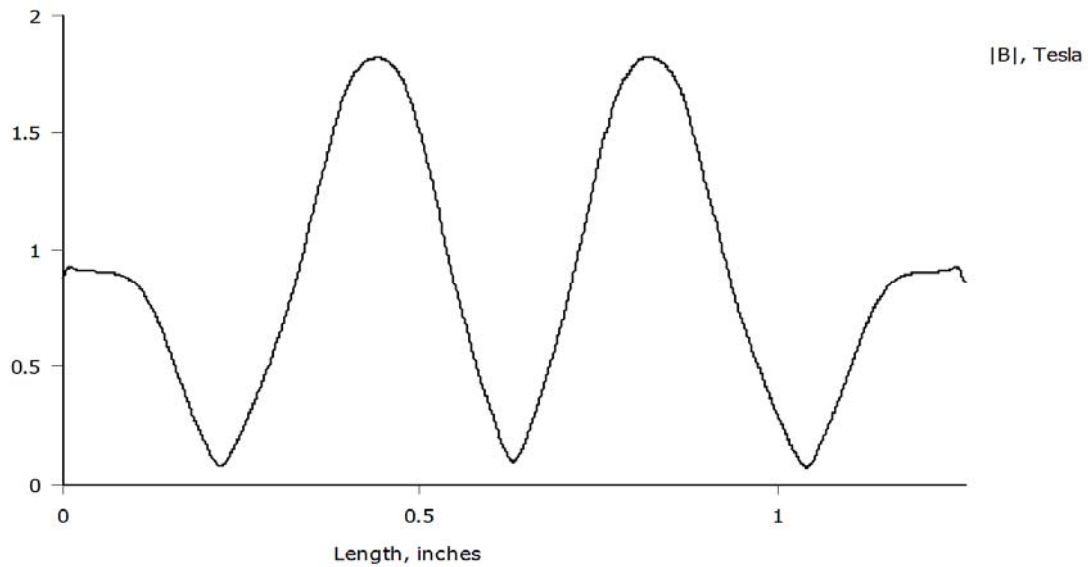


Figure 32: Magnetic Field Intensity Plot Along Wire Coil

Although the FEMM software took a very short time to run the analysis, there are some problems with the software. The conversion from .dwg file does not work very well as the points imported is not at the origin and some parameter inputs are geometry depend. The points can only be moved one by one, which is almost similar to manual input of the points from fresh. In addition, the line plot in Figure 32 does not provide data points, thus average magnetic field around the region cannot be calculated, but can only be estimated from the curve.

3.3 Laminated Copper Wires

Laminated copper wires will be used for the coil windings so that the wire coils will not short out. The wires are to be packed as close as possible so that the magnetic flux is always cutting through the maximum amount of wires. From the formula in chapter 2.2.2.1, the voltage induced is proportional to the length of wire the magnetic field is cutting through it.

The specification of the wire diameter as seen in chapter 2.2.2.1 will determine the gauge of the wires. From the initial calculation conducted in chapter 2.2.2.1, the diameter of the wire is dependent on the current flowing through it as seen from the formula from the same chapter. The calculation uses an AWG 18 wire and was over design from the estimated magnetic field and the diameter of the coil. The diameter of the wires can be further downsized to AWG 22

which has a diameter of 0.65 mm. The maximum current for an AWG 22 wire is 7.0 A. Although it is still overdesign, it is a dimension that is still not too difficult to work with. With a lower diameter, it is more challenging to wrap the wires.

The wire coils require a holder to hold the wires in place to maintain its integrity. A ferrous material can be used to further enhance the magnetic field that cuts through the holder and the wires. Analysis will be conducted in the next chapter to check if the ferrous holder does help to increase the magnetic flux density as it might end up shielding the magnetic field from the inner magnets.

3.3.1 Ansys Magnetostatic Analysis on No Wire Housing

Figure 33 shows the magnetic flux density plot with arrow colour plot in section view. The diagram shows that the magnetic flux are concentrated mostly at the ferrous spacer region and the magnetic field travels straight from the outer spacer to the inner spacer and vice versa. However, the maximum magnetic flux for the plot is lower at 1.90 T as compared to 2.40 T in Figure 24.

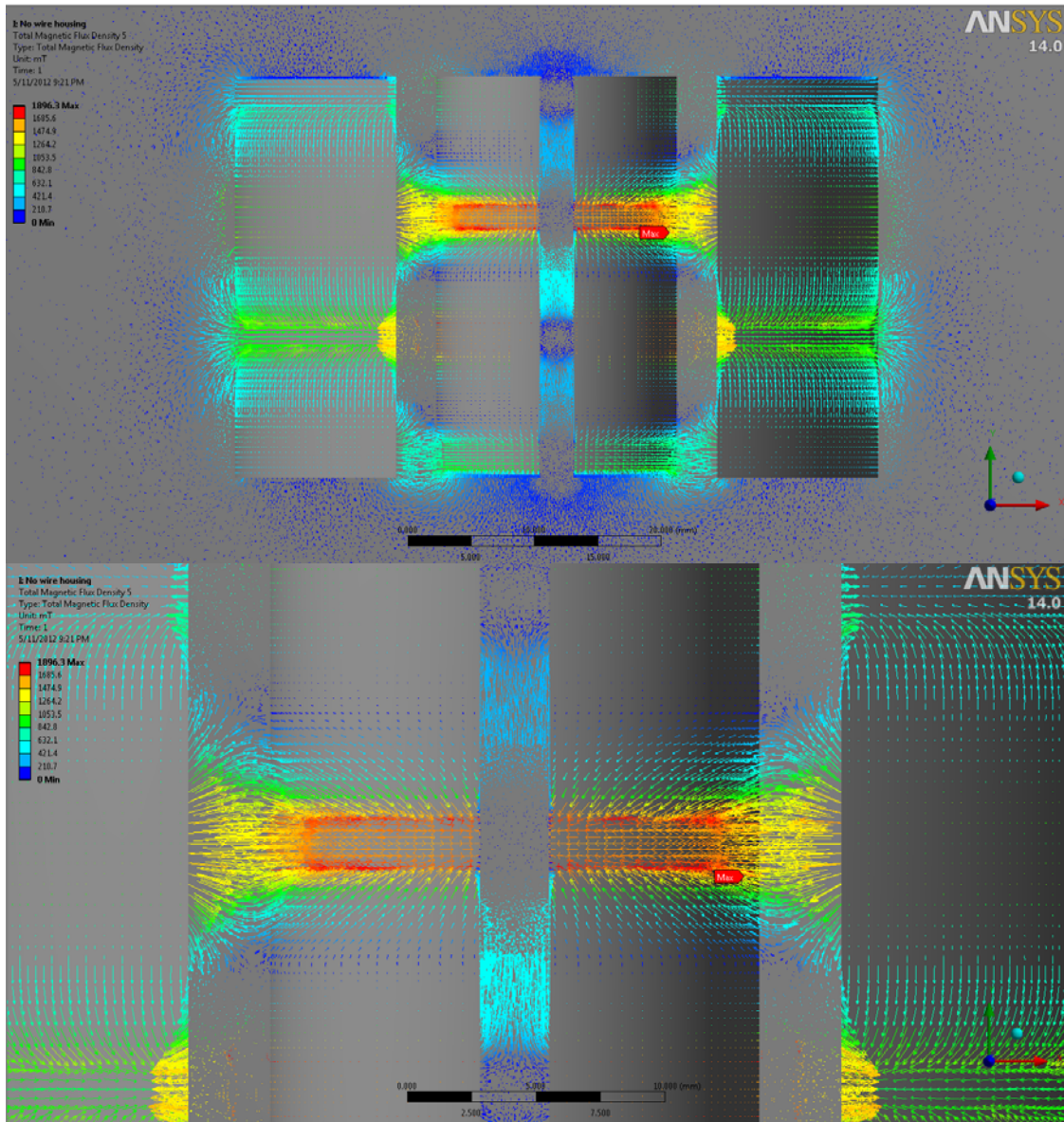


Figure 33: Magnetic Flux Lines (Top) and Zoom in of Analysis (Bottom) for Magnet with no Wire Housing

A line plot is also conducted to know the magnetic flux at the region where the copper coils will pass through. Figure 33 shows the maximum for the air region; the maximum intensity might be at the small air gaps between the wire coil housing and the inner magnets. However, the area of interest is the air gap where the wire will pass through. Therefore, the line plot along the area where the wire coil will move around should be considered and be used for calculation.

From the line plot in Figure 34, the maximum magnetic field intensity is 1.40 T. The coils will experience the peak magnetic field within 3.175 mm of the maximum magnetic field intensity

as it travel pass the spacer. Thus, the average magnetic field intensity will be taken within the region. Appendix 9 shows the tabular form of Figure 34. The average magnetic field intensity is calculated to be 1.32 T within the region, which is lower than with wire coil housing at 1.56 T from Chapter 3.2.1.1.

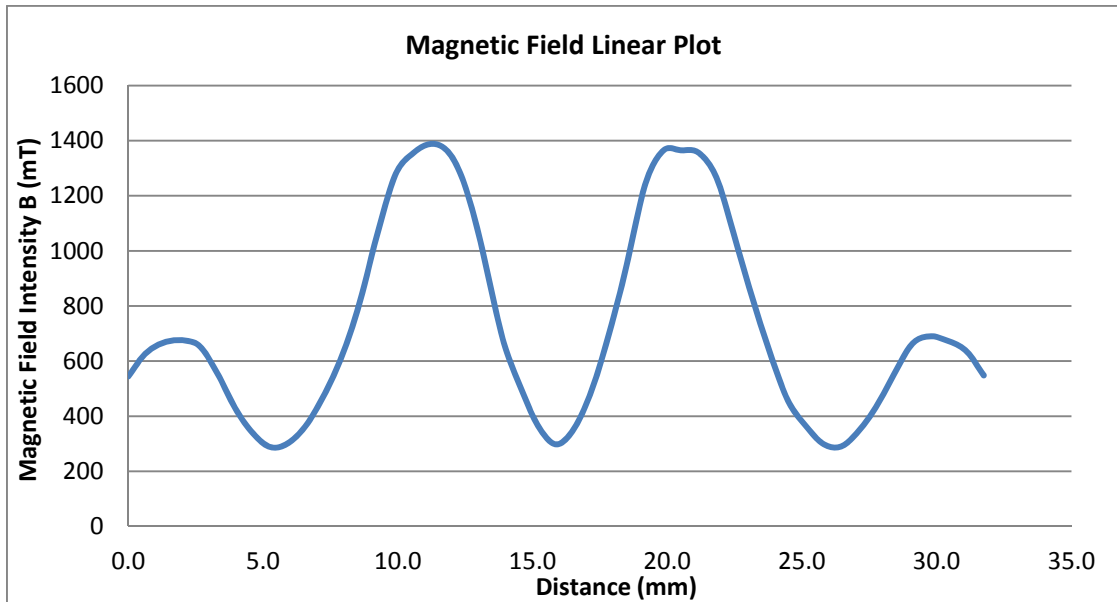


Figure 34: Magnetic Field Intensity Plot for Magnet With No Coil Housing

Through the analysis, it shows that if the wire coil housing is not ferrous, i.e. using aluminium stainless steel or plastic, the magnetic field intensity will be lower. Thus, using 1018 ferrous steel will be used for the wire coil housing.

3.3.2 Wire Coil Orientation

The orientation of the magnets and spacer as seen in Figure 20 shows the magnet like poles facing each other. Figure 35 shows the magnetic field direction due to the orientation. In a normal linear actuator, an in stroke and an out stroke requires a change of direction of the current. In an induced current, it is the same for the direction of the current induced. However, the changing of magnetic field direction among each magnet stack requires the wire to be coiled in a different orientation than just winding it continuously up the wire coil housing.

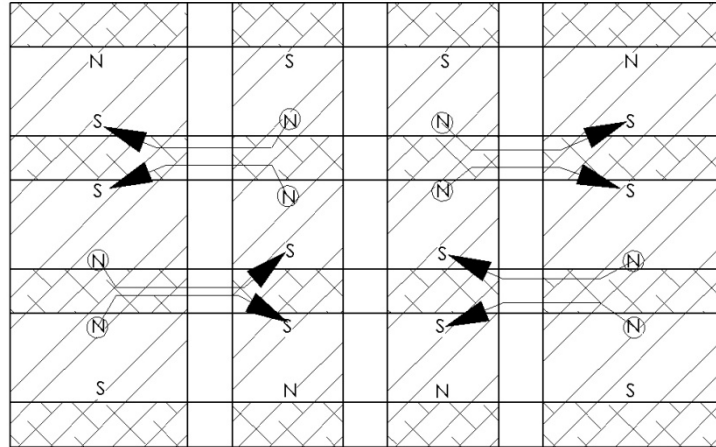


Figure 35: Magnetic Field Direction on 3 magnet spacer layout

The wires can be coiled and have a change in direction for every change in magnetic field. The number of coils for the change is determined by the separation of the center of one spacer to the next. Figure 36 shows the CAD of the wire coils. When the first coil passes through the second spacer, the second coil will pass through the first spacer. The change in direction of the coils will cause the current to be induced in the same direction along the coils and the voltage will be added up in series across all coils that passes the magnetic field. This method of coiling wires will still only allow current to be induced in the same direction for the same stroke; the upstroke and down stroke will still have current induced in different direction.



Figure 36: CAD of Wire Coils Changing Direction

A mini experiment is set up to verify that the voltage will double for the change in direction of the wire coils when magnet has been purchased and the outer casing has been machined. An aluminium rod with enamel wires wound on it will be dropped from a fixed height into the outer ring of magnets. An oscilloscope will be used to measure the peak voltage generated in the coils. The experimental setup is shown in Figure 37.



Figure 37: Simple Experiment on Wire Coil Orientation

3 set of coils are wound on the aluminium rod: One in 10 turns clockwise, one in 20 turns clockwise and the last one is 10 turns clockwise and 10 turns anticlockwise using a single wire shown in Figure 38.



Figure 38: 10 Turns Clockwise (Left), 20 Turns Clockwise (Middle) and 10 Turns Clockwise and 10 Turns Anticlockwise Wire Coils (Right)

Time is taken on a stopwatch to measure the velocity of the coil as it drops down the array of magnets at a fixed drop distance. Table 7 shows the distance, time, velocity and induced

voltage of the enamel wire coil as it drops down the magnet array. The voltage is taken to be the peak voltage of the curve from an oscilloscope.

Type of coils	Time (s)	Distance (m)	Velocity (m/s)	Peak Voltage (V)
10 clockwise coils	50	0.10795	0.00216	0.06
20 clockwise coils	50	0.10795	0.00216	0.06
10 clockwise coils, 10 anticlockwise coils	55	0.10795	0.00196	0.10

Table 7: Coil Drop Velocity and Voltage Induced

From the table, we can see that the induced voltage of the 10 and 20 turn clockwise coils are the same at 0.06V. This is because the magnetic field changes every 9.53mm (ferrous spacer to the next distance). For 20 coils, the total thickness of the coils exceeded 9.53mm and thus the voltage is induced in the opposite direction as the coil passes to the next magnetic field direction while there is still voltage being induced on the current magnetic field direction.

For 10 anticlockwise and 10 clockwise coils, the voltage induced in the first magnetic field will be the same direction as the voltage induced in the opposite magnetic field. Thus, the voltage induced is higher at almost 2 times that induced in the coils.

This experiment is a rough gauge for the change in direction of the coils as there are many other factors that can contribute to the inaccuracy of the experiment for example due to impact of the coils to the magnet as it is being dropped down and the consistency of the drop.

Due to the external diameter of the inner magnet (19.05 mm) and the internal diameter of the outer magnet (25.40 mm), there is only 3.175 mm of space left for the wire coil housing and the wire coils. The wire coil housing is required to have a minimum of 1.0 mm for structural integrity. This left 2.175 mm of gap for the AWG 22 wires where only 2 layers of wire coil can be wound before interfering with the internal diameter of the outer magnet.

3.4 Damper Design

The design of the damper is constrained by a few parameters. Most importantly, it must be able to fit into the original space in the Formula SAE vehicle. It also has to be able to provide

the bump and droop travel as per the original dampers as the linkages for the car are design to be able to perform the travel without interference with other components. Figure 39 shows the CAD of the electromagnetic damper.

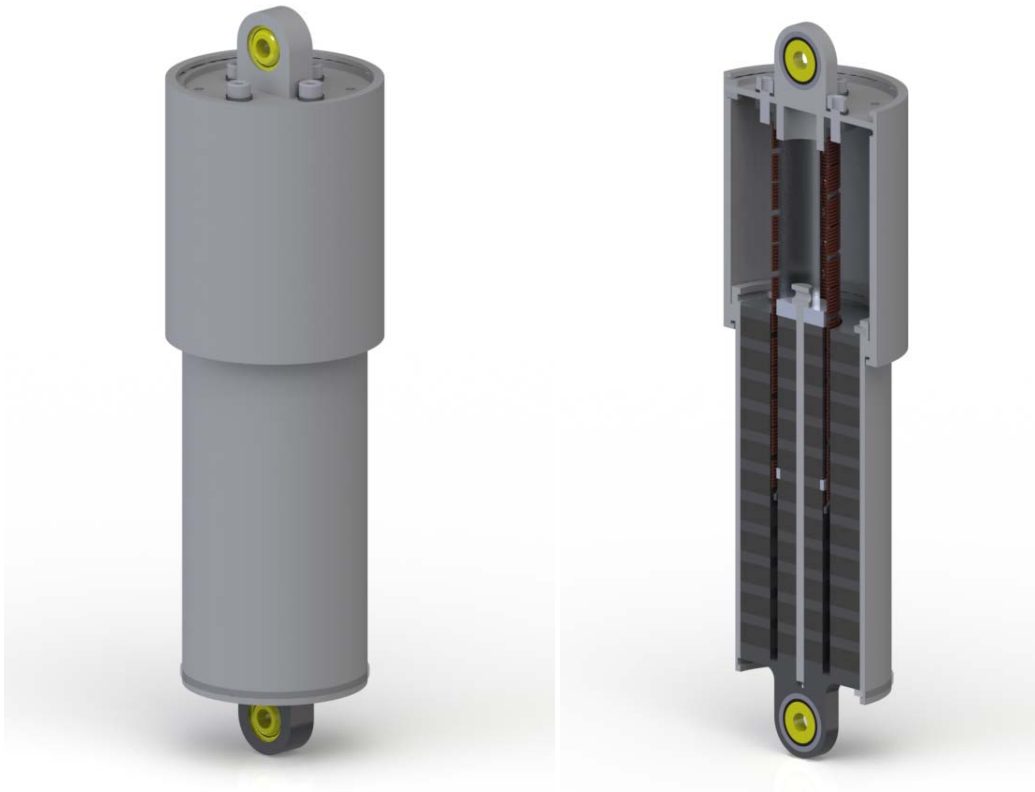


Figure 39: Damper Design (Left) and Sectional View (Right)

Figure 40 shows the section front view of the electromagnetic damper with labels. The component names for the labels are shown in Appendix 10 with pictures of each component for reference. There are a total of 98 components in the electromagnetic damper.

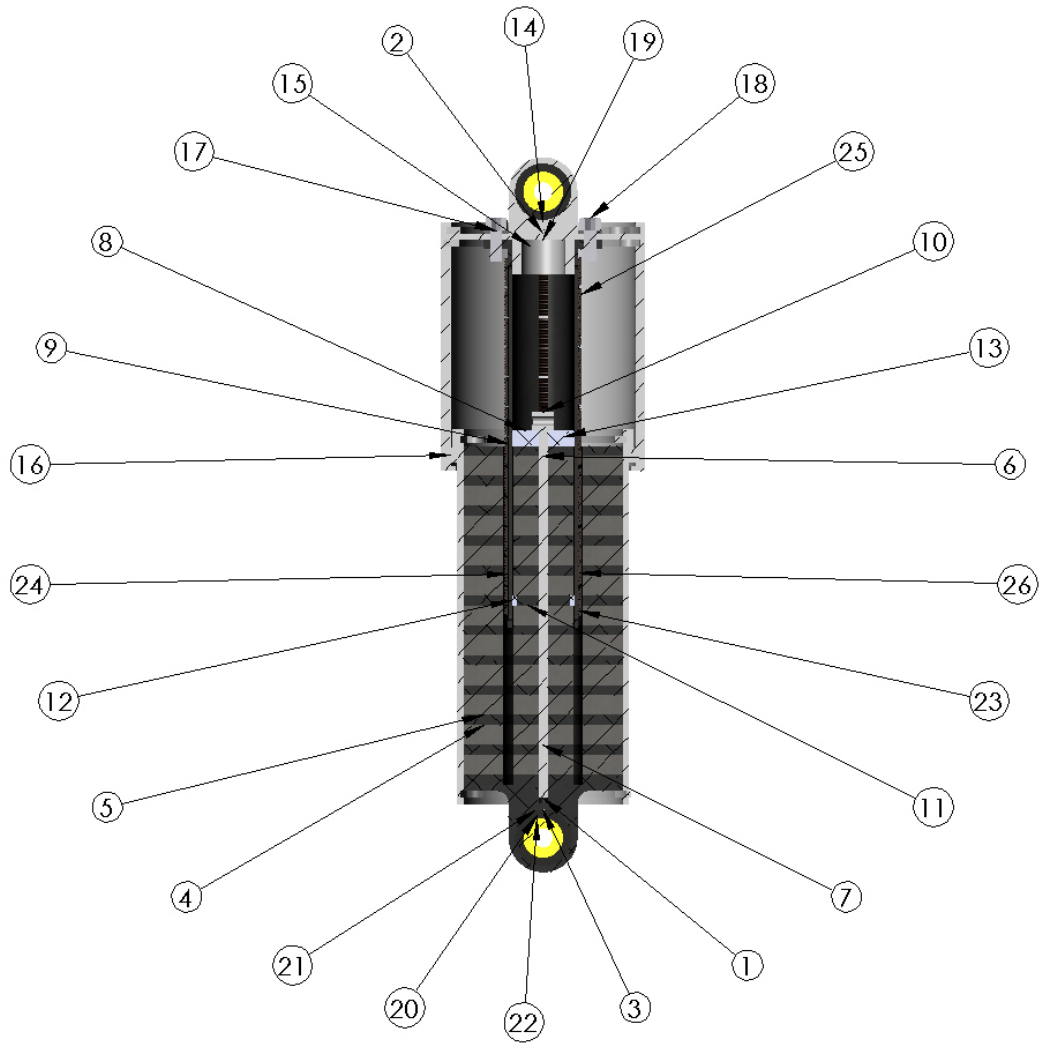


Figure 40: Section View of Electromagnetic Damper

The end of the upper portion in Figure 41 of the damper houses the spherical bearing to enable mounting to the chassis. This upper bearing mount also holds the rebound case and the wire coil housing. The rebound case serves to protect the electromagnetic damper from elements from the environment and also to ensure concentricity with the lower portion of the damper through a nylon outer bushing. The wire coil housing forms the backbone for the wires to be coiled on. It is also a ferrous material to concentrate a higher magnetic field to the wire coils. The wire will exit from one of the holes drilled on the upper bearing mount.

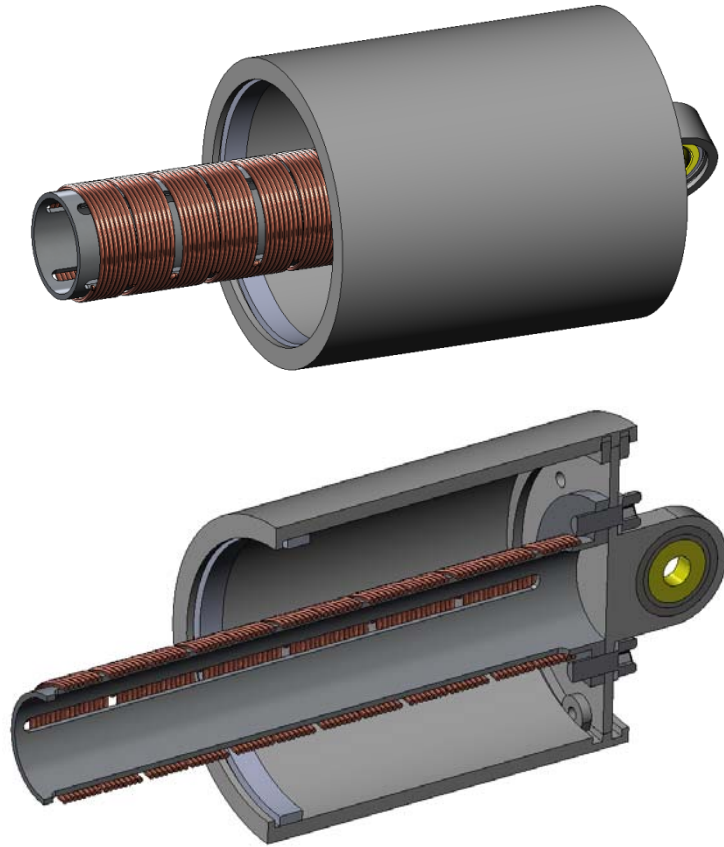
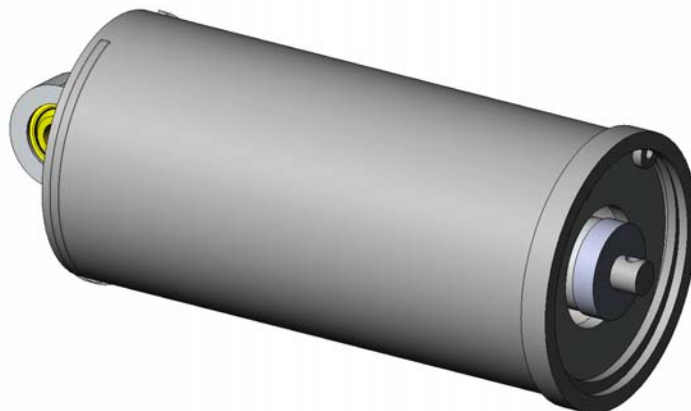


Figure 41: Upper Half of Electromagnetic Damper

The end of the lower portion in Figure 42 of the damper houses a spherical bearing as well to mount to the rocker. The lower bearing mount has a tapped hole in the middle to bolt the inner magnet and spacer cluster through the center magnet bolt. Its end on the opposite side is a nylon inner bushing which serves to keep the wire coil housing from the upper portion of the damper to be in concentric with the inner magnet and spacer cluster



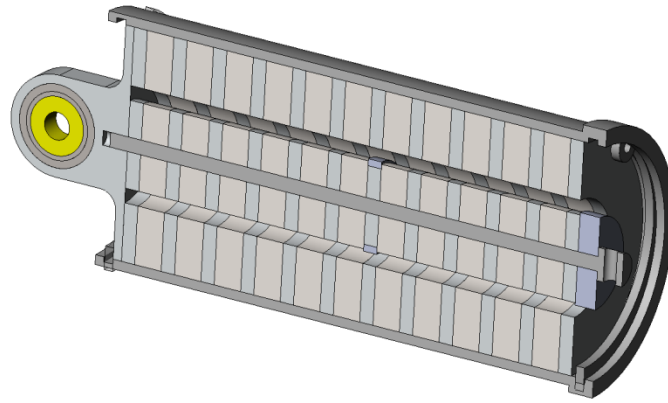


Figure 42: Lower Half of Electromagnetic Damper

The lower bearing mount is attached to the outer casing through a circlip on the bottom. The outer magnet and spacer cluster is inserted through the outer casing and finishes off with another circlip at the end. There is also a central inner bushing in the center of the inner magnet and spacer cluster to help keep the concentricity of the wire coil housing and also as a stopper for maximum bump travel. A nylon outer bushing over the outer casing serves to keep the rebound case in concentricity with the outer case. It is important to keep the magnets and the coils concentric to each other as the spacing between the wire coils and the outer magnets is very small at 0.40 mm and the wire coil housing and inner magnet at 0.50 mm.

3.5 Electromagnetic Damper Power Calculation

The dimensions and number of coils are obtained after designing the electromagnetic damper using CAD. New calculations will be conducted to measure the voltage and current induced from the revised design. Table 8 shows the basic specifications of the electromagnetic damper.

Specifications	Values	Remarks
Fully extended damper length	206 mm	
Fully compressed damper length	156 mm	
Number of Outer Magnet	11	
Number of Outer Spacer	12	
Number of Inner Magnet	11	

Number of Inner Spacer	12	
Number of 1st layer wire coils	180	12 sets of 15 coils each CW and CCW
Number of 2nd layer wire coils	180	12 sets of 15 coils each CW and CCW

Table 8: Electromagnetic Damper Specifications

From the previous chapter 2.2.2.1, a total of 1,637 turns of wire are required to generate 14.4 V for charging a 12 V battery. Since the number of coils for the current design is only 360 coils, it is only 20% and thus a DC-DC step up converter is required to get the voltage up. When 4 electromagnetic dampers are used, it can be wired up in series to add up the usable voltage.

3.5.1 Induced Voltage

The voltage and current induced on the wire coils in an electromagnetic field is proportional to the velocity of the coil. As the velocity of the damper increases, both the voltage and current induced will increase as well.

The voltage induced is calculated by the formula

$$V = Blv$$

The magnetic field intensity is obtained from the analysis conducted in the previous chapter 3.2.1.1. The length of the coils exposed to the magnetic field is obtained from the formula $l = \pi N d_a$. The voltage induced is thus the velocity of the dampers at different time frame of the logged data.

3.5.1.1 Length of Coils

The number of coils changes with the different position of the damper as shown in Figure 43. Calculation will take into account the position of the damper and the number of coils exposed to the magnetic fields.

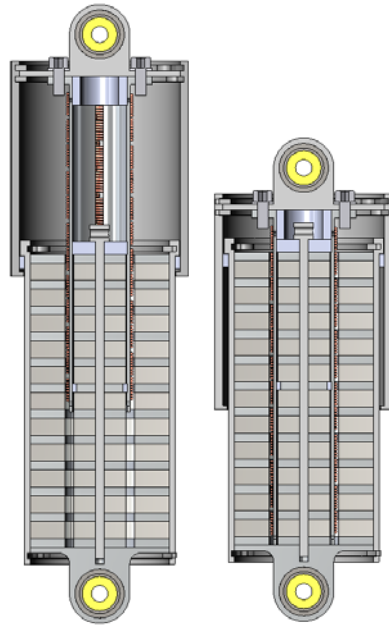


Figure 43: Fully Extended (Left) and Fully Compressed (Right) Damper

The original dampers are design with a full bump length of 156 mm and a full droop length of 206 mm. With the coil windings of 0.6 mm enamel wires, there are 360 coils of wires in the magnetic region of the electromagnetic damper. Within the magnetic region, excluding the first and last spacers, there are 10 spacers where the magnetic field intensity will be the highest. Zooming in for the cross sectional view of the electromagnetic damper as shown in Figure 44, there are around 10 coils exposed to the spacer at any time. Therefore, at full bump, there are 100 coils exposed to the magnetic field. At full droop, there will be only 50 coils exposed to the magnetic field.

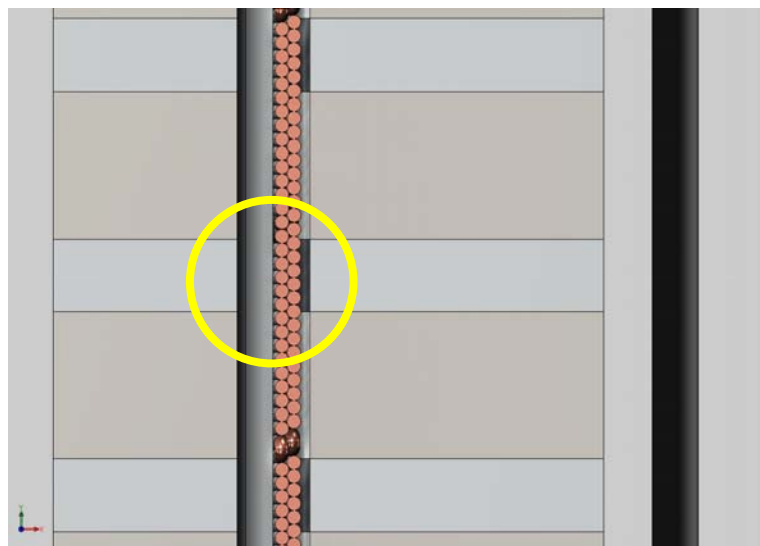


Figure 44: Zoom In View of Wire Coil Interaction with Magnets

An Excel Spreadsheet is used to record the number of coils relative to the position of the damper. It will be used to convert the length of the damper at a particular time to the number of coils exposed to the magnetic field. An assumption is made such that at the start of the logged data, the dampers are all at the neutral position of $181 \text{ mm} \left(\frac{206-156}{2} + 156 \right)$. All other linear potentiometer positions will be referred back to this first position to obtain the length of the damper at the particular time.

3.5.1.2 Average Diameter

The average diameter of the coils around the wire coil housing is obtained from the CAD and can be also calculated. It is the addition of the diameter of wire coil housing with 2 half diameter of the wire coil. The average diameter of the coils around the wire coil housing d_a is 23.48 mm.

3.5.1.3 Voltage Calculation

The values of Table 3 in chapter 2.1.3 will be used as the sample calculation to obtain the voltage induced. At the beginning of the logged data, the damper position from the linear potentiometer is at 48.11 mm. From assumption of the neutral damper length, the linear potentiometer of 48.11 mm is equivalent to the neutral position of 181 mm.

For Position 1, the damper position will give a damper length of:

$$\begin{aligned} \text{Damper Length} &= (44.17 - 48.11) + 181 \\ &= 177.06 \text{ mm} \end{aligned}$$

At 177.06 mm, there will be 80 coils that are exposed to the magnetic field.

The induced open circuit voltage formula $V = Blv$ can be re-written as below and the voltage can be calculated for Position 1:

$$\begin{aligned} V &= Blv \\ &= B\pi N d_a v \end{aligned}$$

$$= 1.56 \times 3.14 \times 80 \times \frac{23.48}{1000} \times 0.00426$$

$$= 0.0392 \text{ V}$$

The induced voltage is very low. It could be due to the low velocity of the dampers from the previous position.

3.5.2 Current

The induced short circuit current is calculated by the formula:

$$I = B\sigma Av$$

The electrical conductivity of copper (σ) is obtained from the website http://www.powerstream.com/Wire_Size.htm From the website, the diameter of the copper laminated wire and the resistance per length is given. The resistivity of the wire can be found by multiplying the area of the wire with the resistance per length. From there, the conductivity can be found by taking the reciprocal of the resistivity and it is found to be $5.78 \times 10^7 \text{ S/m}$.

The induced current for position 1 can be calculated as below:

$$I = B\sigma Av$$

$$= 1.56 \times 5.78 \times 10^7 \times \pi \times \left(\frac{0.6}{2 \times 1000}\right)^2 \times 0.00426$$

$$= 0.109 \text{ A}$$

Similar to the voltage which is dependent on the velocity of the damper, the induced current is low as well.

3.5.3 Power

The power generated can be calculated by using the formula below:

$$P = VI$$

$$= 0.0392 \times 0.109$$

$$= 0.00427 \text{ W}$$

As the power is summed up for the whole Endurance race, the total power for the whole race is 1,720 W. This is only 9.2 % of the calculated damper power of 18,800 W from chapter 2.1.3.

4 Electromagnetic Damper Manufacturing

The electromagnetic damper has very small tolerances for the wire coils to move in the midst of the magnets. It is important to control the tolerance between the manufactured components and the off the shelf components

4.1 Manufacturing

The manufacturing of the components are outsourced to machining shops with tolerances given in the technical drawings. Off the shelf components like the magnets are given to the machining shops to enable them to test fit to the machined components

4.2 Assembly

The assembly of the electromagnetic damper requires the manoeuvre of strong N48 magnets with same poles facing each other. The risk of handling such magnets are high as the magnets can easily snap to the other magnets of different poles. Fingers can get injured quite badly when such situation happens. The magnets can also crack when encountering such impact. As most tool are made of steel, they are also easily attracted to the magnets. Therefore it is very important to handle one magnet at a time and keep the rest of the other magnets isolated.

4.2.1 Magnet Assembly

Figure 45 shows the outer magnets from the supplier. It is split using nylon spacers and packed in thick bubble wraps. In order to take out the magnets, a large force is required using fingers to pull it out from the other magnets. To prevent the stack from breaking up or the extracted magnet from flipping around and attracting back to the magnet stack, a nylon rod is inserted in the middle.

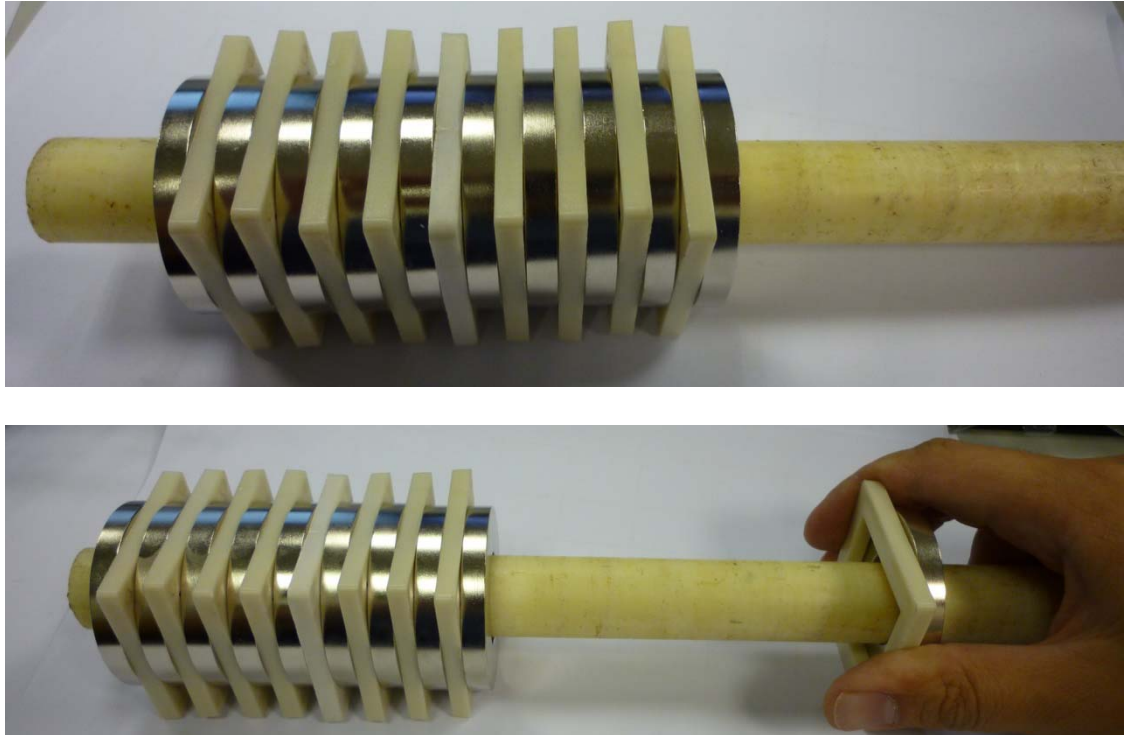


Figure 45: Magnet Stacks (Top) and Method of Extracting Magnets (Bottom)

The next challenge involves in the attraction of the magnets to the ferrous spacers. A magnet have to be attracted to a spacer before inserting into the outer case. If every alternating magnets and spacers are inserted separately, the magnet or the spacer will snap to the spacer or magnet halfway in the outer case. It is impossible to use any tools to control the action when it is in the outer case as the space within is small. It is also almost impossible to use fingers to assemble them together as bringing them to close together will cause the magnet to snap to the spacer with the risk of cracking the magnet or tearing the skin of the fingers if it is trapped between the magnet and the spacer.

A wedge made of wood in Figure 46 is used to slowly ease the magnet to the spacer through an aluminium rod inserted in the middle. The aluminium rod is used to make sure the magnet and the spacer is attracted in concentric to each other. Figure 47 shows the process of attracting the magnet to the spacer. The figure on the right shows the initial phase where the thicker part of the wedge is used to separate the magnet and the spacer. It is then slowly slide out towards the tip to allow the magnet to get closer to the spacer until the wedge is out of the magnet and spacer. As the gap is already very small, the impact when both are attracted is much lesser.



Figure 46: Wedge Made of Wood to Ease the Magnet to the Spacer

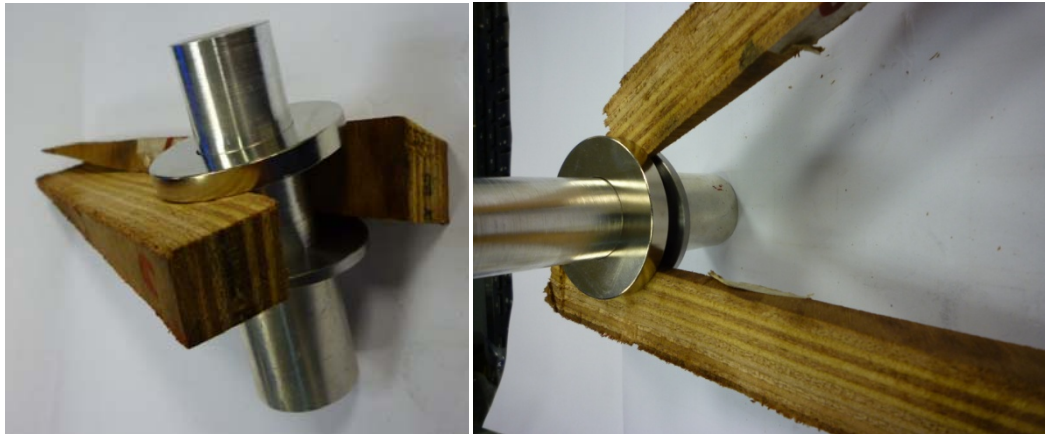


Figure 47: Using the Wedge to Ease the Magnet to the Spacer

Each set of magnet and spacer has to be attracted in the right orientation and the poles of the magnets have to be opposite to each other. The outer casing is machined to be slide fit with the magnet and spacer. When the magnet-spacer is inserted into the outer casing, there is no risk of the magnet-spacer snapping to the other set inside the outer casing as the poles are repelling each other. As the magnets are not manufactured with a good tolerance due to the protective coating outside the magnet, slight press fit is required to push the magnet-spacer down the outer casing. A bench drill as shown in Figure 48 is used to press it in as the base and the head is square and the force required to press the magnet-spacer is not very high. In fact, the slight press fit is beneficial to keep the magnet-spacer in place after pressing it in even though the magnet-spacer below it is repelling it upwards. When the magnet-spacer fully fills the outer casing, a circlip is used to lock the magnets in place.



Figure 48: Bench Drill Used to Press the Magnet-Spacer into the Outer Casing

For the inner magnets and spacer, it is slightly easier to attract the magnet to the spacer as the magnet is smaller and thus the magnetic force is lower. The center magnet bolt helps to hold the magnet-spacer in concentricity and there is less risk in the magnet and spacer flipping and attracting to the magnet-spacer that is already in the center magnet bolt during insertion. It is also externally inserted and thus there is a lot of working space as shown in Figure 49.



Figure 49: Inner Magnet Assembly with Lower Bearing Mount

The final assembly of the inner magnet to the outer magnet proves to be the most challenging. This is because there is a point where there will be opposite poles as the inner magnet assembly is inserted into the outer magnet assembly. As more magnets are inserted, there are

more points with opposite poles and the force required to push the 2 assemblies become higher. A lathe is used to keep the outer magnet and the inner magnet in concentricity through using the tailstock to push the 2 assemblies together.

4.2.2 Wire Coils

AWG 18 wires will be coiled around the wire coil housing. Cyanoacrylate (CA) glue will be used to hold the wire in place. CA glue is important as the wire have to do a turn to convert from clock wise turn to anti clockwise turns. It is not possible to change direction while still keeping the wires tight. The wires are required to be wound tight so as to prevent interference with the other components. Figure 50 shows the complete assembly, with only one layer of wire coils for testing first. It is wrapped with fiber tape to check if there is any interference with the outer magnets.



Figure 50: AWG 18 Wire Coil on Wire Coil Housing

The assembly of the wire coil assembly and the magnet assembly again proves to be challenging. The ferrous wire coil housing keeps on being attracted to the magnets and it can caused the wires to be scrapped during insertion. The inner bushing is the only bushing that helps to hold the wire coil assembly in place for half a depth before the wire coil housing reaches the inner bushing central. Both the bushing have outer diameter that is slide fit with the inner diameter of the wire coil housing.

Figure 51 shows the electromagnetic damper fully assembled and ready for testing. The COM-M6T is a spherical bearing on both ends of the damper to enable mounting to the Formula SAE race car or any testing equipments.



Figure 51: Electromagnetic Damper Fully Assembled

5 Testing Method

Testing of the electromagnetic damper will be conducted on a damper dynamometer coupled with a Cathode Ray Oscilloscope (CRO) as shown in Figure 52. The damper dynamometer will be used to produce the bump and rebound that a damper will go through and the CRO will be used to measure the peak voltage that the electromagnetic damper produces.



Figure 52: Damper Dynamometer (Left) and Cathode Ray Oscilloscope (Right)

5.1 Damper Dynamometer

The damper dynamometer has an adjustable stroke from 10 mm to 200 mm in steps of 10 mm. The load cell is capable of recording load data up to 700 kg, which is sufficient for most automotive dampers. The stroke speed can be up to 500 mm/s.

There is a display showing the RPM of the system on the damper dynamometer itself. It is also linked to a computer through serial cable to output the force-velocity graph. Unfortunately, the link to the computer is not working at the point of testing and thus the testing will be conducted through sweeping through a range of damper velocity and finding the voltage and

current induced. Using the data, it will be fed back to the Endurance race and compute the total power generated.

From Figure 14 in Chapter 2.2.2.1, the damper stroke has a peak of 31 mm. However, the frequency of occurrence starts to get very low from 22.5 mm onwards. In view of this, the damper stroke for the damper dynamometer will be 20 mm as the adjustments are fixed. From Figure 12 in Chapter 2.2.2.1, the more frequently peak velocity of the damper is 0.068 m/s. Since the velocity of the damper dynamometer can be adjusted till 0.5 m/s, the velocity sweep can have a maximum of up till 0.068 m/s. At 0.068 m/s, the RPM of the damper dynamometer with a stroke of 20 mm is calculated as below

$$\begin{aligned}
 RPM &= \frac{v}{\pi d} \times 60 \\
 &= \frac{0.068}{\pi \times 0.02} \times 60 \\
 &= 64.9
 \end{aligned}$$

The velocity sweep for the electromagnetic damper through using RPM control from the damper dynamometer will thus be from 10RPM to 70 RPM so that a better curve can be plotted to compute the power generation for the Endurance race data

5.2 Current Direction

As mentioned in Chapter 3.3.2, the current induced will be alternating in an up and down stroke. A full bridge rectifier will be implemented in the circuit to allow the alternating current to be converted to a direct current. Figure 53 shows the schematics for a full bridge rectifier.

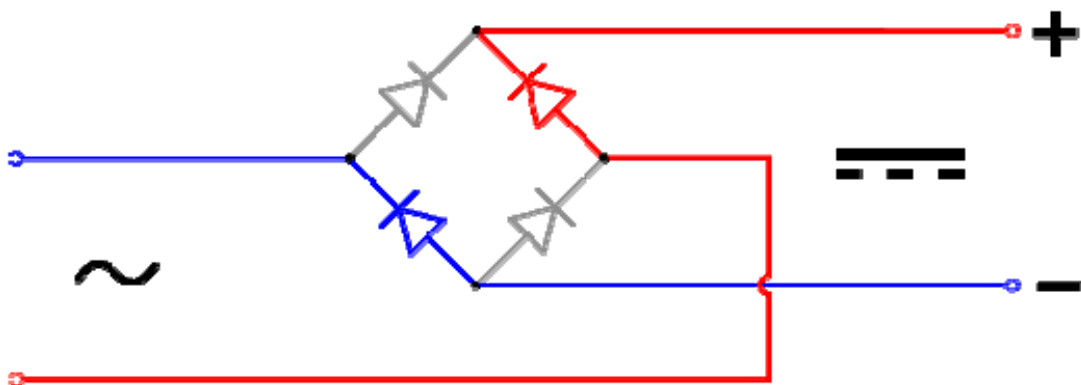


Figure 53: Schematics for a Full Bridge Rectifier

The rectifier diode has a model number of N4004. It can allow up to RMS voltage of 280 V with a rectified current of 1 A with 30 A surge. The datasheet for N4004 is attached in Appendix 11. Figure 54 shows the final product of the full bridge rectifier.

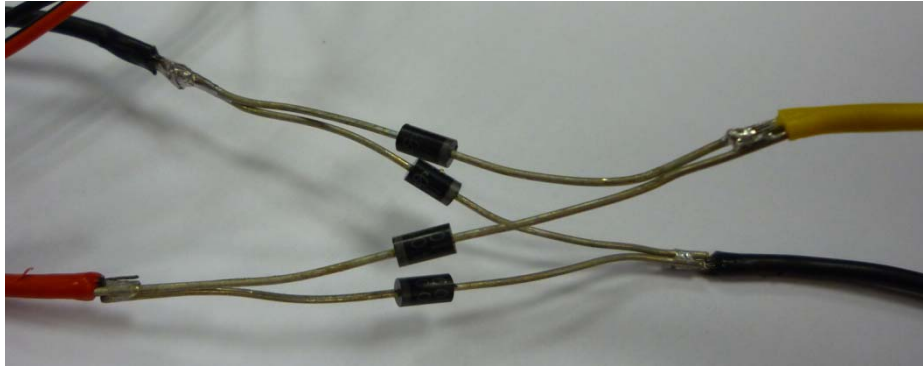


Figure 54: Full Bridge Rectifier

However, the bridge rectifier consumes 0.7 V as the voltage is passed through it. If the voltage generated is lower than 0.7 V, then there are chances that there will be no voltage logged especially at low RPM. The decision on using the bridge rectifier will be decided during the test. If the bridge rectifier is not used, then the Root Mean Square (RMS) of the peak voltage and current will be taken.

5.3 Data Logging

Data logging is done using the Race- Technology DL1 data logger shown in Figure 55. The data logger has a 100Hz update frequency which is suitable to capture the current induced from the electromagnetic damper from the inputs of the damper dynamometer. At a maximum rotation of 70 RPM, or 1.2 Hz, DL1 is still able to log proper data.



Figure 55: Race Technology DL1 Data Logger

The DL1 data logger requires an input of 12 V for power and stores data into a Compact Flash (CF) card. It can read voltage directly from any of its 8 analogue inputs and it also has an RS232 input to link up to its Dash 1 software. For current induced, a current sensor has to be used.

For the current sensor, a current transducer LTS 25-NP from LEM will be used. Figure 56 shows the current transducer and it being wired up. The current transducer has a measurement range of 25 A. It has an analogue voltage range of 2.500 V to 3.125 V. A formula from Appendix 12 will be used to calculate the current from the logged voltage.

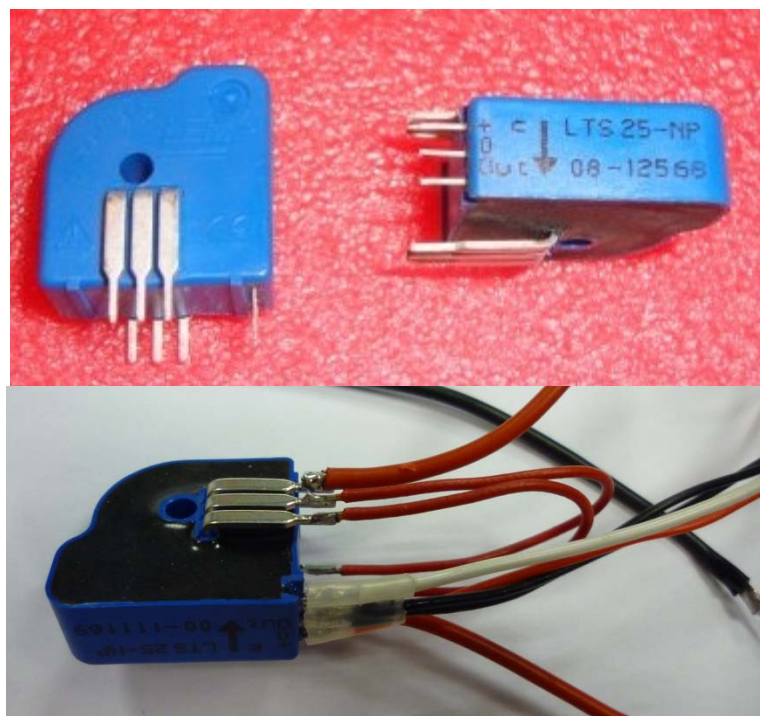


Figure 56: LTS 25-NP Current Transducer (Top) and Current Transducer Being Wired Up (Bottom)

Figure 57 shows the full bridge rectifier, current transducer being output to DL1 data logger. A CRO can be used to monitor the voltage produced in real time. The output from the electromagnetic damper is first connected to the full bridge rectifier, then the positive line goes to the current transducer. A load resistor is connected across the positive and negative terminal after the current transducer and the positive and negative terminals goes to the data logger to measure the voltage. The current transducer has wires that goes to the data logger as well and is drawing power from the data logger.

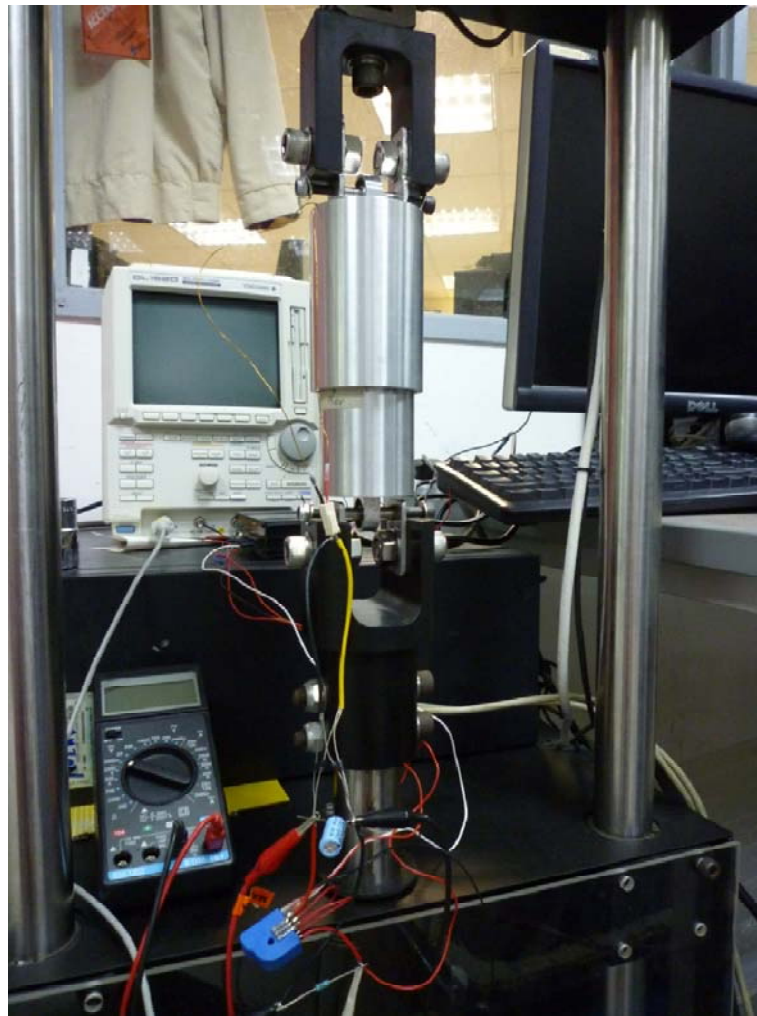


Figure 57: Electromagnetic Damper and Measuring Equipments Setup in Damper Dynamometer

For the first test, a 15 coil setup will be coiled on the wire coil housing to make sure that there are no interference between the components and the wires and there is proper output voltage and current.

5.4 Problems Encountered

For the initial test, the CRO shows some output as shown in Figure 58 below. However, the output becomes zero after a few more runs. There is no logged data at that point as it is an initial testing phase to check the output from the CRO.

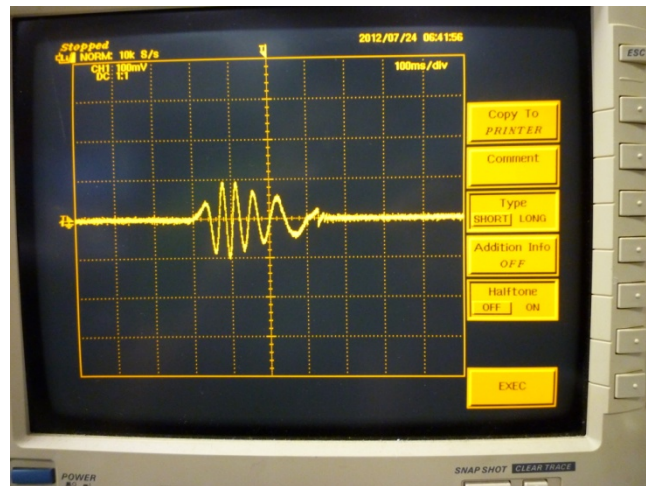


Figure 58: CRO Output

Upon opening up of the electromagnetic damper, the enamel wires are scrapped and there is shorting among the wires. Due to this, the current cannot be induced in the coils. Figure 59 shows the damage of the enamel wires. The masking tape used to tape the upper portion of the wire coil housing is also badly scrapped. Upon closer inspection, the cause of the problem being the lower bearing mount and the center magnet bolt not square causing the whole row of inner magnet to be slanted. This caused the wire coil housing to be pushed to one side and the enamel wires to be in contact with the internal diameter of the outer magnet.



Figure 59: Enamel Wires Being Scrapped (Top), Zoom In of the Damage (Bottom)

Taking apart the center magnet bolt from the lower bearing mount, it can be seen that the center magnet bolt is not perfectly straight and the tapped hole on the lower bearing mount is not straight as well. Figure 60 shows the location of the M3 tapped hole in the lower bearing mount. A straight M3 bolt is also bolted in and the effect of the slanted hole is clearly shown.



Figure 60: Lower Bearing Mount (Left) with Arrow Showing Tapped Hole Location, Bolt Inserted into Lower Bearing Mount Badly Slanted

Although the tapped hole and the center magnet bolt is slanted, there is no sign of the inner magnet not concentric with the outer magnet during assembly. The center magnet bolt could have been dented and damage the tapped hole on the lower bearing mount while the electromagnetic damper is in operation. The thread might also have stripped in the process. Due to this, the electromagnetic damper have to be re-designed to make sure that the upper portion of the damper is in concentricity with the lower portion of the damper.

6 Design Change and Improvement

The main objective of the design change is to ensure that the upper portion of the electromagnetic damper is in concentricity with the lower portion during motion. There will be a total of 4 design changes to the electromagnetic damper as shown in Figure 61.

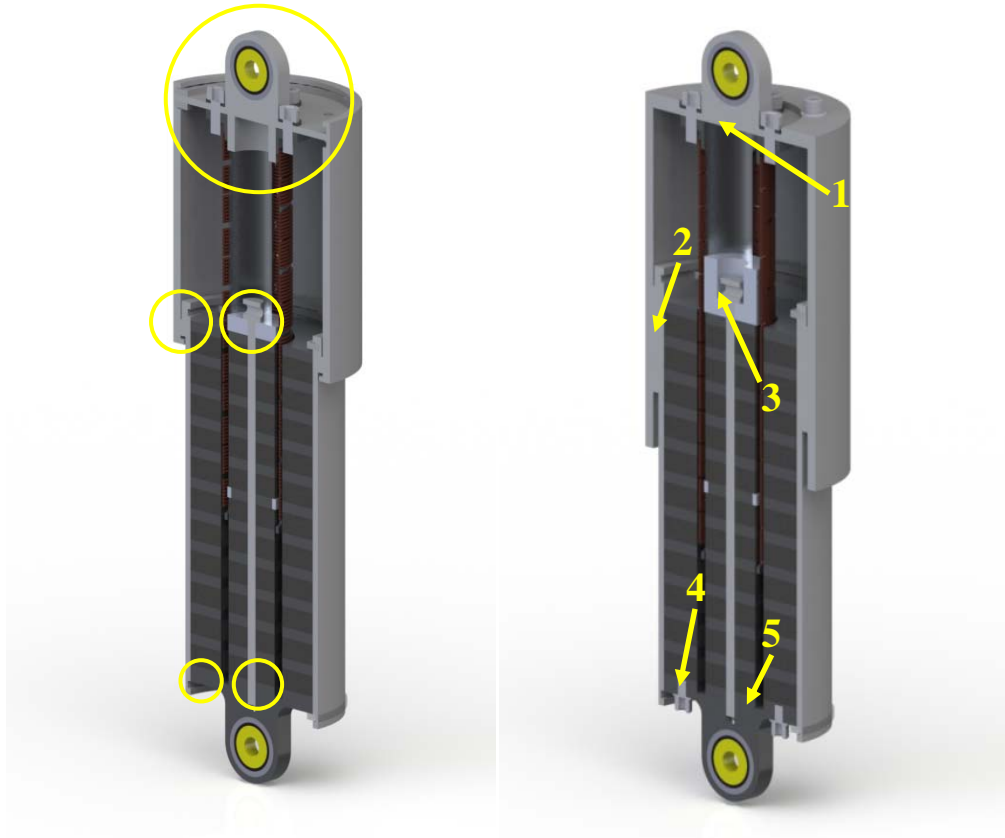


Figure 61: Design Change for Electromagnetic Damper

The 4 design changes are shown in Table 9:

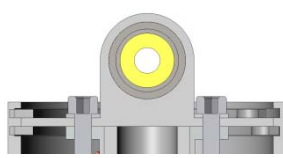
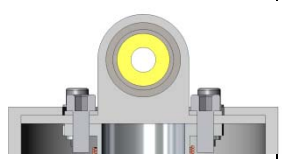
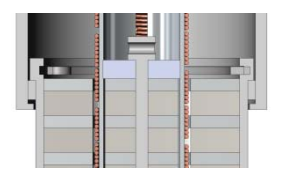
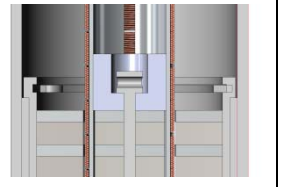
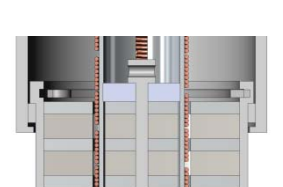
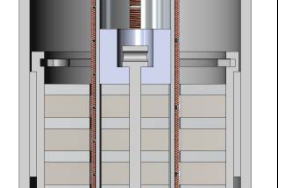

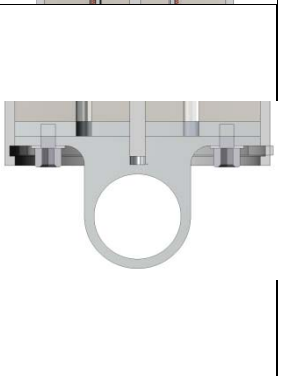
No	Part	Function	Design Change	Design 1 Illustration	Design 2 Illustration
1	Upper Bearing Mount	Ensure wire coil housing is center and concentric	From circlip to one piece and bolted		
2	Inner Bushing	Ensure wire coil housing is concentric to inner magnet	Longer bushing		
3	Outer Bushing	Ensure top part of damper is concentric with lower part of damper	Longer Bushing		
4	Lower Bearing Mount	Ensure lower bearing mount, outer casing and outer magnet is concentric with inner magnet	Lower bearing mount bolted to outer spacer		
5	Lower Bearing Mount	Ensure inner magnet array is perpendicular to lower bearing mount	Epoxy spacer to lower bearing mount	NIL	NIL

Table 9: Design change table

For changes 2 and 3, the main purpose is to lengthen the bushing that keeps the upper portion of the damper, the lower portion of the damper and the wire coil housing concentric to each other. For changes 1, 4 and 5, the purpose is to make sure the sub assembly of the wire coil housing to the upper portion of the damper and the magnets to the lower portion of the damper is true and concentric to each other.

Figure 62 shows the section view of the 2nd iteration of the electromagnetic damper design. Appendix 13 lists the bill of materials for the electromagnetic damper. In total, there are 6 components to be replaced.

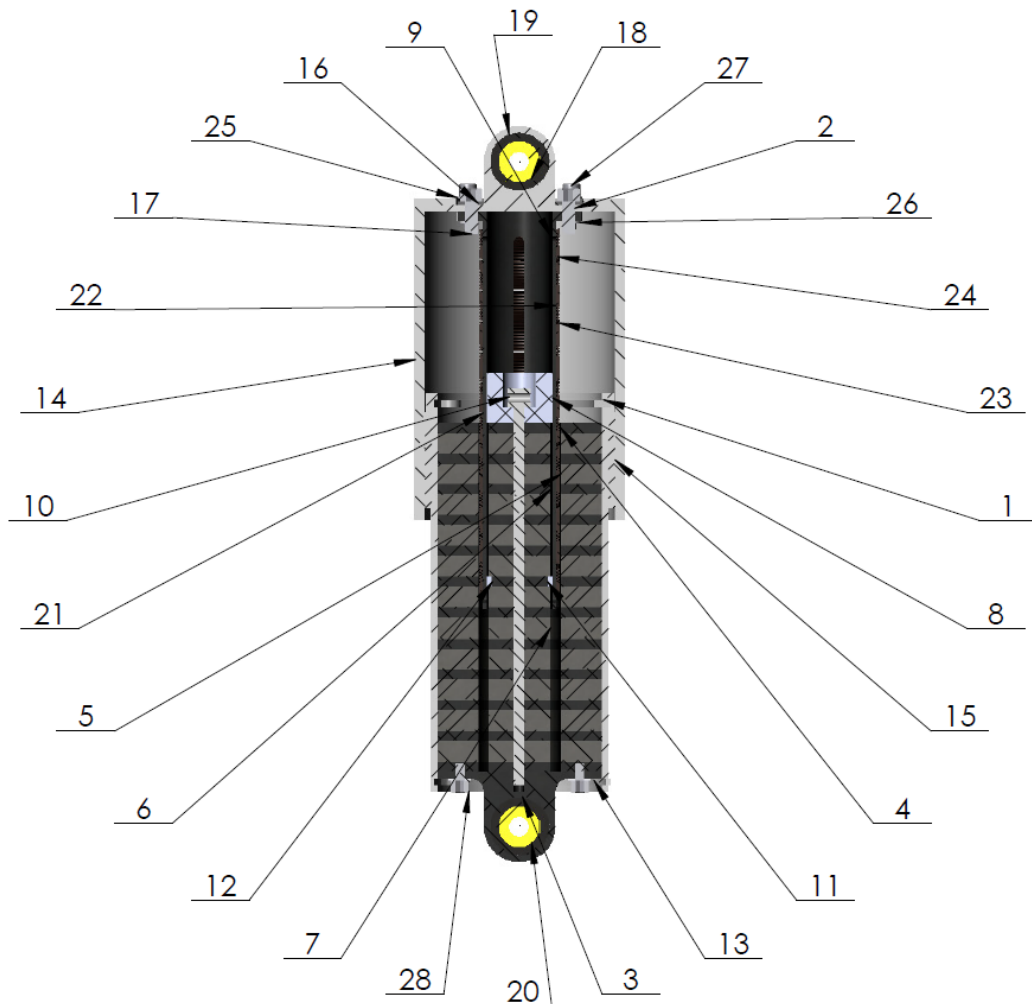


Figure 62: Section View of Electromagnetic Damper 2nd Design

6.1 Design Change (Without Inner Magnet)

The newly machined components that came back shows similar problems after assembly and going through a damper dynamometer run. The conclusion of the damage could be due to the size of the thread (M3) being too small and the tolerance of the magnet internal diameter, the center magnet bolt outer diameter and the location of the tap hole in the lower bearing mount. Due to the shortage of time and funds, it is decided to do away with the center magnet and the voltage and current induced will be checked with the calculated data to find the difference between calculated and test data.

6.2 Ansys Magnetostatic Analysis

Analysis Magnetostatic analysis is once again conducted to obtain magnetic field intensity of the new design without the inner magnets. Figure 63 shows the magnetic flux density plot with arrow colour plot in section view. The diagram shows that the magnetic flux is concentrated mostly at the ferrous spacer region. Right after the wire coil housing, it is almost shielded to no magnetic field. The maximum magnetic flux for the plot is the highest at 3.70 T.

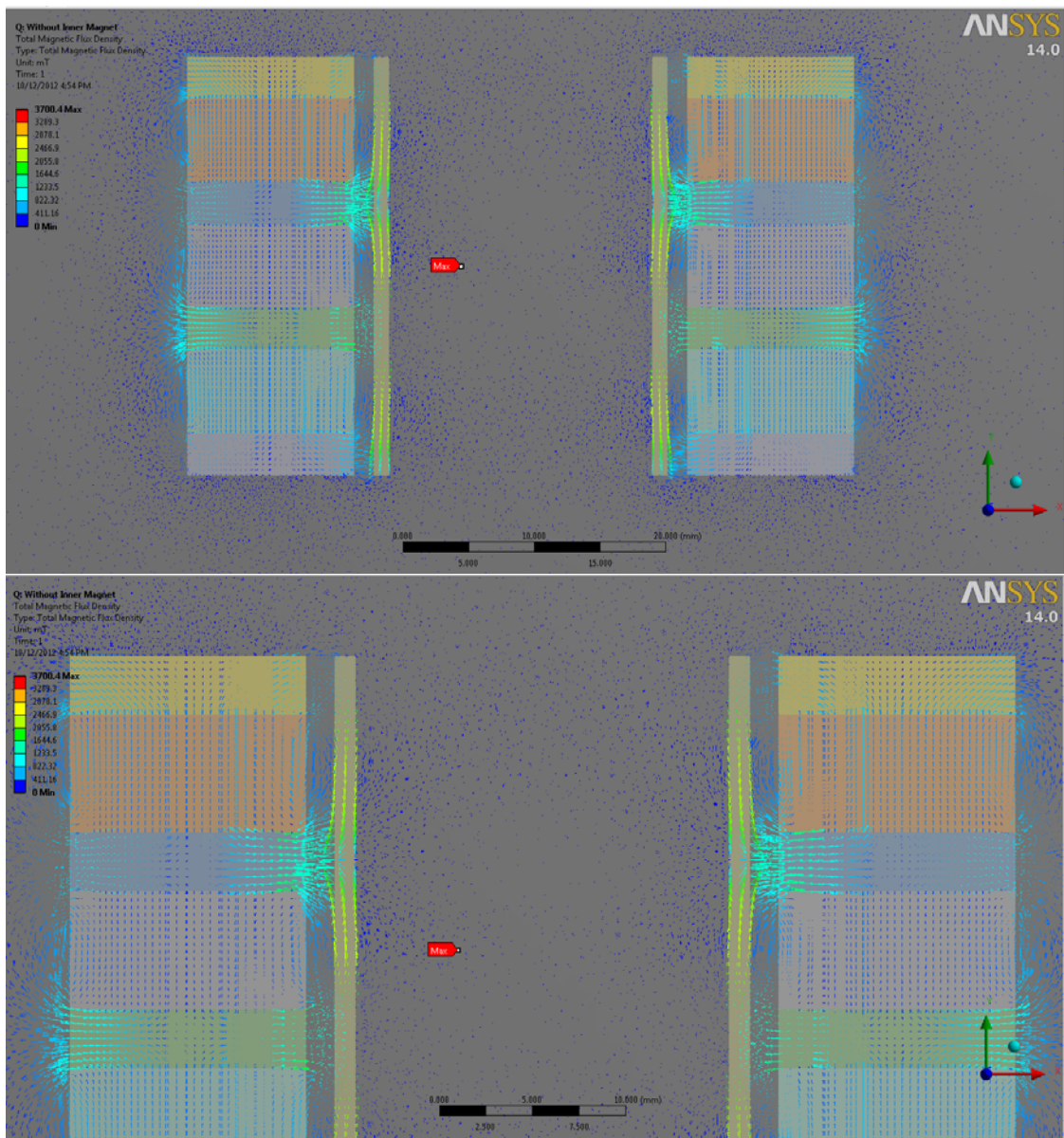


Figure 63: Magnetic Flux Lines (Top) and Zoom in of Analysis (Bottom) for No Inner Magnet

A line plot is also conducted to know the magnetic flux at the region where the copper coils will pass through. Figure 63 shows the maximum for the air region; the maximum intensity

might be at the small air gaps between the wire coil housing and the inner magnets. However, the area of interest is the air gap where the wire will pass through. Therefore, the line plot along the area where the wire coil will move around should be considered and be used for calculation.

From the line plot in Figure 64, the maximum magnetic field intensity is 1.26 T. The coils will experience the peak magnetic field within 3.175 mm of the maximum magnetic field intensity as it travel pass the spacer. Thus, the average magnetic field intensity will be taken within the region. Appendix 14 shows the tabular form of Figure 64. The average magnetic field intensity is calculated to be 1.09 T within the region.

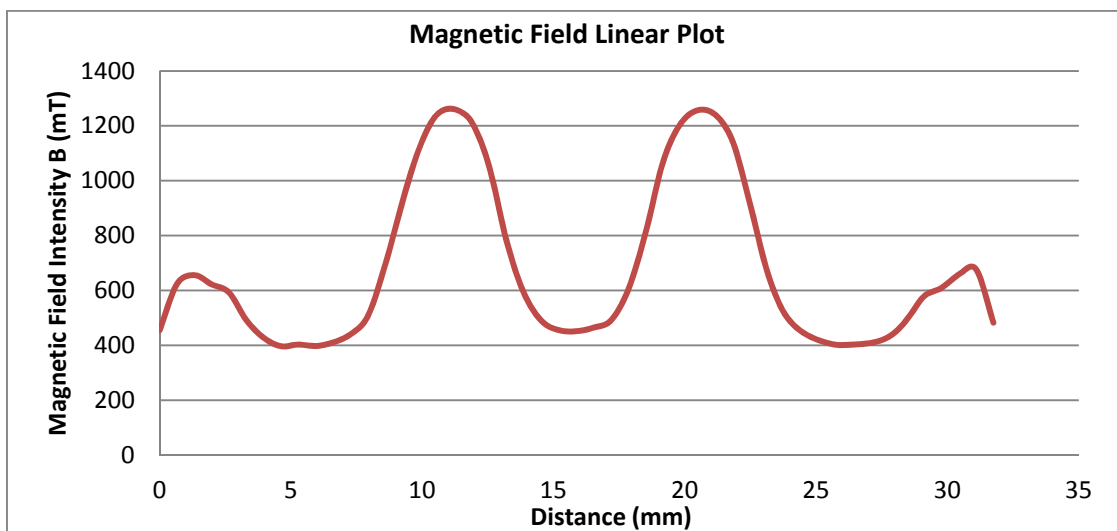


Figure 64: Magnetic Field Intensity Plot for No Inner Magnet

6.2.1 Voltage and Current Calculation

Taking the formula and the sample position in Chapter 3.5.1.3, the induced voltage can be recalculated as below:

$$\begin{aligned}
 V &= Blv \\
 &= B\pi Nd_a v \\
 &= 1.09 \times 3.14 \times 80 \times \frac{23.48}{1000} \times 0.00426 \\
 &= 0.0274 \text{ V}
 \end{aligned}$$

The voltage is around 0.01 V lower than previously calculated. Since the voltage is low, the bridge rectifier cannot be used. The sinusoidal wave of the voltage will be logged and the RMS value will be taken.

The induced current from Chapter 3.5.2 can be calculated as below:

$$\begin{aligned}
 I &= B\sigma Av \\
 &= 1.09 \times 5.78 \times 10^7 \times \pi \times \left(\frac{0.6}{2 \times 1000}\right)^2 \times 0.00426 \\
 &= 0.0759 \text{ A}
 \end{aligned}$$

The power generated can be calculated by using the formula below:

$$\begin{aligned}
 P &= VI \\
 &= 0.0274 \times 0.0759 \\
 &= 0.00208 \text{ W}
 \end{aligned}$$

The power summed up for the whole Endurance race using the Excel Spreadsheet calculation is reduced to 840 W from 1,720 W from Chapter 3.5.3.

6.3 Testing and Results Evaluation

The new setup is tested again in the damper dynamometer at every 10 RPM up to 80 RPM. A load resistor of 1 Ω is used as a load so that current data can be logged. The RMS value of the voltage and current will be calculated as the full bridge rectifier is not suitable for use as the voltage consumed is too high.

6.3.1 Theoretical Calculations

Theoretical calculation was also done to compare the calculated results versus the tested results. The travel and the position of the damper where the compression starts are taken to be the same as the tested value. Table 10 shows the new data used for the calculation for the new damper setup.

Data	Value	Remarks
Magnetic Field	1.24 T	No Inner Magnet Setup

Number of coils	125	Max velocity occurs at damper neutral
Load Resistor	1 Ω	

Table 10: New Data for Calculation

The values of Table 3 in chapter 2.1.3 will be used as the sample calculation to obtain the voltage, current and power for 10 RPM:

$$\begin{aligned}
 V &= Blv \\
 &= B\pi Nd_a v \\
 &= 1.09 \times 3.14 \times 125 \times \frac{23.48}{1000} \times 0.0105 \\
 &= 0.1055 \text{ V}
 \end{aligned}$$

The internal resistance of the wires contribute to the overall resistance of the circuit. It is considered to be connected to the load resistor in series. For a single layer AWG 22 wire coil,

$$\begin{aligned}
 \text{Internal Resistance } r &= l \times \Omega \text{ per km} \\
 &= \pi Nd_a \times \Omega \text{ per km} \\
 &= 3.14 \times 180 \times \frac{23.48}{1000} \times \frac{52.939}{1000} \\
 &= 0.7025\Omega
 \end{aligned}$$

Current across 1 Ω resistor

$$\begin{aligned}
 I &= \frac{V}{R + r} \\
 &= \frac{0.1055}{1 + 0.7025} \\
 &= 0.0620 \text{ A}
 \end{aligned}$$

Voltage across 1 Ω resistor

$$\begin{aligned}
 V &= R \times I \\
 &= 1 \times 0.0620 \\
 &= 0.0620 \text{ V}
 \end{aligned}$$

Power dissipated across 1 Ω resistor

$$\begin{aligned}
 P &= I^2 \times R \\
 &= 0.0620^2 \times 1 \\
 &= 0.00384 \text{ W}
 \end{aligned}$$

6.3.2 Results Table

The results are saved in the CF card and are shown in Appendix 15. The voltage logged data from Appendix 15 only shows the positive portion as the logger can only log DC voltage. The entire negative portion is not logged. Table 11 shows the calculated and tested voltage and current and the percentage changes.

RPM	Velocity (m/s)	Induced Voltage	Internal Resistance	1 Ω Calculation		1 Ω Test			
				Current at 1 Ω	Voltage at 1 Ω	Test Voltage	Test Current	% Δ Voltage	% Δ Current
10	0.0105	0.1052	0.703	0.0618	0.0618	0.0233	0.0640	-62.2	+3.6
20	0.0209	0.2105	0.703	0.1236	0.1236	0.0570	0.0905	-53.9	-26.8
30	0.0314	0.3157	0.703	0.1854	0.1854	0.0608	0.0905	-67.2	-51.2
40	0.0419	0.4210	0.703	0.2472	0.2472	0.0771	0.1267	-68.8	-48.7
50	0.0524	0.5262	0.703	0.3090	0.3090	0.0940	0.0905	-69.6	-70.7
60	0.0628	0.6315	0.703	0.3708	0.3708	0.1146	0.0905	-69.1	-75.6
70	0.0733	0.7367	0.703	0.4326	0.4326	0.1315	0.1720	-69.6	-60.3
80	0.0838	0.8420	0.703	0.4944	0.4944	0.1450	0.1267	-70.7	-74.4

Table 11: Comparison of Calculated and Test Voltage and Current

From Table 11, there is a drastic drop in the voltage and current induced. The voltage dropped by an average of 70.5% and the current drop by an average of 56.5%. As the setup and calculation methods are the same, the reason for the extremely low voltage and current could be due to the following reasons:

1. The wire coils are not tightly packed and thus the number of coils exposed to the magnetic field is lower. The wire coils per direction might also become larger if not tightly pack thus causing the coil height to be larger than 9.525 mm. This cause the induced voltage and current to cancel out each other.
2. The magnets are not producing the magnetic field as advertised in the specifications.
3. The Ansys Magnetostatic analysis was not accurate due to the inaccurate input from the specifications.

Table 12 shows the comparison for the tested and calculated power. The average percentage drop for the power is 82.4%. With that, the total power generated is calculated to be only 148 W for the whole Endurance race from a total of 840 W from Chapter 6.2.1. The power generated is very low, and it is based on one set of coils with no inner magnet. With the initial design from Chapter 3.5.3 with a total power generation of 1,720 W, the power can be roughly estimated to be 302.7 W, which is still very low. Due to the low power generation, it is not very worth it to implement an electromagnetic damper in a Formula SAE race vehicle.

RPM	Velocity (m/s)	Calculated Power at 1 Ω	1 Ω Test	
			Power	% Power
10	0.0105	0.0038	0.0015	-60.9
20	0.0209	0.0153	0.0052	-66.2
30	0.0314	0.0344	0.0055	-84.0
40	0.0419	0.0611	0.0098	-84.0
50	0.0524	0.0955	0.0085	-91.1
60	0.0628	0.1375	0.0104	-92.5
70	0.0733	0.1872	0.0226	-87.9
80	0.0838	0.2455	0.0184	-92.5

Table 12: Comparison of Calculated and Tested Power

6.4 Design Improvement

From the evaluation from the previous chapter, 2 major problems of the Formula SAE race vehicle electromagnetic damper are due to the voltage and current being too low, and the tolerance of the manufactured components causing damages. The next few chapters will be focus on the possible design changes that can be implemented for a better system.

6.4.1 Additional Coils

More coils can be added on the outside of the rebound casing to tap on the magnetic field due to the outer magnets as shown in Figure 65. More than one set of coils can be added if space is permitted.

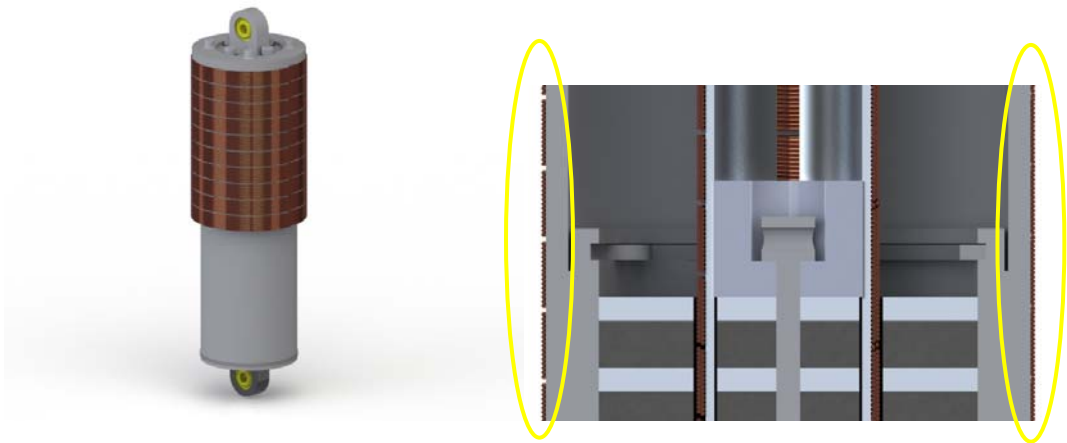


Figure 65: Electromagnetic Damper with Coils on the Outside (Left) and Section View (Right)

In order for the magnetic field to be travelling in the radial direction, rings of ferrous spacer will be positioned outside of the coils. Without the ferrous spacer on the outside, the magnetic field will tend to curl back to the spacer above or below depending on its pole as shown in Figure 66.

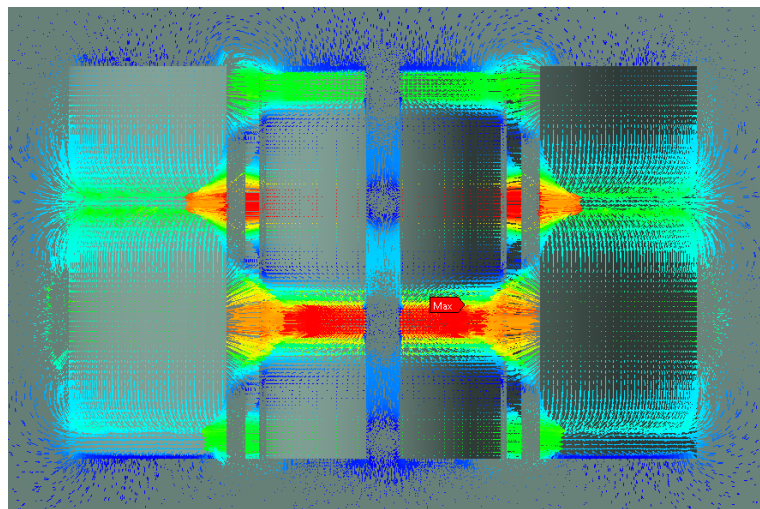


Figure 66: Ansys Magnetostatic Analysis on Original Design

To direct the magnetic fields in the radial direction, a "toothed" ferrous outer ring have to be placed outside the outer magnet array as shown in Figure 67. Ansys Magnetostatic analysis will be conducted to determine the magnetic field at the outer portion.

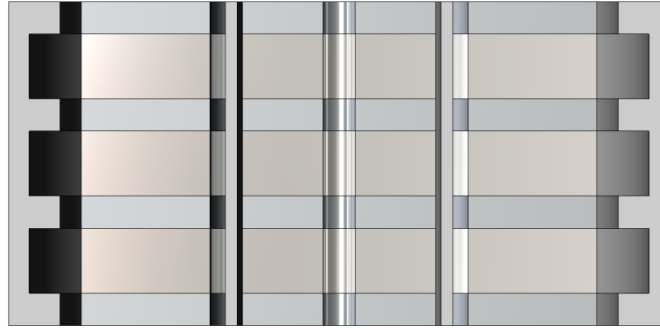


Figure 67: Section View of 3 Magnet Setup

From the Ansys Magnetostatic analysis in Figure 68, it can be seen that the "tooth" ferrous outer ring is directing the magnetic field outwards from the outer magnet. By plotting the magnetic field along the region (circled), the average magnetic field intensity is 1.16 T. Appendix 16 shows the plot of the magnetic field along the region.

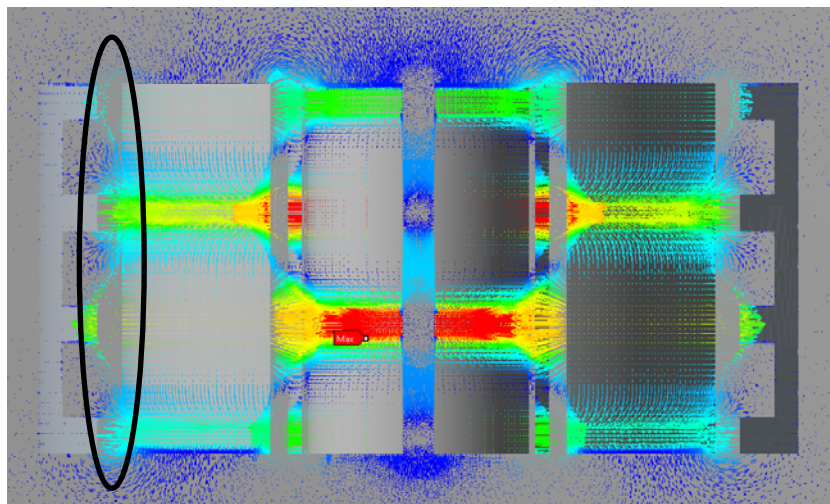


Figure 68: Ansys Magnetostatic Analysis for Coils on the Outside

Calculation is conducted to find out the addition power from the outer coils. Since there is less restriction in space, more coils can be added to tap on the magnetic field. Assume there are 3 sets of coils on the outside of the electromagnetic damper. The new specifications are shown in Table 13.

Specifications	Values	Remarks
Coil Average Diameter	66.64 mm	
Average Magnetic Field	1.16 T	
Number of Coils	405	Between 220 to 270 exposed coils Refer to Chapter 3.5.1.1

Table 13: Specifications of Wire Coils on the Outside

With the input values, the total power generated during an Endurance Race for the outside coils are computed in an Excel Spreadsheet similar to Chapters 3.5.1, 3.5.2 and 3.5.3. The outer coils along is able to generate a maximum power of 8,645 W for an Endurance Race. Coupled with the inner coils of 1,720 W, a total of 10,365 W can be generated. From the experimental power drop of 82.4% from the calculation in Chapter 6.3.2, the power generated goes up to around 1,824 W.

The advantage of this system is that minimal modification is required for the current design. However, adding the coils outside means it will be taking up the place of the springs. As the laminated wires are very delicate, it might be damaged by the springs or the dirt from the environment.

6.4.2 Larger Inner Magnets

The inner magnet is relatively small as compared to the larger magnet. Increasing its size might increase the magnetic field of the system. Since designing with other magnets means customizing the magnet, it will also be worthwhile to use a N52 magnet instead of N48.

A few inner magnet dimensions will be analyzed using Ansys Magnetostatic analysis. Table 14 and Figure 69 show the different values of diameter being tested. Configuration 1 is the original diameter configuration. The diameter in configuration 2 is an even smaller inner magnet for verification. The next 3 configurations are diameter with increasing inner magnet diameter.

Configuration	Outer Magnet		Inner Magnet	
	External Diameter (mm)	Internal Diameter (mm)	External Diameter (mm)	Internal Diameter (mm)
1	50.8	25.4	19.05	3.175
2	50.8	20.4	14.05	3.175
3	50.8	30.4	24.05	3.175
4	50.8	35.4	29.05	3.175
5	50.8	40.4	34.05	3.175

Table 14: Magnet Diameter Size Iterations

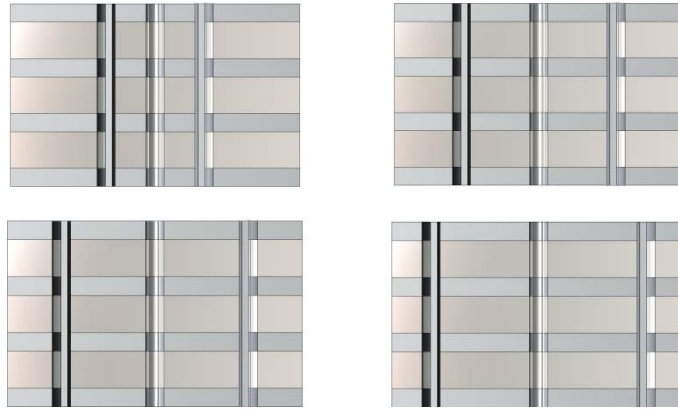


Figure 69: Magnet Diameter Size Iterations

The internal diameter of the wire coil housing is kept to be 1.0 mm larger than the external diameter of the magnet and at 1.6 mm thickness. The magnetic field intensity is taken at 0.3 mm (half wire diameter) outside the outer diameter of the wire coil housing to find out the actual magnetic field that passes through the wires.

Figure 70 shows the magnetic field plot from Ansys Magnetostatic analysis. Appendix 17 shows the table for the plot. The average magnetic field is calculated for the region that the magnetic field are travelling radially. The average magnetic field for configuration 1 to 5 is 1.52 T, 1.60T, 1.42 T, 1.27 T and 1.04 T respectively.

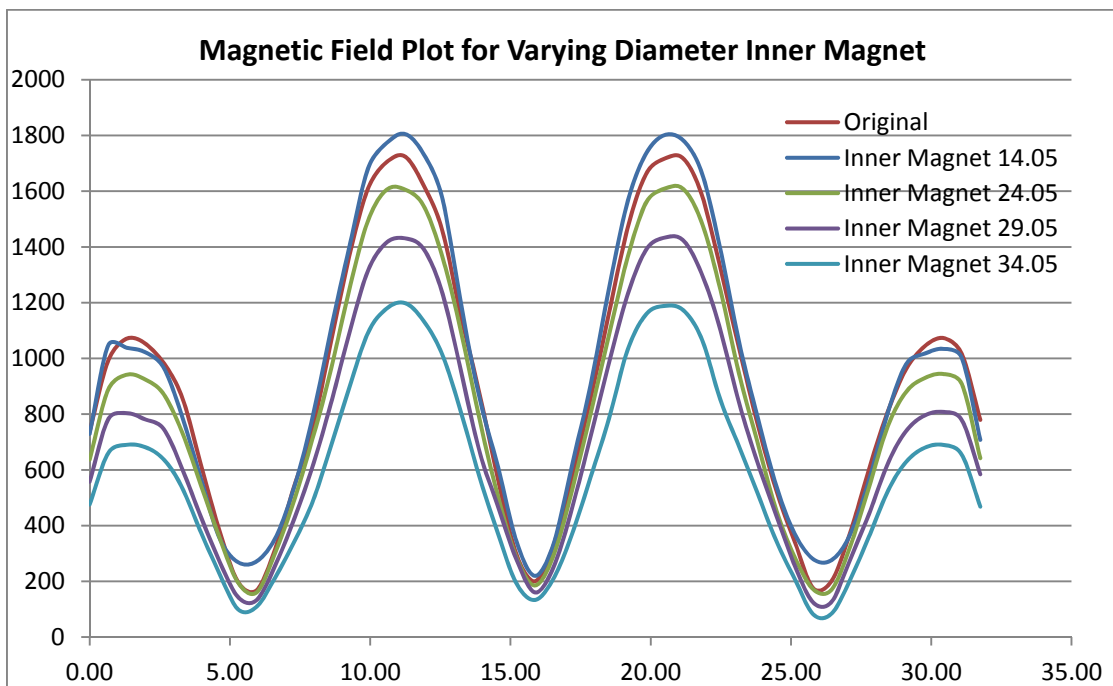


Figure 70: Magnetic Field Plot for Varying Inner Magnet Diameter

Surprisingly, the smallest diameter inner magnet of 14.05 mm has the highest peak and average magnetic field. It could be due to the outer magnet getting larger and thus producing stronger magnetic fields as compared to the inner magnet becoming larger. The strength of the magnetic field should be affected by the volume of the magnet itself

6.4.3 Thicker Magnets

Since the volume of the magnet can affect the magnetic field produced, magnets of different thickness will also be simulated if magnets were to be customised.

Table 15 and Figure 71 show the different configuration of the magnet and spacer thickness. The original magnet and spacer is also compared. From the original configuration, a half height magnet from the original will be used for verification, and then it will be 25%, 50%, 75%, and 100% thicker magnet from the original.

Configuration	Magnet Thickness (mm)	Spacer Thickness (mm)
Half Height	3.1750	1.58750
25% Thicker	7.9375	3.96875
50% Thicker	9.5250	4.26250
75% Thicker	11.1125	5.55625
100% Thicker	12.7000	6.35000

Table 15: Magnet and Spacer Thickness Configuration

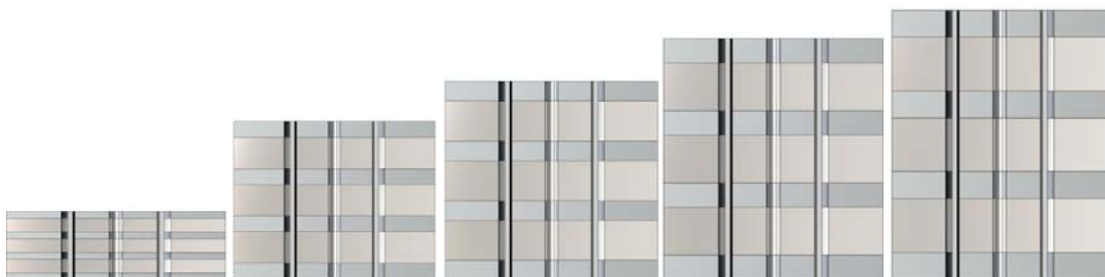


Figure 71: Magnet and Spacer Thickness Configuration

The spacer between the magnets will be kept to half the magnet thickness as it was shown that it is the best magnet to spacer thickness combination in Chapter 3.2.1.3. The internal and external diameter of the inner and outer magnets will be kept to the original dimension. The

wire coil housing will be kept to the same inner and outer diameter, only the length varies according to the total length of the setup.

Figure 72 shows the magnetic field plot from Ansys Magnetostatic analysis. Appendix 18 shows the table for the plot. The average magnetic field is calculated for the region that the magnetic field are travelling radially. The average magnetic field from half height, original to 100% thicker is 0.86T, 1.69 T, 1.69 T, 1.70 T and 1.56 T respectively.

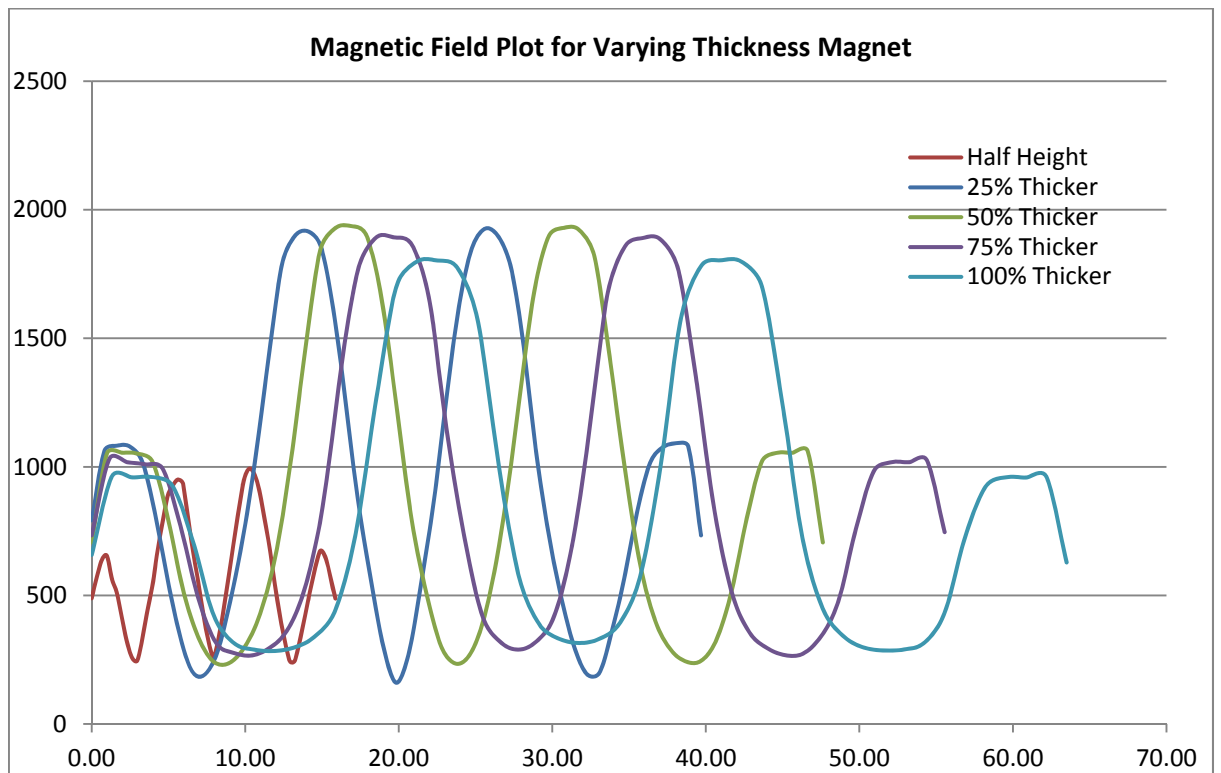


Figure 72: Magnet Field Plot for Varying Thickness Magnet

There is not much difference between the original thicknesses up to 50% thicker magnet. The highest magnetic field is only 0.01 T higher than the original. However, it is worth the change as the thicker magnet means thicker spacer. This will allow more coils of wires to be exposed to the magnetic field and thus more power can be generated.

7 Results Evaluation on Road Vehicle

The calculation of power generation in Chapter 6.3.2 shows that there is not much power produced by the electromagnetic dampers to generate electricity to charge batteries in a Formula SAE race vehicle. Based on the calculations in Chapter 6.3.2, an electromagnetic damper will be design for road going vehicles. Since there are more space in road vehicles, more magnets and coils can be set up to harness the power. Furthermore, with a larger suspension travel in road vehicles, the velocity and coils exposed will be more than the Formula SAE race vehicle.

7.1 Road Profile

Road profile data was not available for local roads, and with reference to US patent 6,952,060 B2 [12], the velocity of the bump ranges from 0.1 m/s to 1.0 m/s. The average bump height is from 1.0 mm to 6.0 mm. Frequency of travel ranges from 50 Hz to 1.7 kHz between vehicle speeds of 25 to 65 mph. Figure 73 shows the typical road data in the United States.

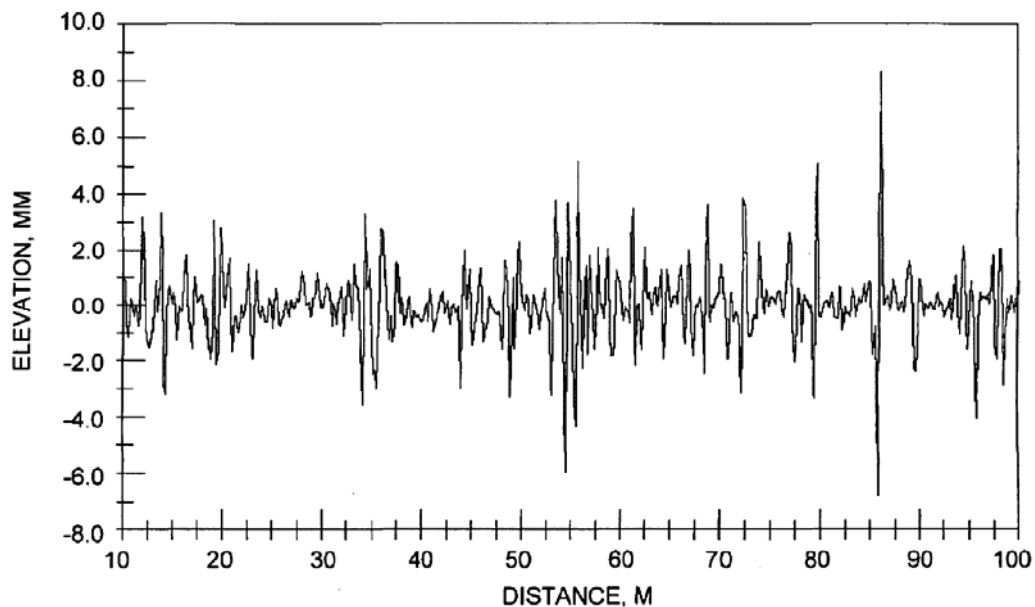


Figure 73: Road Profile Data

7.2 Damper Design

The electromagnetic damper design will be based on a road car front damper. As there is an ongoing project for a road vehicle using a Toyota Picnic front damper, dimensions will be

modelled after the damper for the electromagnetic damper. As the damper resides inside the springs, the inner dimension of the springs is taken. The dimensions are taken to be 14.0 cm in diameter and 26.0 cm in length. Due to the large dimension available, a series of ring magnets and wire coils can be used and they can be configured to be in series or parallel to configure the voltage required.

7.2.1 Laminated Wire

Figure 74 shows the 4 magnet setup for Ansys Magnetostatic analysis. There are a total of 4 sets of magnets in the setup and 4 sets of wire coils in the system. The air gap between each wire coil housing and the magnets is determined by the maximum short circuit current induced and thus the gauge of the wires used.

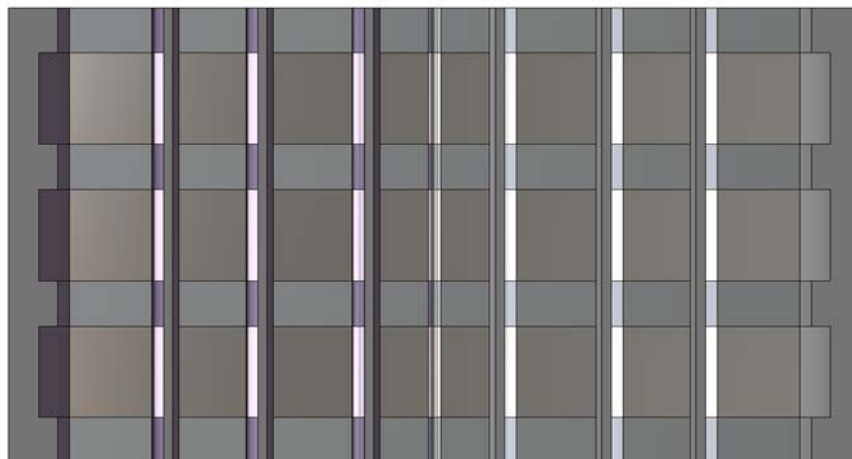


Figure 74: 4-Magnet Setup

The magnetic field induced will be taken to be 1.5 T as most simulations from Ansys Magnetostatic analysis on magnets range from 1.2 T to 1.7 T. From Chapter 3.5.2, the current is calculated using the formula $I=B\sigma Av$. AWG 22 wires will be first used for calculation. At the median vertical velocity of 0.5 m/s, the current is calculated as below:

$$\begin{aligned}
 I &= B\sigma Av \\
 &= 1.50 \times 5.78 \times 10^7 \times \pi \times \left(\frac{0.6}{2 \times 1000}\right)^2 \times 0.5 \\
 &= 34.1 \text{ A}
 \end{aligned}$$

This current would require an AWG 13 laminated wire with 1.83 mm in diameter. From Chapter 6.3.2, the experimental current will drop by an average of 50.5% to 17.2 A from the theoretical calculation. For RMS current, the current will drop to 12.2 A since there is up and down stroke causing the current to change direction at each stroke. With that, an AWG 18 wire can be used as its current capacity is 16.0 A. By packing the wire coils tight in 3 layers, the space required would be 3.0 mm as shown in Figure 75.

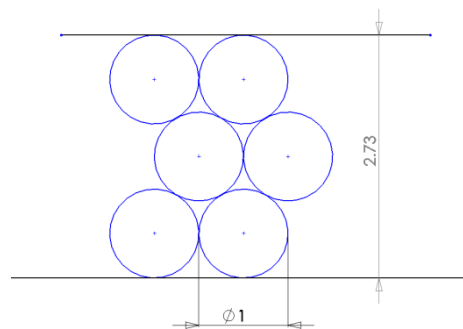


Figure 75: Wire Coil Cross Section

7.2.2 Magnet Setup and Analysis

Ansys Magnetostatic analysis will be used to conduct the magnet configuration. In Figure 74, a 4-magnet set is displayed. A 3-magnet set in Figure 76 will also be simulated to find out the magnetic field at each air gap. The magnetic field will be added up together to find out the configuration that produces the highest magnetic field since the voltage and current is proportional to the magnetic field.



Figure 76: 3-Magnet Layout

7.2.2.1 Multiple Step Wire Coil Housing

There is one modification on the wire coil housing as shown in Figure 76 circled 1. The wire coil housing has multiple steps at the region above and below every ferrous spacer. Figure 77 shows a small section of the wire coil housing. These steps serve 2 functions:

1. To concentrate and direct the magnetic field from the one ferrous spacer to the next as the gap has increased to 3.0 mm
2. To keep the wire coil windings in place and location and allows easy winding.

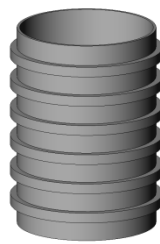


Figure 77: Multiple Step Wire coil Housing

7.2.2.2 Ferrous Spacer Gap

The next modification is the ring of air gap around the ferrous spacer on each surface as shown in Figure 76 circled 2. The cross sectional view is also shown in Figure 78. The purpose of the air gap is to direct the magnetic fields from the magnets evenly to the coil near its inner diameter and the coils near its outer diameter so that the wire coil gets an even share of the magnetic field and not bias towards the larger magnet.



Figure 78: Ferrous Spacer and Cross Section View

7.2.2.3 Ansys Magnetostatic Analysis

Table 16 shows the consolidation of 3-magnet and 4-magnet iteration using Ansys Magnetostatic analysis. The iteration consists of different inner diameter and outer diameter of each of the magnets. A gap of 0.5 mm is left between the magnet outer diameter and wire coil

housing inner diameter. The wire coil housing will be 1.0 mm thick and the air gap for the wire coils will be 3 mm.

Set	Dimension (mm)				Magnetic Field (mT)				
4 Magnet Set									
1	6.865	23.365	39.865	60.635	589	976	1422	1324	4311
2	8.865	25.365	37.865	60.635	1141	848	1380	1577	4946
3	8.865	25.365	39.865	60.635	1081	1078	1414	1361	4934
4	8.865	25.365	41.865	60.635	1103	1090	1387	1231	4811
5	8.865	25.365	43.865	60.635	924	1102	1196	1235	4457
6	8.865	25.365	45.865	60.635	1054	1253	1283	1054	4644
7	10.865	27.365	43.865	60.635	982	937	1276	1136	4331
8	12.865	29.365	45.865	60.635	1060	1020	1098	1045	4223
9	14.865	31.365	47.865	60.635	1095	1040	1006	852	3993
10	8.865	23.365	37.865	60.635	870	765	1401	1567	4603
3 Magnet Set									
11	9.865	35.865	60.635	-	1055	1753	1355	-	4163
12	11.865	36.865	60.635	-	2193	1791	1712	-	5697
13	13.865	37.865	60.635	-	1174	1706	1300	-	4180
14	15.865	38.865	60.635	-	1188	1694	1237	-	4119
15	17.865	39.865	60.635	-	1217	1602	1292	-	4111
16	19.865	40.865	60.635	-	1262	1540	1246	-	4048
17	21.865	41.865	60.635	-	1310	1469	1135	-	3914
18	23.865	42.865	60.635	-	1329	1400	1182	-	3911
19	25.865	43.865	60.635	-	1500	1302	1323	-	4125

Table 16:3- Magnet and 4-Magnet Iterations

Set 12 of the 3-magnet setup is chosen as it produces the highest magnetic field combined as compared to the highest of the 4-magnet setup. Each wire coil will be wound and separate from the wire coils above or below so that the error of wire coils not wrapped properly and keep to the design height will not be accumulated throughout the whole wire coil assembly. Wires wrapped in this way will also allow different voltage and current configuration by wiring the output of the wire coils in series or in parallel.

Figure 79 shows the Ansys Magnetostatic analysis of Set 12. From the figure, the magnetic field lines are distributed at the ferrous spacer evenly to the left and right of the spacer. The stepped profile at the wire coil housing also helps to pull more magnetic fields in the radial direction.

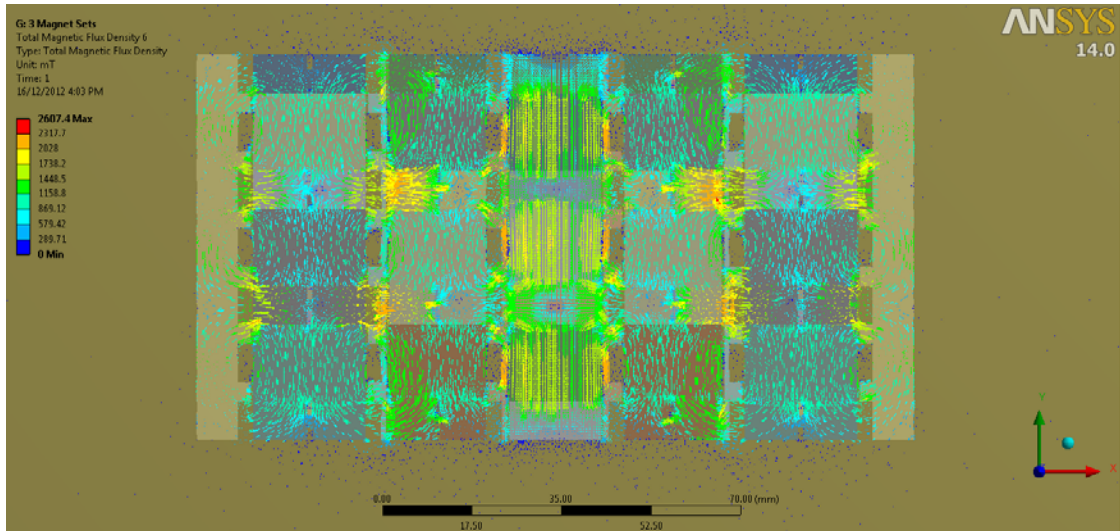


Figure 79: Ansys Magnetostatic Analysis of 3- Magnet Setup Set 12

From the line plot in Figure 80, there are spikes before and after the central spacer location. These spikes are due to the stepped profile of the wire coil housing. In between the spikes, there is a drop in magnetic field. However, it is almost flat rather than peaking and dropping off like in earlier plots without any steps. This flat profile allows for a higher overall average magnetic field and also allows the voltage and current to be induced. The average magnetic field intensity will be taken within the 3 regions. The average magnetic field intensity for region 1 is 1.08 T, region 2 is 1.5 T and region 3 is 1.2 T.

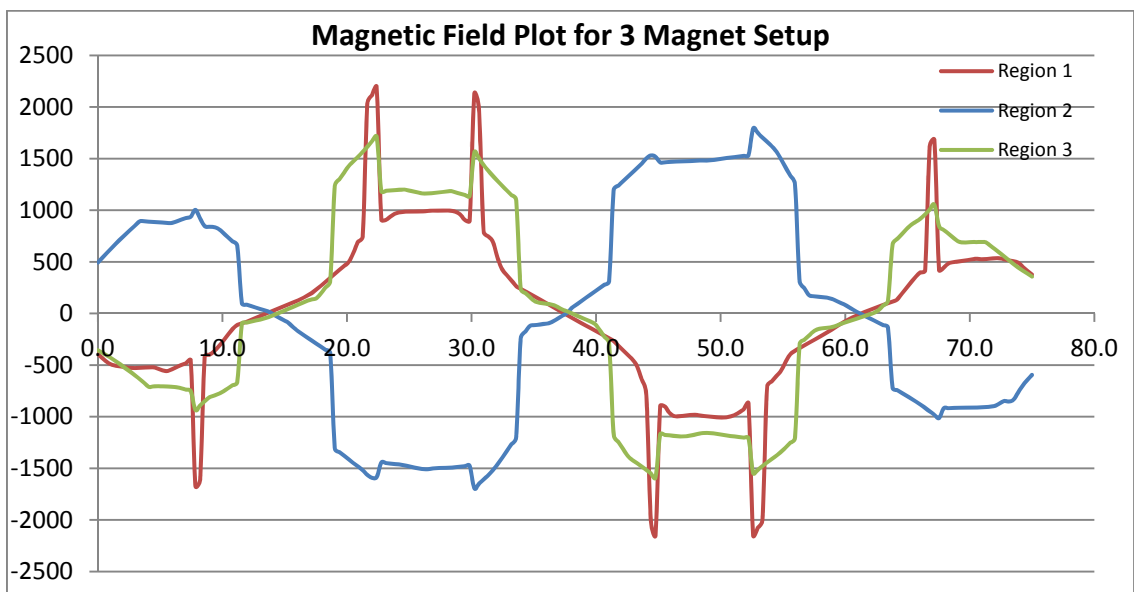


Figure 80: Magnetic Field Intensity Plot for 3-Magnet Setup

7.2.3 Damper CAD

Figure 81 shows the road car damper design. There are a 306 inner, middle and outer wire coils each, giving a total wire length of 210 m. This is a significant increase in wire length due to the large size of road car damper.

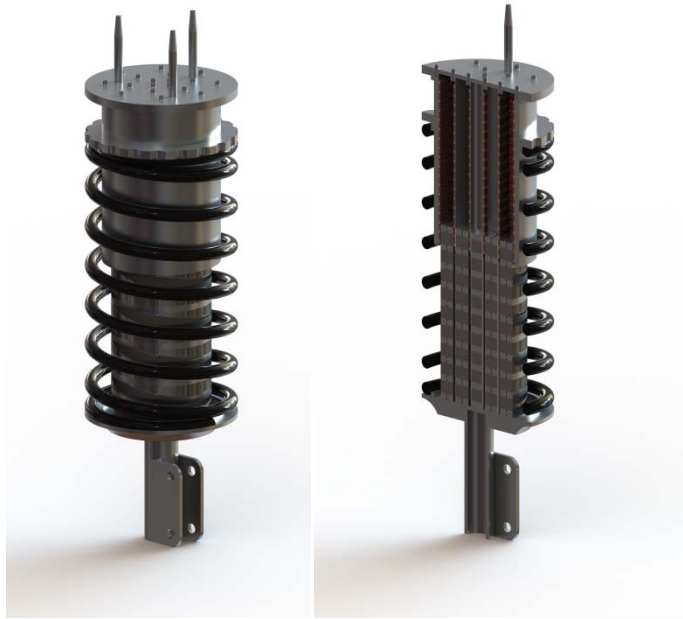


Figure 81: Road Car Electromagnetic Damper (Left) and Section View (Right)

The wire coils in Figure 82 below will fit inside a 7.5 mm indentation which is the thickness of the ferrous spacer where the magnetic field will be the strongest. Instead of continuing the wires immediately to the upper or lower coils from the original wire coils, there is a spacing of 3.75 mm to allow for coils not wounded properly.

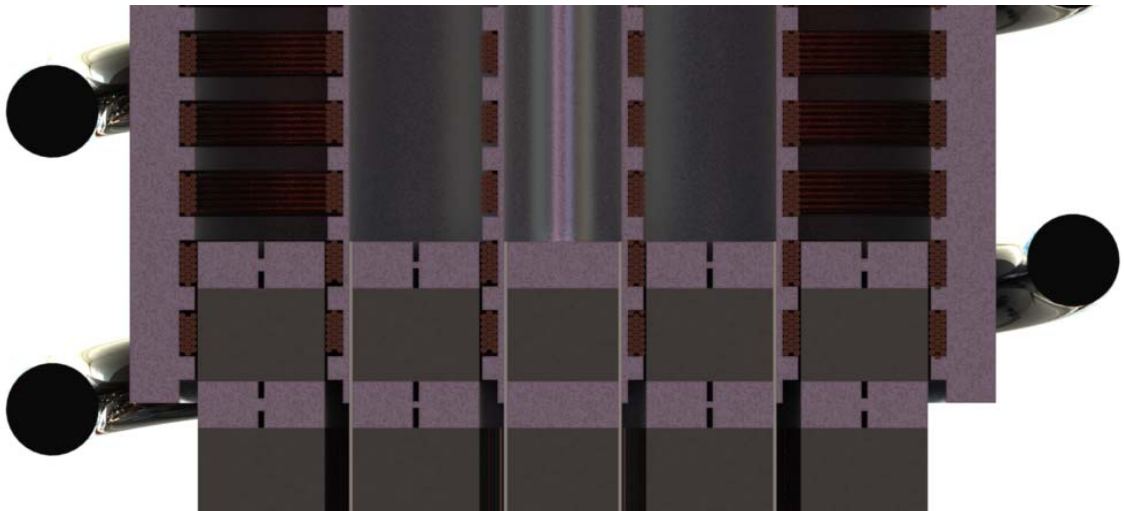


Figure 82: Close up Section View of Road Car Electromagnetic Damper

The other features of the damper are for fitting to a road car MacPherson strut assembly.

7.2.4 Voltage and current calculation

Open circuit voltage and short circuit current will be calculated for each of the set of coils to find the maximum voltage and current generated.. A range of vertical velocities will also be calculated for the setup. Instead of using 306 coils from Chapter 7.2.4, 150 coils will be used as the damper in Figure 81 shows that half the coils will be exposed to the magnetic field at neutral position. All the coils will only be exposed to magnetic field when the damper is at full bump which is not very common.

Table 17 shows the voltage and current induced at various damper vertical velocity. From Chapter 7.1 where the suspension travel is between 1.0 mm to 6.0 mm, the wire coils will be travelling within the 7.5 mm spacer thickness. If there is higher suspension travel, more coils will be exposed to the magnetic field from the 150 coils and higher voltage can be induced.

Vertical Velocity	Coil	Open Circuit Voltage (V)	Short Circuit Current (A)	Maximum Power (W)	RMS Power (W)	Tested Power (W)
0.10	Inner	1.20	2.03	2.45	1.23	0.22
	Middle	5.21	2.83	14.77	7.38	1.30
	Outer	6.95	2.30	15.99	7.99	1.41
0.20	Inner	2.41	4.07	9.80	4.90	0.86
	Middle	10.42	5.67	59.07	29.53	5.20
	Outer	13.91	4.60	63.95	31.98	5.63
0.30	Inner	3.61	6.10	22.05	11.03	1.94
	Middle	15.63	8.50	132.90	66.45	11.70
	Outer	20.86	6.90	143.89	71.95	12.66
0.40	Inner	4.82	8.14	39.20	19.60	3.45
	Middle	20.85	11.33	236.27	118.14	20.79
	Outer	27.82	9.20	255.81	127.91	22.51
0.50	Inner	6.02	10.17	61.25	30.63	5.39
	Middle	26.06	14.17	369.17	184.59	32.49
	Outer	34.77	11.49	399.70	199.85	35.17
0.60	Inner	7.23	12.21	88.21	44.10	7.76
	Middle	31.27	17.00	531.61	265.80	46.78
	Outer	41.73	13.79	575.57	287.79	50.65
0.70	Inner	8.43	14.24	120.06	60.03	10.57
	Middle	36.48	19.83	723.58	361.79	63.68
	Outer	48.68	16.09	783.42	391.71	68.94
0.80	Inner	9.63	16.28	156.81	78.40	13.80
	Middle	41.69	22.67	945.08	472.54	83.17
	Outer	55.64	18.39	1023.24	511.62	90.05
0.90	Inner	10.84	18.31	198.46	99.23	17.46
	Middle	46.90	25.50	1196.12	598.06	105.26
	Outer	62.59	20.69	1295.04	647.52	113.96
1.00	Inner	12.04	20.34	245.02	122.51	21.56
	Middle	52.12	28.33	1476.69	738.35	129.95

	Outer	69.55	22.99	1598.82	799.41	140.70
--	-------	-------	-------	---------	--------	--------

Table 17: Road Car Electromagnetic Damper Power Generation

The coils are also assumed to be wired in series between the inner, middle and outer coils. Different configurations can be wired such that the voltage can be increased through series connection or current increased through parallel connection of different coils to fine tune to the voltage and current required.

From Table 17, the maximum power induced is taken by using the formula $P=VI$. The RMS power is due to the frequency of oscillation of the damper as voltage of different polarity will be induced as the damper move up and down stroke. The tested power is taken by reducing the RMS power by 84.2% from the tested data in Chapter 6.3.2.

Figure 83 above shows the plot for tested power versus damper vertical velocity for inner, middle and outer coils. The middle and outer coils are producing almost similar output and can be used to charge the main batteries for electric vehicle. The average output power for the middle and outer coils are around 52 W per stroke and the power produced can be quite significant for frequencies between 50 Hz and 1.7 kHz from Chapter 7.1 for vehicle travelling between 45 mph to 65 mph. For the inner coils where power is lesser at an average of 8.3 W, it can be used to charge the onboard auxiliary battery.

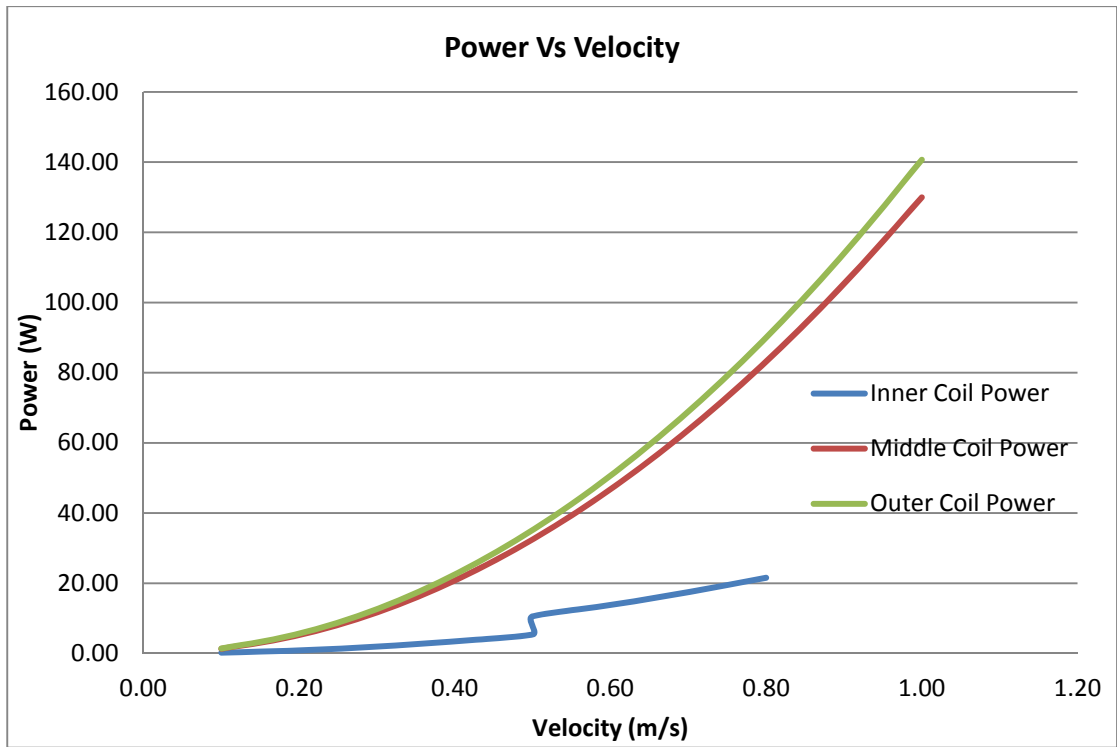


Figure 83: Power Vs Velocity Plot for Road Car Electromagnetic Damper

8 Conclusion

The use of electromagnetic dampers in Formula SAE race vehicle proves to be not effective due to the limited space for wire coils and magnets and also the low travel length which translates to low damper velocities. In addition, with the lack of space for the magnet and wire coils, fabrication demands a higher tolerance. Any discrepancy in tolerance causes a large drop in the efficiency of the damper power generation.

The laminated wires that are bought off the shelf have some kinks present and this makes the wire coils extremely difficult to be wound tightly together. This cause the clockwise and anticlockwise coils to move out of the high magnetic flux zones and in fact causes voltages and current to be induced in opposite direction and cancel out each other.

The N48 magnets were also producing not high enough magnetic fields for the wire coils. Since the magnetic field of the magnets is dependent on the volume of the magnet itself, the lack of space for the Formula SAE damper once again restricts the amount of magnetic field produced. Even when the highest strength commercially available N52 magnet is used in the simulation, the magnetic field does not increase by a lot. Until a stronger magnet is commercially available, it is still difficult to achieve a magnetic field intensity if around 2.0 T.

The use of test data on a road car electromagnetic damper proves to be worthwhile due to the large size available for multiple magnets and wire coils to be packaged inside. The change in wire coil housing and ferrous spacer design in the expense of manufacturing also allows less margin of error for the winding of wire coils and allows a higher magnetic flux across the wire coils.

The only downside of the road car electromagnetic damper is its weight. From CAD, the weight of the damper is around 18 kg. This is due to the weight of the magnets and ferrous spacer which takes up most of the volume of the damper as compared to traditional hydraulic dampers with hydraulic fluids. As the dampers contribute to half the unsprung mass of the suspension system, it can have a significant impact on the dynamic performance of the vehicle.

References

- [1] Clegg, S.J. A Review of Regenerative Braking Systems Institute for Transport Studies Working Paper 471, 1996
- [2] E. Minazara, D. Vasic and F. Costa. Piezoelectric Generator Harvesting Bike Vibrations Energy to Supply Portable Devices
- [3] Pirisi. A, Grimaccia. F, Mussetta. M and Riccardo. E.Z. Novel Speed Bumps Design and Optimization for Vehicles' Energy Recovery in Smart Cities, ISSN 1996-1073
- [4] Zhu. Z, Norbert C. Cheung and K.W.E Cheng. Application of Linear Switched Reluctance Motor for Active Suspension System in Electric Vehicle The 25th World Battery, Hybrid and Fuel Cell Electric Vehicle Symposium & Exhibition, 2010
- [5] Zhu. L and Knospe. C.R. Modeling of Nonlaminated Electromagnetic Suspension Systems IEEE/ASME TRANSACTIONS ON MECHATRONICS, VOL. 15, NO. 1, 2010
- [6] Milliken. W.F, Milliken. D.L. Race Car Vehicle Dynamics. SAE International. 1992
- [7] Shian, C., H. Ren, and Senlin, L. *New Reclaiming Energy Suspension and its Working Principle* Chinese Journal of Mechanical Engineering, 2007. 13(11): pp. 177-182.
- [8] Ren, H., C. Shian, and L. Senlin, A Permanent Magnetic Energy Regenerative Suspension. ZL 200520072480.9, 2005.
- [9] Shian, C., H. Ren, and Senlin, L. Operation Theory and Structure Evaluation of *Reclaiming Energy Suspension*. Transactions of the Chinese Society for Agricultural Machinery, 2006. 37(5): pp. 5-9.
- [10] Yong-chao, Z., et al., Isolation and Energy Regenerative Performance Experimental Verification of Automotive Electrical Suspension. Journal of Shanghai Jiaotong University, 2008. 42(6): pp. 874-877.
- [11] Zhengquan, W. and C. Yu, Brief Introduction to Structure and Principle of *Electromagnetic Shock Absorber*. Motor Technology, 2007. 8: pp. 56-59.

[12] Ronald, G. And Peter, Z., Trustees of Tufts College (2005), Medford, MA (US), US
Pat. 6,952,060

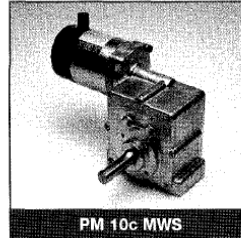
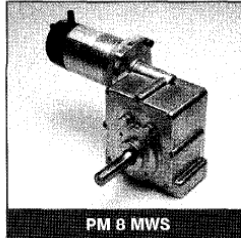
Appendix

Appendix 1: Rocker Rotation Frequency

RPM	Frequency	RPM	Frequency	RPM	Frequency
0.000	23930	3.354	0	6.708	0
0.078	70731	3.432	0	6.786	0
0.156	20348	3.510	0	6.864	0
0.234	10802	3.588	0	6.942	0
0.312	6163	3.666	0	7.020	0
0.390	3631	3.744	0	7.098	0
0.468	2104	3.822	0	7.176	0
0.546	1232	3.900	0	7.254	1
0.624	706	3.978	0	7.332	0
0.702	442	4.056	0	7.410	2
0.780	241	4.134	0	7.488	0
0.858	137	4.212	0	7.566	0
0.936	72	4.290	0	7.644	1
1.014	39	4.368	0	7.722	0
1.092	28	4.446	0	7.800	0
1.170	13	4.524	0	7.878	0
1.248	11	4.602	0	7.956	0
1.326	8	4.680	0	8.034	0
1.404	3	4.758	0	8.112	0
1.482	2	4.836	0	8.190	1
1.560	0	4.914	0	8.268	1
1.638	0	4.992	0	8.346	1
1.716	0	5.070	0	8.424	0
1.794	0	5.148	0	8.502	1
1.872	0	5.226	0	8.580	0
1.950	0	5.304	0		
2.028	1	5.382	0		
2.106	0	5.460	0		
2.184	0	5.538	0		
2.262	0	5.616	0		
2.340	0	5.694	0		
2.418	0	5.772	0		
2.496	0	5.850	0		
2.574	0	5.928	0		
2.652	0	6.006	0		
2.730	0	6.084	0		
2.808	0	6.162	0		
2.886	0	6.240	0		
2.964	0	6.318	0		
3.042	0	6.396	0		
3.120	0	6.474	0		
3.198	0	6.552	0		
3.276	0	6.630	0		

Appendix 2: Low Torque Motor Specification Sheet

Gearbox Type: MWS <i>Speed Range: 1.1 – 64 r.p.m.</i>	Worm and Multi-Spur Reduction Gear Units Variable Speed – D.C. Permanent Magnet Enclosure: – Totally enclosed (IP 54)
--	---



■ **Voltage, Construction, Connections, Motor Performance**
Specifications and Optional Extras see page 68 in main catalogue for full details.

(1 Nm = 8.85 lbs. ins.) (1 Nm = 10.2 cmkp)

Gearbox Specification Motor Speed 1500 r.p.m.			PM 7 MWS		PM 8 MWS		PM 9 MWS		PM 10c MWS		PM 11c MWS	
			Cont	1 Hour	Cont	1 Hour	Cont	1 Hour	Cont	1 Hour	Cont	1 Hour
			Motor Rating 7.5 watts	Motor Rating 10 watts	Motor Rating 12.5 watts	Motor Rating 15 watts	Motor Rating 19 watts	Motor Rating 24 watts	Motor Rating 20 watts	Motor Rating 25 watts	Motor Rating 33 watts	Motor Rating 40 watts
FINAL R.P.M.	GEARBOX RATIO		OUTPUT TORQUE (Nm)									
	WORM	SPUR										
1.1	40:1	35.17	26	35	43	45	45	-	-	-	-	-
1.6	27:1	35.17	20	27	33	45	45	-	-	-	-	-
2	18 1/2:1	35.17	16	21	26	34	40	45	45	-	-	-
3	12 1/2:1	35.17	12	16	21	27	31	39	33	45	45	-
5	9 1/3:1	35.17	10	13	16	22	25	32	26	33	43	45
6	7 1/4:1	35.17	8	11	14	18	21	26	22	27	36	44
8	5 1/6:1	35.17	6	8	10	14	16	20	17	21	27	33
10	4 1/3:1	35.17	5	7	8	11	13	16	13	17	22	27
12	8 1/3:1	15.06	4	5	7	9	10	13	11	13	17	21
14	7 1/4:1	15.06	4	5	6	8	9	12	10	12	16	19
16	6 1/4:1	15.06	3	4	5	7	8	10	9	11	14	17
24	4 1/8:1	15.06	2	3	4	5	6	7	6	7	10	12

Appendix 3: Damper Velocity Frequency

Velocity	Frequency	Velocity	Frequency	Velocity	Frequency	Velocity	Frequency	Velocity	Frequency
0.001	44830	0.062	145	0.123	7	0.184	0	0.245	0
0.002	9717	0.063	141	0.124	4	0.185	1	0.246	0
0.003	8364	0.064	119	0.125	4	0.186	0	0.247	0
0.004	5922	0.065	134	0.126	4	0.187	0	0.248	0
0.005	5929	0.066	134	0.127	4	0.188	0	0.249	0
0.006	4559	0.067	109	0.128	4	0.189	0	0.25	0
0.007	4578	0.068	113	0.129	0	0.19	1	0.251	0
0.008	3663	0.069	93	0.13	5	0.191	0	0.252	0
0.009	3586	0.07	97	0.131	2	0.192	0	0.253	0
0.010	2989	0.071	86	0.132	4	0.193	0	0.254	0
0.011	2849	0.072	88	0.133	3	0.194	0	0.255	0
0.012	2485	0.073	82	0.134	7	0.195	0	0.256	0
0.013	2411	0.074	67	0.135	2	0.196	0	0.257	0
0.014	2264	0.075	81	0.136	2	0.197	0	0.258	0
0.015	2090	0.076	68	0.137	1	0.198	0	0.259	1
0.016	1948	0.077	62	0.138	4	0.199	0	0.26	0
0.017	1774	0.078	51	0.139	1	0.2	0	0.261	0
0.018	1693	0.079	74	0.14	2	0.201	0	0.262	0
0.019	1618	0.08	50	0.141	0	0.202	0	0.263	0
0.020	1498	0.081	52	0.142	1	0.203	0	0.264	0
0.021	1471	0.082	44	0.143	4	0.204	0	0.265	0
0.022	1257	0.083	61	0.144	0	0.205	0	0.266	0
0.023	1241	0.084	46	0.145	2	0.206	0	0.267	0
0.024	1174	0.085	51	0.146	3	0.207	0	0.268	0
0.025	1148	0.086	44	0.147	1	0.208	0	0.269	0
0.026	1047	0.087	48	0.148	1	0.209	0	0.27	0
0.027	973	0.088	31	0.149	0	0.21	0	0.271	0
0.028	942	0.089	34	0.15	1	0.211	0	0.272	0
0.029	841	0.09	38	0.151	1	0.212	0	0.273	0
0.030	880	0.091	31	0.152	1	0.213	0	0.274	0
0.031	708	0.092	28	0.153	0	0.214	0	0.275	0
0.032	814	0.093	28	0.154	0	0.215	0	0.276	0
0.033	696	0.094	27	0.155	1	0.216	0	0.277	0
0.034	656	0.095	25	0.156	2	0.217	0	0.278	0
0.035	625	0.096	23	0.157	4	0.218	0	0.279	0
0.036	629	0.097	29	0.158	2	0.219	0	0.28	0
0.037	552	0.098	17	0.159	0	0.22	0	0.281	0
0.038	571	0.099	21	0.16	0	0.221	0	0.282	0
0.039	458	0.1	15	0.161	0	0.222	0	0.283	0
0.040	504	0.101	22	0.162	1	0.223	0	0.284	0
0.041	408	0.102	8	0.163	1	0.224	0	0.285	0
0.042	480	0.103	15	0.164	0	0.225	0	0.286	0
0.043	385	0.104	14	0.165	1	0.226	0	0.287	0
0.044	392	0.105	12	0.166	0	0.227	0	0.288	0
0.045	354	0.106	14	0.167	1	0.228	0	0.289	0
0.046	365	0.107	13	0.168	2	0.229	0	0.29	0
0.047	339	0.108	13	0.169	2	0.23	0	0.291	0
0.048	307	0.109	15	0.17	0	0.231	0	0.292	0
0.049	285	0.11	12	0.171	1	0.232	0	0.293	0
0.05	291	0.111	9	0.172	1	0.233	0	0.294	0
0.051	242	0.112	9	0.173	0	0.234	0	0.295	0
0.052	269	0.113	11	0.174	0	0.235	0	0.296	0
0.053	228	0.114	8	0.175	0	0.236	0	0.297	0
0.054	241	0.115	5	0.176	0	0.237	0	0.298	0
0.055	194	0.116	8	0.177	0	0.238	0	0.299	0
0.056	189	0.117	4	0.178	1	0.239	0	0.3	0
0.057	197	0.118	10	0.179	0	0.24	0	0.301	0
0.058	195	0.119	1	0.18	0	0.241	0	0.302	0
0.059	182	0.12	9	0.181	0	0.242	0	0.303	0
0.06	180	0.121	5	0.182	0	0.243	0	0.304	0
0.061	151	0.122	2	0.183	0	0.244	0	0.305	0

Appendix 4: American Wire Gauge Table

AWG gauge	Conductor Diameter Inches	Conductor Diameter mm	Ω s per 1000 ft.	Ω s per km	Maximum amps for chassis wiring	Maximum amps for power transmission
0000	0.46	11.684	0.049	0.16072	380	302
000	0.4096	10.40384	0.0618	0.202704	328	239
00	0.3648	9.26592	0.0779	0.255512	283	190
0	0.3249	8.25246	0.0983	0.322424	245	150
1	0.2893	7.34822	0.1239	0.406392	211	119
2	0.2576	6.54304	0.1563	0.512664	181	94
3	0.2294	5.82676	0.197	0.64616	158	75
4	0.2043	5.18922	0.2485	0.81508	135	60
5	0.1819	4.62026	0.3133	1.027624	118	47
6	0.162	4.1148	0.3951	1.295928	101	37
7	0.1443	3.66522	0.4982	1.634096	89	30
8	0.1285	3.2639	0.6282	2.060496	73	24
9	0.1144	2.90576	0.7921	2.598088	64	19
10	0.1019	2.58826	0.9989	3.276392	55	15
11	0.0907	2.30378	1.26	4.1328	47	12
12	0.0808	2.05232	1.588	5.20864	41	9.3
13	0.072	1.8288	2.003	6.56984	35	7.4
14	0.0641	1.62814	2.525	8.282	32	5.9
15	0.0571	1.45034	3.184	10.44352	28	4.7
16	0.0508	1.29032	4.016	13.17248	22	3.7
17	0.0453	1.15062	5.064	16.60992	19	2.9
18	0.0403	1.02362	6.385	20.9428	16	2.3
19	0.0359	0.91186	8.051	26.40728	14	1.8
20	0.032	0.8128	10.15	33.292	11	1.5
21	0.0285	0.7239	12.8	41.984	9	1.2
22	0.0254	0.64516	16.14	52.9392	7	0.92
23	0.0226	0.57404	20.36	66.7808	4.7	0.729
24	0.0201	0.51054	25.67	84.1976	3.5	0.577
25	0.0179	0.45466	32.37	106.1736	2.7	0.457
26	0.0159	0.40386	40.81	133.8568	2.2	0.361
27	0.0142	0.36068	51.47	168.8216	1.7	0.288
28	0.0126	0.32004	64.9	212.872	1.4	0.226
29	0.0113	0.28702	81.83	268.4024	1.2	0.182
30	0.01	0.254	103.2	338.496	0.86	0.142
31	0.0089	0.22606	130.1	426.728	0.7	0.113
32	0.008	0.2032	164.1	538.248	0.53	0.091
33	0.0071	0.18034	206.9	678.632	0.43	0.072
34	0.0063	0.16002	260.9	855.752	0.33	0.056
35	0.0056	0.14224	329	1079.12	0.27	0.044
36	0.005	0.127	414.8	1360	0.21	0.035
37	0.0045	0.1143	523.1	1715	0.17	0.0289
38	0.004	0.1016	659.6	2163	0.13	0.0228
39	0.0035	0.0889	831.8	2728	0.11	0.0175
40	0.0031	0.07874	1049	3440	0.09	0.0137

Source: http://www.powerstream.com/Wire_Size.htm


Appendix 5: Misumi South East Asia Gear Catalogue

Spur Gears

-Pressure Angle 20° Module 0.5-

CAD Data Folder Name: 19_Gears

*All prices are in S\$ and subjected to change without prior notice



Type	Material	Surface Treatment	Accessory
Straight Bore	S45C	Blackening Electroless Nickel Plating	Set Screw *Except Straight Bore Type.
Straight Bore+Tap			
GEABN			
GEABB	Free Cutting Brass Bar		
GEABG			
GEAHS	SUS304		

Shaft Bore Specifications

Straight Bore	Straight Bore+Tap

⊗ Straight Bore + Tap is not applicable to A Shape.

Gear Shape

KShape

AShape

BShape

Accuracy JSB 1702 (Class 4)

For alterations on tooth width and hub dimensions, refer P.1241

Part Number	No. of Teeth	B	Gears Shape	Shaft Bore Dia. P _{IT} 1mm Increment	d	D	H	L	E ₁	E ₂	M (Coarse Thread)	* Allowable Transmission Force (N) Sending Strength			Unit Price				
												S45C	Free-cutting Brass Bar	SUS304	Straight Bore	GEABN (P.1) GEABB (P.1) GEABG (P.2)	GEAB	GEABS	
Straight Bore GEAHS	15	8	K	3-5	7.5	8.5	9	18	10	3	M3	0.72	0.16	0.41	13.32	14.28	14.28	14.28	
	16				8	9						0.79	0.17	0.45	14.28	15.24	15.24	15.80	
	18				9	10						10	0.95	0.21	0.54	14.76	15.72	15.72	17.17
	20				10	11						11	1.12	0.24	0.64	16.36	17.33	17.33	18.77
	24				12	13						8.5	0.42	0.09	0.24	13.80	14.76	14.76	18.77
	25				12	13							0.54	0.12	0.31	14.28	15.24	15.24	21.66
	26	12.5	13.5	0.58	0.13	0.33	14.60	15.56	15.56	22.62									
	28	13	14	0.61	0.13	0.35	14.76	15.72	15.72	23.58									
	29	14	15	0.68	0.15	0.39	14.92	15.88	15.88	24.55									
	30	15	16	0.74	0.16	0.42	16.36	17.33	17.33	26.15									
	Straight Bore+Tap GEABN GEABB GEABG GEAB GEABS	35	3	A	3-6 or 6.35	16	17	10	8	5		2.5	0.80	0.17	0.46	14.60	15.56	15.56	15.56
		36				17.5	18.5						0.91	0.20	0.52	15.24	16.20	16.20	16.20
38		18				19	0.94				0.20		0.54	15.40	16.36	16.36	16.36		
40		20				21	0.72				0.16		0.41	17.49	18.45	18.45	18.45		
42		21				22	0.76				0.17		0.43	19.25	20.22	20.22	21.50		
45		22.5				23.5	0.83				0.18		0.48	19.25	20.22	20.22	24.55		
48		24	25	0.90	0.20	0.51	19.25	20.22	20.22	25.51									
50		25	26	0.95	0.21	0.54	19.57	20.54	20.54	26.31									
*52		26	27	0.99	0.22		19.89	20.86	20.86										
*60		30	31	1.18	0.26		21.86	22.62	22.62										
*70		35	36	1.42	0.31		25.03	25.99	25.99										
*80		40	41	1.65	0.36		26.31	27.27	27.27										
*100	50	51	2.13	0.46		38.83	39.79	39.79											
*120	60	61	2.58	0.56		43.48	44.44	44.44											

* marked No. of teeth is not available for GEABS. ⊗ Shaft Bore Diameter 6.35 is available.

* Allowable Transmission Forces in the table are reference values calculated with prescribed conditions. For conditions, refer P.1222

⊗ For the price of GEABB, multiply the unit price in the table by 1.1.

⊗ For the price of GEABG, multiply the unit price in the table by 1.2. (Round down to the nearest cent.)

⊗ When tooth shape is not specified, No. of teeth 15-20 (B-B) will be K shape, 20 (B-B)-120 will be B shape.

Order Estimate

Part Number - **K** - **B** - **Teeth** - **P**

GEABN 0.5 - 20 - 3 - B - 3

GEAHS 0.5 - 30 - 3 - A - 5

GEABS 0.5 - 15 - 8 - K - 5

⊗ A flat charge of S\$21.56 for 3 or more identical pieces

Keys to Ship

5 Days

Express A S\$8.02/piece

PS8

Price

Volume Discount Rate

Quantity	1-3	10-12	13-14	15-20
Rate	1st Price	5%	10%	15%

⊗ Round down to the nearest one cent. P.87

Revisions

Part Number	Rev	B	P	(KC90, KTC...etc)
GEAHS 0.5	02	3	A	5 - KC120
GEABS 0.5	02	3	A	5 - KFC15-K3.0

Alterations Code	Set Screw	Side Through Holes	Female Thread Hole Dimensions	
	KC90	KC120	KFC / KTC	
			TPC	
Spec.	<p>Adds another set screw at position 90°.</p> <p>⊗ Applicable to B shape only.</p> <p>⊗ Not applicable to Straight Bore Type.</p>	<p>Adds another set screw at position 120°.</p> <p>⊗ Applicable to B shape only.</p> <p>⊗ Not applicable to Straight Bore Type.</p>	<p>Machines through holes on the side surface (KFC / KTC: 1mm increment; 0.5mm increment)</p> <p>⊗ Applicable to A shape only.</p> <p>⊗ P-K-A-KFC(KTC)-01-K-4</p> <p>K Selection K3.0-K6.0 Options/Note KFC15-K3.5 KTC</p>	<p>Changes the tapped hole dimension to M4.</p> <p>Options/Note TPC4</p> <p>⊗ Applicable to B shape only.</p> <p>⊗ Not applicable to Straight Bore Type.</p>
Price Adder	3.21	3.21	11.23	
			Free of Charge	



Round Rack Gears / Worm / Worm Wheel

- L Dimension Standard / L Configurable Pressure Angle 20° -

CAD Data Folder Name: 19_Gears

*All prices are in \$S and subjected to change without prior notice

Round Rack Gears

RoHS

Type		Material	Surface Treatment
L Dimension Fixed	L Dimension Configurable		
RGMA	RGMAL	S45C	Blackening
RGMAS	RGMASL	SUS303	-

Precision RGMA / RGMAL JIS B1702 Class 4
RGMAS / RGMASL JIS B1702 Class 5

L Dimension Fixed								L Dimension Configurable								
Part Number Type	Module	Number	Pitch Circle Dia. (mm)	D (mm)	(L)	h	Unit Price	Part Number Type	Module	Fall Length from Increment	D (mm)	h	Unit Price			
													L50-99	L100-199	L200-300	L301-500
RGMA (S45C)	0.5	300	192	8	301.6	7.5	90.66	RGMAL (S45C)	0.5	50-300	8	7.5	74.77	84.23	97.07	-
		300	120		7.2	91.13	75.25						84.71	97.55	-	
	1.0	300	95	10	298.4	9	73.96		1.0	10	9	61.13	68.83	80.38	124.98	
		500	159		499.5	119.57	77.01									84.71
	1.5	300	63	15	300	13.5	82.15		1.5	15	13.5	89.31	77.01	84.71	132.94	
		500	106		500	125.14	82.15									88.56
	2.0	300	47	20	300	18	98.19		2.0	20	18	75.73	82.15	88.56	142.79	
		500	79		500	136.37	98.19									104.61
	2.5	300	38	25	300	22.5	162.37		2.5	25	22.5	91.77	98.19	104.61	168.78	
		500	63		500	162.37	116.32									122.74
	3.0	300	31	30	300	27	116.32		3.0	30	27	109.90	116.32	122.74	196.96	
		500	53		500	190.44	141.19									158.84
RGMAS (SUS303)	0.5	300	192	8	301.6	7.5	170.67	RGMASL (SUS303)	0.5	50-300	8	7.5	141.19	158.84	177.29	-
		300	120		7.2	142.31	117.60						132.36	148.25	-	
	1.0	300	95	10	298.4	9	170.22		1.0	10	9	91.13	102.52	116.64	176.16	
		500	159		499.5	168.75	91.13									102.52
	1.5	300	63	15	300	13.5	119.85		1.5	15	13.5	107.01	113.75	120.33	193.33	
		500	106		500	180.50	107.01									113.75
	2.0	300	47	20	300	18	126.43		2.0	20	18	120.01	126.43	132.94	206.97	
		500	79		500	200.55	120.01									126.43
	2.5	300	38	25	300	22.5	210.50		2.5	25	22.5	125.95	132.36	138.78	216.91	
		500	63		500	210.50	125.95									132.36
	3.0	300	31	30	300	27	170.39		3.0	30	27	163.97	170.39	176.80	277.08	
		500	53		500	270.66	163.97									170.39

Order Example: Part Number - Length L
RGMA1.0 - 500
RGMAL0.8 - 205

Days to Ship: 5 Days Express A 288.00/piece per P88

Price: Volume Discount Rate (Round down to the nearest one cent.) P87

Alterations: Part Number - Length L - (MC / WMC)
RGMA1.0 - 500 - MC5

Alterations Code	One End Female Thread	Both Ends Female Thread																								
	MC	WMC																								
Spec.	<table border="1" style="font-size: x-small;"> <tr><th>Ordering Code</th><th>MC5</th></tr> <tr><th>Module</th><th>M Selection</th></tr> <tr><td>0.5</td><td>3 4 5</td></tr> <tr><td>0.8</td><td>3</td></tr> <tr><td>1.0</td><td>4 5</td></tr> <tr><td>1.5-3.0</td><td>4 5 6</td></tr> </table>	Ordering Code	MC5	Module	M Selection	0.5	3 4 5	0.8	3	1.0	4 5	1.5-3.0	4 5 6	<table border="1" style="font-size: x-small;"> <tr><th>Ordering Code</th><th>WMC5</th></tr> <tr><th>Module</th><th>M Selection</th></tr> <tr><td>0.5</td><td>3 4 5</td></tr> <tr><td>0.8</td><td>3</td></tr> <tr><td>1.0</td><td>4 5</td></tr> <tr><td>1.5-3.0</td><td>4 5 6</td></tr> </table>	Ordering Code	WMC5	Module	M Selection	0.5	3 4 5	0.8	3	1.0	4 5	1.5-3.0	4 5 6
Ordering Code	MC5																									
Module	M Selection																									
0.5	3 4 5																									
0.8	3																									
1.0	4 5																									
1.5-3.0	4 5 6																									
Ordering Code	WMC5																									
Module	M Selection																									
0.5	3 4 5																									
0.8	3																									
1.0	4 5																									
1.5-3.0	4 5 6																									
Price Adder	6.42	12.84																								

Worm

RoHS

WGEAU

Material: S45C
Tooth Surface Hardness: 12HRC or less
Accuracy Class: JIS B 1702 Class 4 or equivalent (Tooth Surface Finish: Rolled)

Surface Treatment: Blackening
Accessory: Set Screw M4

Worm Wheel

RoHS

WGEAH

Material: Phosphor Bronze (CAS502)
Accuracy Class: JIS B 1702 Class 4 or equivalent (Tooth Surface: Machined)

Worm										Worm Wheel		
Part Number Type	Module	Number of Starts	Shaft Bore Dia. P11 Straight Bore-Top	Twisting Direction	Advance Angle	d	D	L	ℓ	Unit Price 1 - 5 pcs.	Backlash (mm)	Reduction Rate
WGEAU	0.8	1	6	R (Right)	3°17'	14	15.6	30	5	8.34	0.04-0.22	1/10
		2	6		6°54'	19	1.89	1/20				
	1.0	1	6		3°35'	16	18	32	5	8.50		1/15
		2	6	7°11'					8.66	1/40		

Worm Wheel											
Part Number Type	Module	No. of Teeth	Shaft Bore Dia. P11 Straight Bore	Teeth Width	d	D	B	H	ℓ	Unit Price 1 - 5 pcs.	
WGEAH	0.8	20	2	5	16.11	17.6	12			15	0.86
		30	1	5	24.04	25.6	18			19	1.89
		40	1	6	24.16	25.6	9	18	9	19	1.87
		50	1	8	32.05	33.8	20			23	3.24
		50	1	8	40.06	41.8	25			27	4.90
WGEAH	1.0	20	2	6	20.05	23	16			18	1.58
		30	1	6	20.16	23	16			18	1.54
		40	1	9	30.07	33	10	20	10	23	3.38
		50	1	9	30.24	33	20			23	3.35
		50	1	9	40.06	43	26			28	5.79
		50	1	9	50.10	53	30		33	8.76	

Order Example: Part Number - No. of Teeth - Shaft Bore Dia. P11 - Teeth Width - Hardness
WGEAU1.0 - 20 - 1 - 6 - R
WGEAH1.0 - 20 - 2 - 6 - R

Days to Ship: 7 Days

*For orders larger than indicated quantity, please request a quotation.

*For orders larger than indicated quantity, please request a quotation.

Appendix 6: Ring Magnet Sources

OD mm	ID mm	T mm	Price SGD	Type	Source
12.7000	3.1750	1.5875	0.76		Ebay
12.7000	3.1750	3.1750	1.84	N48	Ebay
12.7000	6.3500	3.1750	1.84	N48	Ebay
19.0500	3.1750	3.1750	2.76	N48	Ebay
19.0500	12.7000	3.1750	2.25	N42	Ebay
19.0500	3.1750	4.7625	3.72	N38	Ebay
19.0500	7.9375	4.7625	2.48	N48	Ebay
15.0000	5.0000	5.0000	3.24	N48	Ebay
15.0000	10.0000	5.0000	2.89	N48	Ebay
12.7000	6.3500	6.3500	2.32	N48	Ebay
19.0500	3.1750	6.3500	2.69	N48	Ebay
19.0500	6.3500	6.3500	6.72	N48	Ebay
19.0500	12.7000	6.3500	3.84	N48	Ebay
25.4000	6.3500	6.3500	24.86	N48	Ebay
25.4000	12.7000	6.3500	26.74	N48	Ebay
38.1000	6.3500	6.3500	29.58	N48	Ebay
38.1000	12.7000	6.3500	29.58	N48	Ebay
50.8000	12.7000	6.3500	40.59	N48	Ebay
50.8000	25.4000	6.3500	39.33	N48	Ebay
6.3500	3.1750	12.7000	1.13	N42	Ebay
50.8000	25.4000	25.4000	108.99	N48	Ebay
12.7000	3.1750	3.1750	1.45	N52	kjmagnetics
19.0500	6.3500	6.3500	5.00	N52	kjmagnetics
25.4000	7.9375	6.3500	8.54	N52	kjmagnetics
25.4000	4.9530	12.7000	17.00	N52	kjmagnetics
19.0500	6.3500	19.0500	13.62	N52	kjmagnetics
12.0000	7.0000	3.0000	1.45	N50	Lifton magnets
20.0000	6.0000	6.0000	5.90	N50	Lifton magnets
20.0000	10.0000	6.0000	5.68	N50	Lifton magnets
50.0000	25.0000	6.0000	23.09	N50	Lifton magnets
20.0000	10.0000	10.0000	9.21	N50	Lifton magnets
22.0000	4.0000	22.0000	18.55	N50	Lifton magnets
6.0000	2.0000	3.0000	7.22	N42	Misumi
8.0000	3.0000	3.0000	6.74	N42	Misumi
8.0000	4.0000	3.0000	6.74	N42	Misumi
10.0000	3.0000	3.0000	7.22	N42	Misumi
10.0000	4.0000	3.0000	7.22	N42	Misumi
10.0000	5.0000	3.0000	7.22	N42	Misumi
10.0000	6.0000	3.0000	7.22	N42	Misumi
12.0000	4.0000	3.0000	7.86	N42	Misumi
12.0000	5.0000	3.0000	7.86	N42	Misumi
12.0000	6.0000	3.0000	7.86	N42	Misumi
12.0000	8.0000	3.0000	7.86	N42	Misumi
14.0000	6.0000	3.0000	8.34	N42	Misumi
14.0000	8.0000	3.0000	8.34	N42	Misumi
18.0000	6.0000	3.0000	9.15	N42	Misumi
18.0000	8.0000	3.0000	9.15	N42	Misumi
18.0000	12.0000	3.0000	9.15	N42	Misumi
20.0000	6.0000	3.0000	9.47	N42	Misumi
20.0000	8.0000	3.0000	9.47	N42	Misumi
20.0000	10.0000	3.0000	9.47	N42	Misumi
20.0000	12.0000	3.0000	9.47	N42	Misumi
25.0000	6.0000	3.0000	12.84	N42	Misumi
25.0000	8.0000	3.0000	12.84	N42	Misumi
25.0000	10.0000	3.0000	12.84	N42	Misumi
25.0000	12.0000	3.0000	12.84	N42	Misumi
8.0000	3.0000	5.0000	7.38	N42	Misumi
8.0000	4.0000	5.0000	7.38	N42	Misumi
10.0000	3.0000	5.0000	7.86	N42	Misumi
10.0000	5.0000	5.0000	7.86	N42	Misumi
10.0000	6.0000	5.0000	7.86	N42	Misumi
12.0000	4.0000	5.0000	8.66	N42	Misumi
12.0000	6.0000	5.0000	8.66	N42	Misumi
12.0000	8.0000	5.0000	8.66	N42	Misumi
14.0000	6.0000	5.0000	9.15	N42	Misumi
14.0000	8.0000	5.0000	9.15	N42	Misumi
20.0000	6.0000	5.0000	11.23	N42	Misumi
20.0000	12.0000	5.0000	11.23	N42	Misumi
25.0000	6.0000	5.0000	15.40	N42	Misumi
25.0000	12.0000	5.0000	15.40	N42	Misumi
30.0000	12.0000	5.0000	17.01	N42	Misumi
11.4000	10.0000	2.0000	3.17	N50	Supemagnet man
12.7000	6.3500	1.0000	1.28	N50	Supemagnet man
6.2000	2.1000	2.2000	0.61	N52	Supemagnet man
19.0000	12.0000	3.0000	4.58	N52	Supemagnet man
6.3500	3.1700	3.1700		N45	Supemagnet man
9.5200	6.3500	3.1750	1.65	N50	Supemagnet man
6.0000	3.1000	5.0000		N52	Supemagnet man
19.0500	12.7000	5.0000		N50	Supemagnet man
35.0000	25.0000	5.0000	15.56	N50	Supemagnet man
12.7000	6.3500	6.3500	1.71	N50	Supemagnet man
19.0400	9.5350	6.3500	6.10	N50	Supemagnet man
45.0000	35.0000	8.0000		N50	Supemagnet man

Appendix 7: Ansys Magnetostatic Analysis Linear Plot Data (Ebay.com Magnet)

Distance (mm)	Magnetic Field Intensity (mT)	Distance (mm)	Magnetic Field Intensity (mT)
0	688.12	16.032	193.54
0.31436	815.97	16.347	257.24
0.62871	958.14	16.661	351.71
0.94307	1017.3	16.975	456.74
1.2574	1014	17.29	569.17
1.5718	1003.8	17.604	688.28
1.8861	1003.5	17.918	844.41
2.2005	992.45	18.233	1007.3
2.5149	957.49	18.547	1182.4
2.8292	895.01	18.861	1324.6
3.1436	810.84	19.176	1456.1
3.4579	719.86	19.49	1551.2
3.7723	603.2	19.804	1607.9
4.0866	508.29	20.119	1660.5
4.401	412.33	20.433	1687
4.7153	318.02	20.748	1685
5.0297	240.36	21.062	1680.7
5.3441	185.31	21.376	1654
5.6584	160.02	21.691	1587.5
5.9728	174.58	22.005	1505
6.2871	222.1	22.319	1371.2
6.6015	293.97	22.634	1233.6
6.9158	373.72	22.948	1090.3
7.2302	459.1	23.262	949.43
7.5446	557.5	23.577	819.52
7.8589	666.11	23.891	698.52
8.1733	797.65	24.205	590.69
8.4876	939.15	24.52	485.33
8.802	1095.3	24.834	391.29
9.1163	1238.2	25.149	304.97
9.4307	1362.3	25.463	227.03
9.745	1497.7	25.777	171.28
10.059	1587.6	26.092	143.18
10.374	1667.8	26.406	166.71
10.688	1690	26.72	233.08
11.002	1696.2	27.035	315.89
11.317	1694.9	27.349	409.38
11.631	1669.6	27.663	515.76
11.946	1621.7	27.978	629.29
12.26	1570	28.292	736.84
12.574	1435.6	28.606	822.63
12.889	1285.4	28.921	896.25
13.203	1134.7	29.235	935.86
13.517	976.05	29.55	963.76
13.832	832.14	29.864	995.62
14.146	692.5	30.178	1012.5
14.46	564.86	30.493	1021.7
14.775	444.86	30.807	1016.9
15.089	337.82	31.121	956.31
15.403	251.69	31.436	810.43
15.718	194.36	31.75	675.01
Average			1564.5625


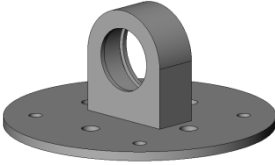
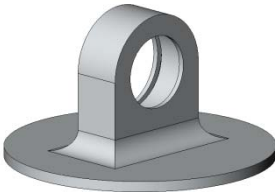


Appendix 8: Ansys Magnetostatic Analysis Linear Plot Data (Ebay.com Magnet)

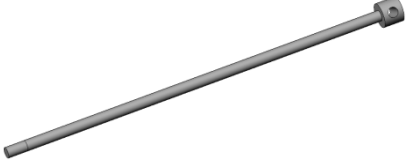



Distance (mm)	Magnetic Field Intensity (mT)	Distance (mm)	Magnetic Field Intensity (mT)
0	696.69	15.149	187.75
0.29703	971.41	15.446	260.31
0.59406	1169.5	15.743	363.77
0.89109	1331.5	16.04	484.82
1.1881	1332.6	16.337	632.5
1.4851	1330.4	16.634	785.5
1.7822	1334.2	16.931	963.01
2.0792	1325.8	17.228	1169.2
2.3762	1293.5	17.525	1384.4
2.6733	1217.4	17.822	1623.5
2.9703	1078.6	18.119	1810.9
3.2673	926.52	18.416	1983.6
3.5644	752.39	18.713	2074.7
3.8614	601.36	19.01	2098.8
4.1584	464.79	19.307	2108.9
4.4554	351.9	19.604	2099.1
4.7525	268.15	19.901	2090.3
5.0495	208.19	20.198	2099.3
5.3465	188.56	20.495	2020.6
5.6436	209.44	20.792	1867.6
5.9406	260.16	21.089	1710
6.2376	330.49	21.386	1486.5
6.5347	422.4	21.683	1287.7
6.8317	520.43	21.98	1092.5
7.1287	631.51	22.277	924.08
7.4257	776.19	22.574	774.46
7.7228	924.06	22.871	627.98
8.0198	1092.5	23.168	516.56
8.3168	1287.7	23.465	422.43
8.6139	1486.5	23.762	333.74
8.9109	1710	24.059	263.07
9.2079	1867.6	24.356	210.26
9.505	2020.6	24.653	188.55
9.802	2099.4	24.95	208.19
10.099	2090.4	25.248	268.13
10.396	2099.1	25.545	351.87
10.693	2108.7	25.842	464.73
10.99	2098.6	26.139	601.29
11.287	2074.5	26.436	752.32
11.584	1983.5	26.733	926.44
11.881	1810.8	27.03	1078.6
12.178	1623.5	27.327	1217.3
12.475	1384.4	27.624	1293.4
12.772	1169.3	27.921	1325.7
13.069	962.99	28.218	1334.2
13.366	785.47	28.515	1330.3
13.663	632.46	28.812	1332.7
13.96	484.79	29.109	1331.5
14.257	363.74	29.406	1149.5
14.554	260.28	29.703	927.09
14.851	187.74	30	634.72
		Average	1965.58

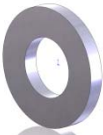
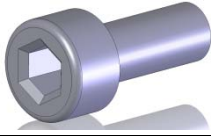
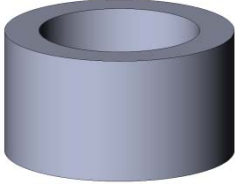
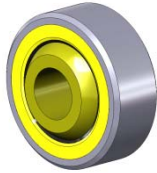




Appendix 9: Ansys Magnetostatic Analysis Linear Plot Data (No Wire Coil Housing)

Distance (mm)	Magnetic Field Intensity (mT)
0.00000	544.52
0.66146	629.86
1.32290	667.22
1.98440	675.57
2.64580	654.14
3.30730	554.98
3.96880	427.84
4.63020	337.17
5.29170	286.96
5.95310	303.87
6.61460	369.03
7.27600	480.42
7.93750	620.29
8.59900	818.80
9.26040	1068.30
9.92190	1279.20
10.58300	1355.80
11.24500	1388.20
11.90600	1355.20
12.56800	1216.20
13.22900	964.27
13.89100	681.05
14.55200	505.67
15.21400	363.50
15.87500	297.58
16.53600	353.81
17.19800	495.26
17.85900	704.88
18.52100	960.55
19.18200	1241.40
19.84400	1363.50
20.50500	1365.20
21.16700	1356.00
21.82800	1265.50
22.49000	1054.60
23.15100	830.61
23.81300	631.02
24.47400	457.68
25.13500	365.72
25.79700	298.99
26.45800	290.12
27.12000	348.26
27.78100	438.09
28.44300	557.04
29.10400	663.67
29.76600	689.99
30.42700	672.63
31.08900	637.59
31.75000	547.82

Appendix 10: Bill of Materials for Electromagnetic Damper

No.	Part Name	CAD Picture	QTY.
1	Outer Casing		1
2	Upper Bearing Mount		1
3	Lower Bearing Mount		1
4	Outer Spacer 50.8 x 25.4 x 3.175		12
5	Outer Magnet 50.8 x 25.4 x 6.35		11
6	Inner Spacer 19.05 x 3.175 x 3.175		11
7	Inner Magnet 19.05 x 3.175 x 6.35		11
8	Inner Bushing		1

9	Wire Coil Housing		1
10	Center Magnet Bolt		1
11	Inner Spacer 17 x 3.175 x 3.175		1
12	Inner Bushing Central		1
13	RTWN52		2
14	Rebound Case		1
15	RTWN60		2
16	Outer Bushing		1

17	12 Washer M4(small)		4
18	12 SOC M4X 10		4
19	Compression Stop Bushing		1
20	COM M6T		2
21	Clockwise Coil - Small		6
22	Anticlockwise Coil - Small		6
23	Clockwise Coil - Small - Outer		6
24	Anticlockwise Coil - Small - Outer		6

Appendix 11: N4004 Diode Datasheet

1N4001 THRU 1N4007

1.0 AMP. Silicon Rectifiers



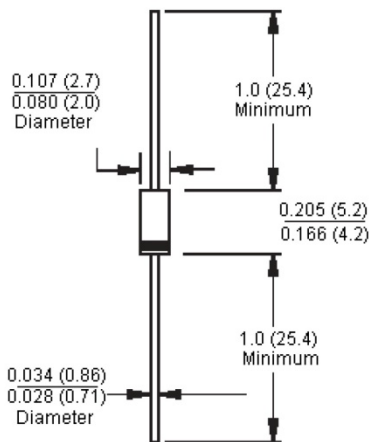
Features:

- Low forward voltage drop.
- High current capability.
- High reliability.
- High surge current capability.



Voltage Range
50 to 1300 Volts
Current
1.0 Ampere

DO-41



Dimensions : Inches (Millimetres)

Mechanical Data:

Cases	: Moulded plastic.
Epoxy	: Rate flame retardant.
Lead	: Axial leads, solderable per MIL-STD-202, method 208 guaranteed.
Polarity	: Colour band denotes cathode end.
High temperature soldering guaranteed	: 260°C/10 second/0.375 inches, (9.5mm) lead lengths at 5lbs., (2.3kg) tension.

<http://www.farnell.com>
<http://www.newark.com>
<http://www.cpc.co.uk>



1N4001 THRU 1N4007

1.0 AMP. Silicon Rectifiers



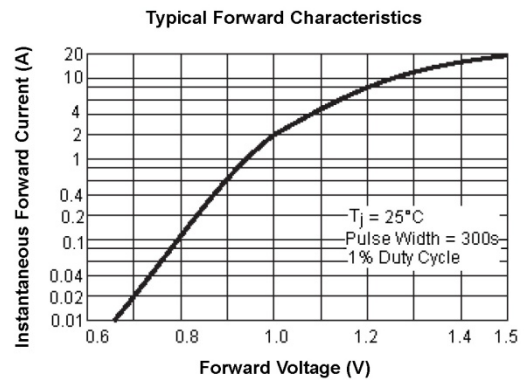
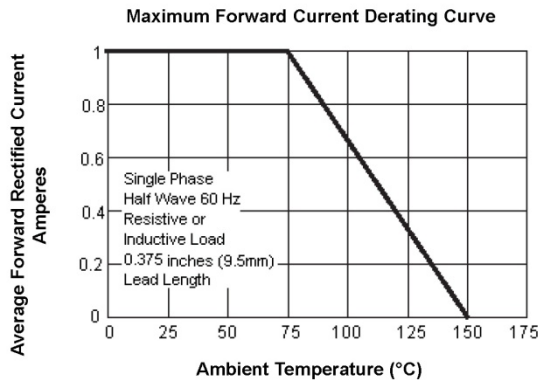
Maximum Ratings and Electrical Characteristics:

Rating at 25°C ambient temperature unless otherwise specified.
 Single phase, half wave, 60Hz, resistive or inductive load.
 For capacitive load, derate current by 20%.

Type Number	Symbol	1N4001	1N4002	1N4003	1N4004	1N4005	1N4006	1N4007	Units
Maximum recurrent peak reverse voltage	V_{RRM}	50	100	200	400	600	800	1000	V
Maximum RMS voltage	V_{RMS}	35	70	140	280	420	560	700	
Maximum DC blocking voltage	V_{DC}	50	100	200	400	600	800	1000	
Maximum average forward rectified current 0.375 Inches (9.5mm) lead length at $T_A = 75^\circ\text{C}$	$I_{(AV)}$	1.0							A
Peak forward surge current, 8.3ms single half sine-wave superimposed on rated load (JEDEC method)	I_{FSM}	30							
Maximum instantaneous forward voltage at 1.0A	V_F	1.0							V
Maximum DC reverse current at $T_A = 25^\circ\text{C}$ at rated DC blocking voltage at $T_A = 100^\circ\text{C}$	I_R	5.0 50							μA
Maximum full load reverse current, full cycle average 0.375 inches (9.5mm) lead length at $T_A = 75^\circ\text{C}$	HT_{IR}	30							μA
Typical junction capacitance (Note 1)	C_j	10							pF
Typical thermal resistance (Note 2)	$R\theta_{JA}$	65							$^\circ\text{C}/\text{W}$
Operating and storage temperature range	T_J, T_{STG}	-65 to +150							$^\circ\text{C}$

Note: 1. Measured at 1MHz and Applied Reverse Voltage of 4.0 Volts DC
 2. Mount on Cu-Pad Size 5 x 5mm on PCB.

Ratings and Characteristic Curves (1N4001)



<http://www.farnell.com>
<http://www.newark.com>
<http://www.cpc.co.uk>



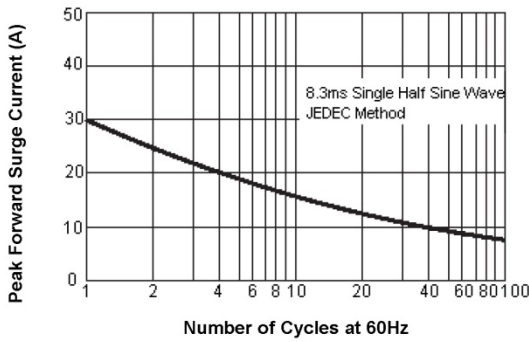
1N4001 THRU 1N4007

1.0 AMP. Silicon Rectifiers

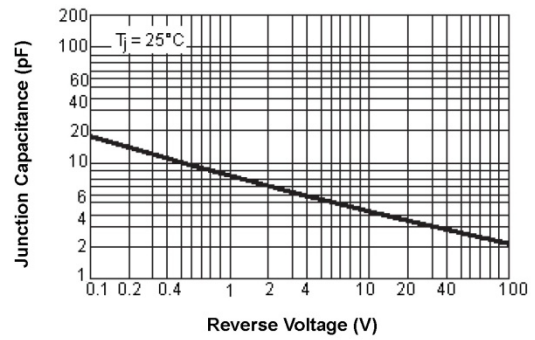


Ratings and Characteristic Curves (1N4001)

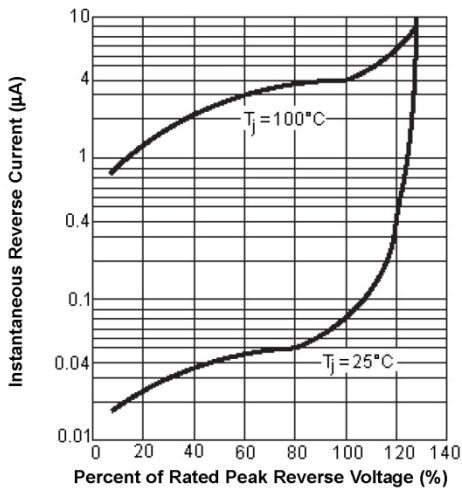
Maximum Non-Repetitive Forward Surge Current



Typical Junction Capacitance



Typical Reverse Characteristics



Disclaimer This data sheet and its contents (the "Information") belong to the Premier Farnell Group (the "Group") or are licensed to it. No licence is granted for the use of it other than for information purposes in connection with the products to which it relates. No licence of any intellectual property rights is granted. The Information is subject to change without notice and replaces all data sheets previously supplied. The Information supplied is believed to be accurate but the Group assumes no responsibility for its accuracy or completeness, any error in or omission from it or for any use made of it. Users of this data sheet should check for themselves the information and the suitability of the products for their purpose and not make any assumptions based on information included or omitted. Liability for loss or damage resulting from any reliance on the Information or use of it (including liability resulting from negligence or where the Group was aware of the possibility of such loss or damage arising) is excluded. This will not operate to limit or restrict the Group's liability for death or personal injury resulting from its negligence. SPC Multicom is the registered trademark of the Group. © Premier Farnell plc 2010.

<http://www.farnell.com>
<http://www.newark.com>
<http://www.cpc.co.uk>





Current Transducer LTS 25-NP

For the electronic measurement of currents : DC, AC, pulsed, mixed, with a galvanic isolation between the primary circuit (high power) and the secondary circuit (electronic circuit).

$$I_{PN} = 8 - 12 - 25 \text{ A}$$



Preliminary



Electrical data

I_{PN}	Primary nominal r.m.s. current	25	At
I_p	Primary current, measuring range	0 .. ± 80	At
V_{OUT}	Analog output voltage @ I_p	$2.5 \pm (0.625 \cdot I_p / I_{PN})$	V
	$I_p = 0$	2.5 ¹⁾	V
N_s	Number of secondary turns ($\pm 0.1\%$)	2000	
R_L	Load resistance	≥ 2	k Ω
R_M	Internal measuring resistance ($\pm 0.5\%$)	50	Ω
TCR_M	Thermal drift of R_M	< 50	ppm/K
V_C	Supply voltage ($\pm 5\%$)	5	V
I_C	Current consumption @ $V_C = 5$ V	Typ $20 + I_p^2 / (V_{OUT} \cdot R_L)$	mA
V_d	R.m.s. voltage for AC isolation test, 50/60 Hz, 1 mn	3	kV
V_s	R.m.s. rated voltage	525 ²⁾	V

Accuracy - Dynamic performance data

X	Accuracy @ $I_{PN}, T_A = 25^\circ\text{C}$	± 0.2	%
	Accuracy with R_M @ $I_{PN}, T_A = 25^\circ\text{C}$	± 0.7	%
ϵ_L	Linearity	< 0.1	%
TCV_{OUT}	Thermal drift of V_{OUT} @ $I_p = 0$	Typ 50	Max 100 ppm/K
TCE_G	Thermal drift of the gain	-10°C .. +85°C	50 ⁴⁾ ppm/K
V_{CM}	Residual voltage @ $I_p = 0$, after an overload of $3 \times I_{PN}$		± 0.5 mV
	$5 \times I_{PN}$		± 2.0 mV
	$10 \times I_{PN}$		± 2.0 mV
t_n	Reaction time @ 10 % of I_{PN}	< 50	ns
t_r	Response time @ 90 % of I_{PN}	< 200	ns
di/dt	di/dt accurately followed	> 100	A/ μ s
f	Frequency bandwidth (0 .. -0.5 dB)	DC .. 100	kHz
	(-0.5 .. -1 dB)	DC .. 200	kHz

General data

T_A	Ambient operating temperature	-10 .. +85	$^\circ\text{C}$
T_s	Ambient storage temperature	-25 .. +100	$^\circ\text{C}$
m	Mass	10	g
	Standards	EN 50178	

Notes : ¹⁾ Absolute value @ $T_A = 25^\circ\text{C}$, $2.475 < V_{OUT} < 2.525$
²⁾ Please see the operation principle on the other side
³⁾ Pollution class 2, Overvoltage category III
⁴⁾ Only due to TCR_M

Features

- Closed loop (compensated) multi-range current transducer using the Hall effect
- Unipolar voltage supply
- Insulated plastic case recognized according to UL 94-V0
- Compact design for PCB mounting
- Incorporated measuring resistance
- Extended measuring range.

Advantages

- Excellent accuracy
- Very good linearity
- Very low temperature drift
- Optimized response time
- Wide frequency bandwidth
- No insertion losses
- High immunity to external interference
- Current overload capability.

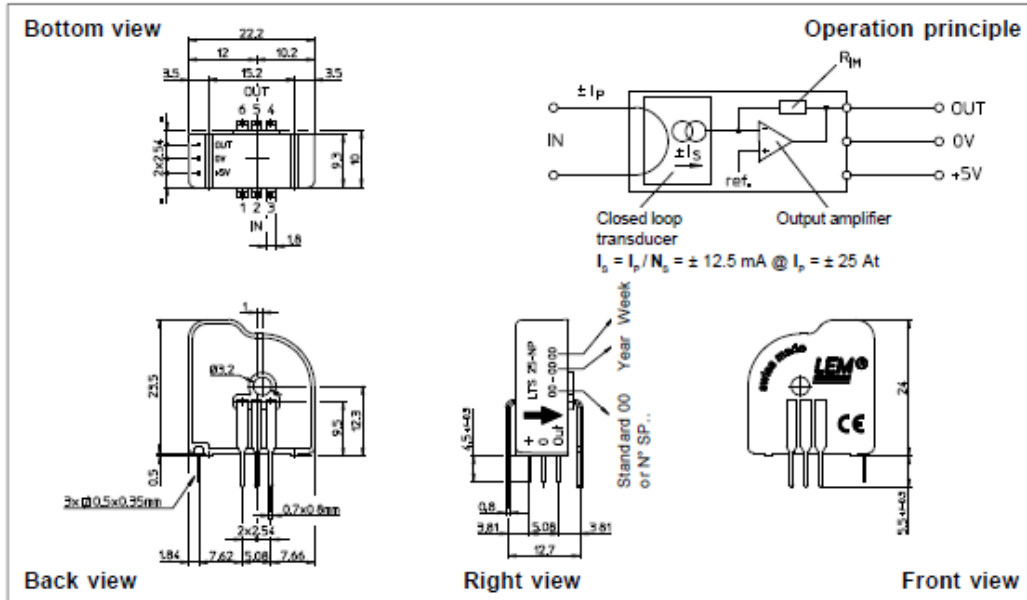
Applications

- AC variable speed drives and servo motor drives
- Static converters for DC motor drives
- Battery supplied applications
- Uninterruptible Power Supplies (UPS)
- Switched Mode Power Supplies (SMPS)
- Power supplies for welding applications.

Copyright protected.

990810/5

Dimensions LTS 25-NP (in mm. 1 mm = 0.0394 inch)



Number of primary turns	Primary nominal r.m.s. current I_{pN} [A]	Nominal output voltage V_{OUT} [V]	Primary resistance R_p [mΩ]	Primary insertion inductance L_p [μH]	Recommended connections
1	± 25	2.5 ± 0.625	0.18	0.013	
2	± 12	2.5 ± 0.600	0.81	0.05	
3	± 8	2.5 ± 0.600	1.62	0.12	

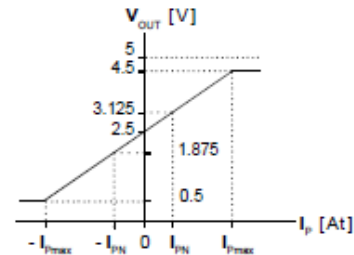
Mechanical characteristics

- General tolerance ± 0.2 mm
- Fastening & connection of primary 6 pins 0.7 x 0.8 mm
Recommended PCB hole 1.3 mm
- Fastening & connection of secondary 3 pins 0.5 x 0.35 mm
Recommended PCB hole 0.8 mm
- Additional primary through-hole ∅ 3.2 mm

Remark

- V_{OUT} is positive when I_p flows from terminals 1, 2, 3 to terminals 6, 5, 4

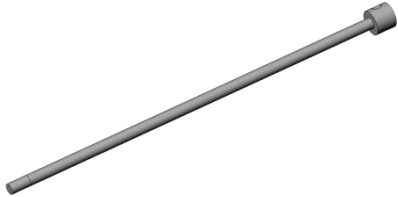
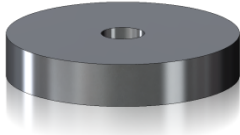
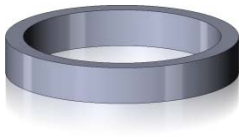


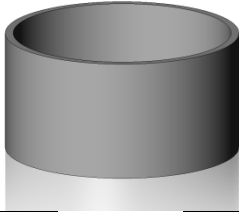
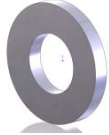
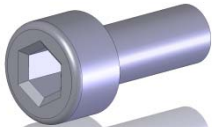
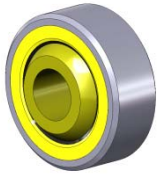
Output Voltage - Primary Current


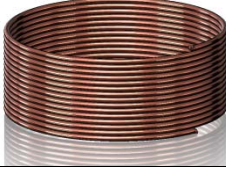

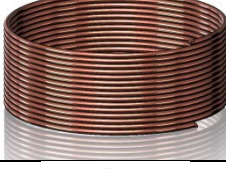

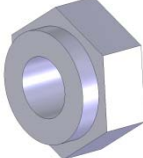
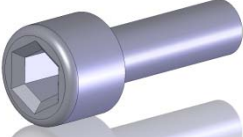
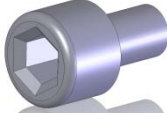


LEM reserves the right to carry out modifications on its transducers, in order to improve them, without previous notice.

Appendix 13: Bill of Materials for Electromagnetic Damper 2nd Design

No	Part Name	CAD Picture	Qty
1	Outer Casing		1
2	Upper Bearing Mount		1
3	Lower Bearing Mount		1
4	Outer Spacer 50.8 x 25.4 x 3.175		12
5	Outer Magnet 50.8 x 25.4 x 6.35		11
6	Inner Spacer 19.05 x 3.175 x 3.175		11
7	Inner Magnet 19.05 x 3.175 x 6.35		11
8	Inner Bushing		1
9	Wire Coil Housing		1

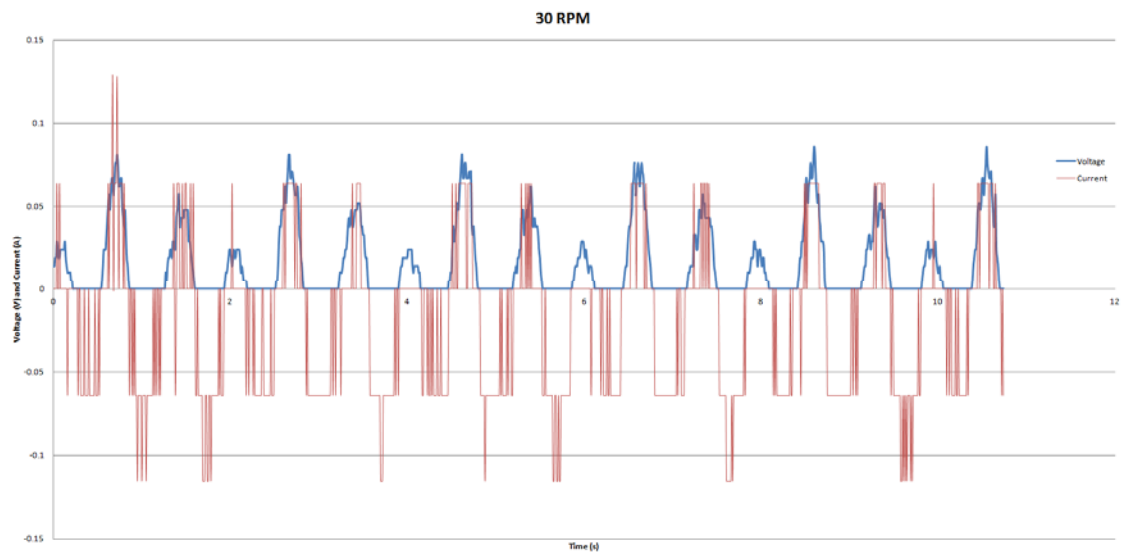
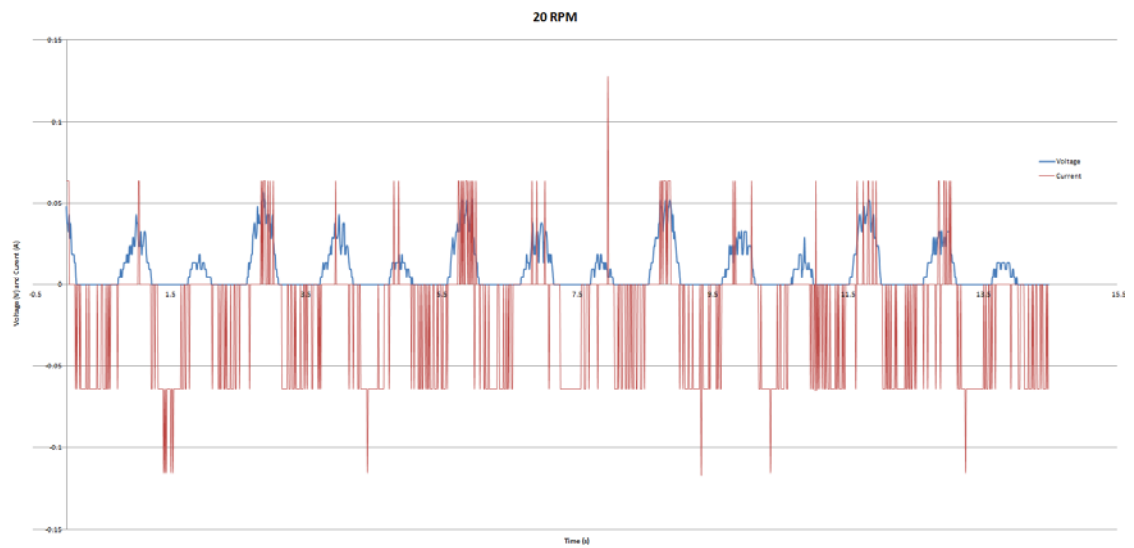
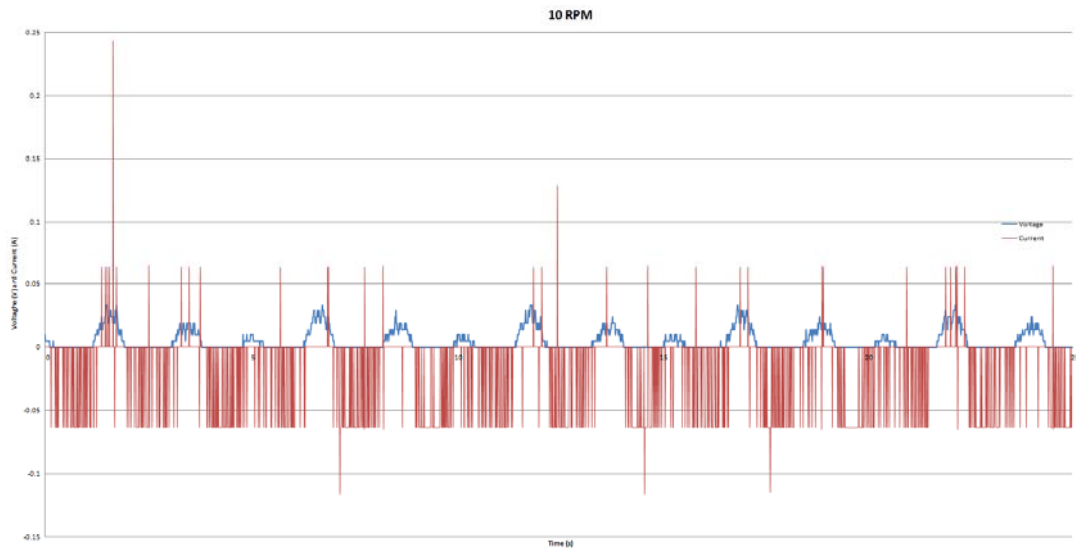
10	Center Magnet Bolt		1
11	Inner Spacer 17 x 3.175 x 3.175		1
12	Inner Bushing Central		1
13	RTWN52		2
14	Rebound Case		1
15	Outer Bushing		1
16	12 Washer M4(small)		4
17	12 SOC M4X 10		4
20	COM M6T		2

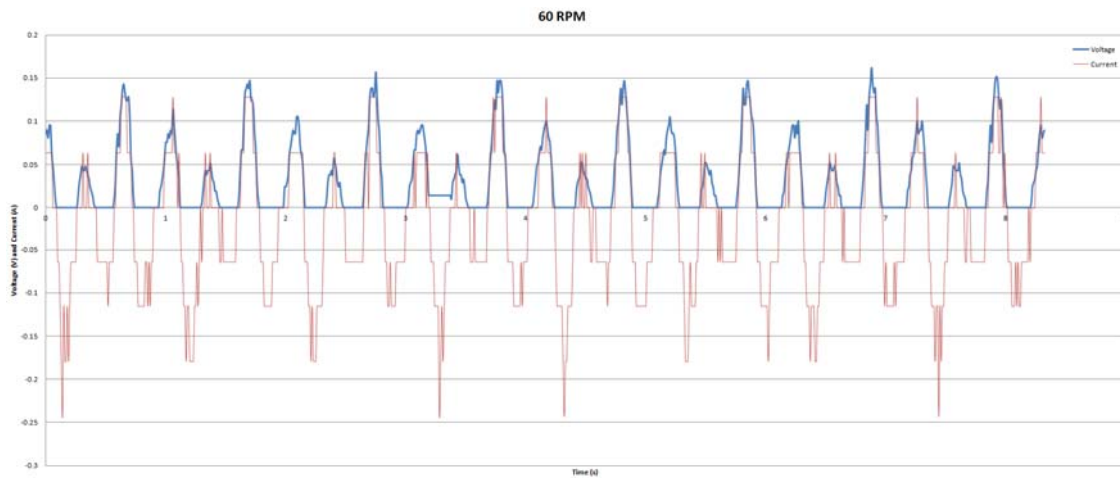
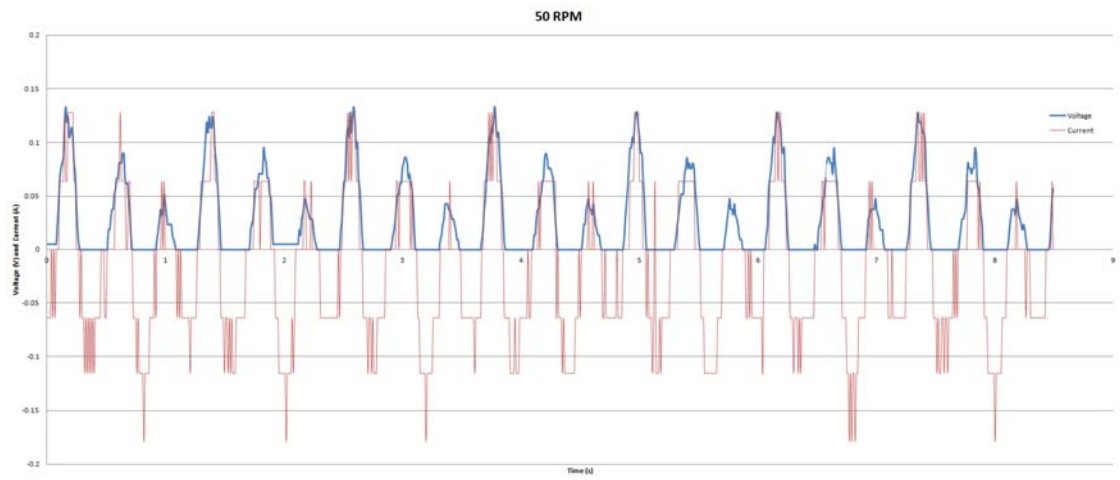
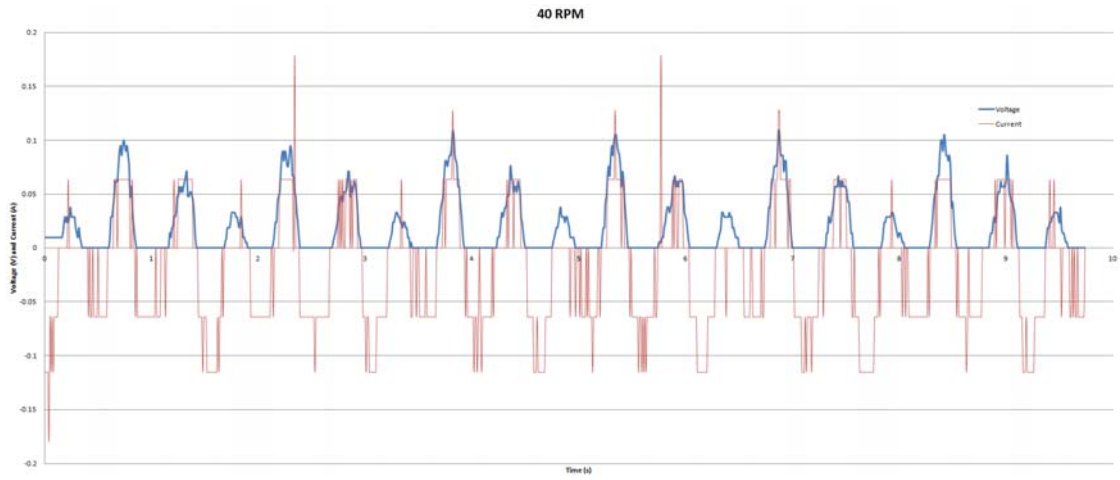
21	Clockwise Coil - Small		6
22	Anticlockwise Coil - Small		6
23	Clockwise Coil - Small - Outer		6
24	Anticlockwise Coil - Small - Outer		6
25	13 Washer M3		12
26	13 Lock nut M3		4
27	13 SOC M3X 10		4
28	13 SOC M3X 05		4

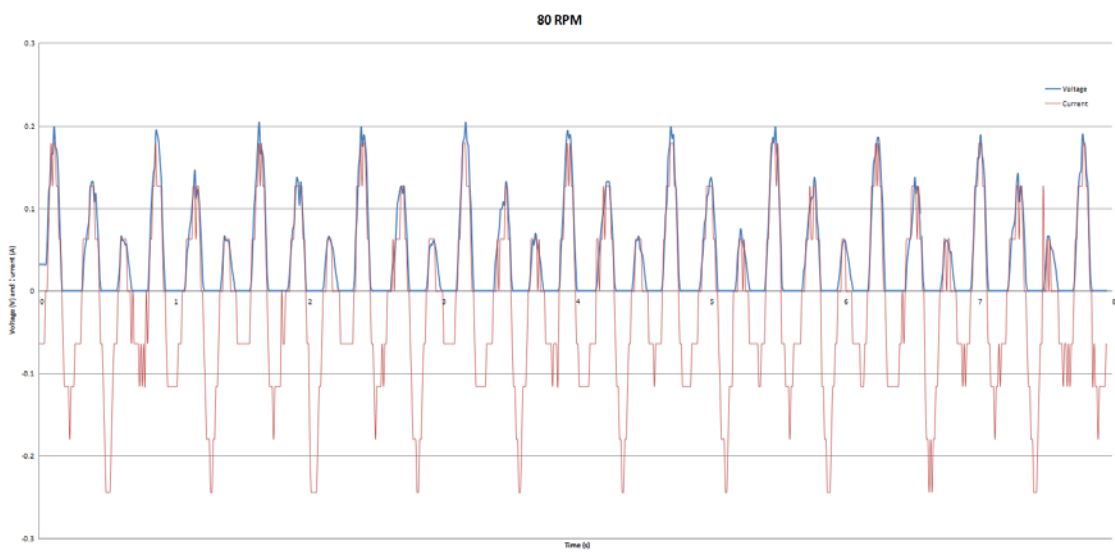
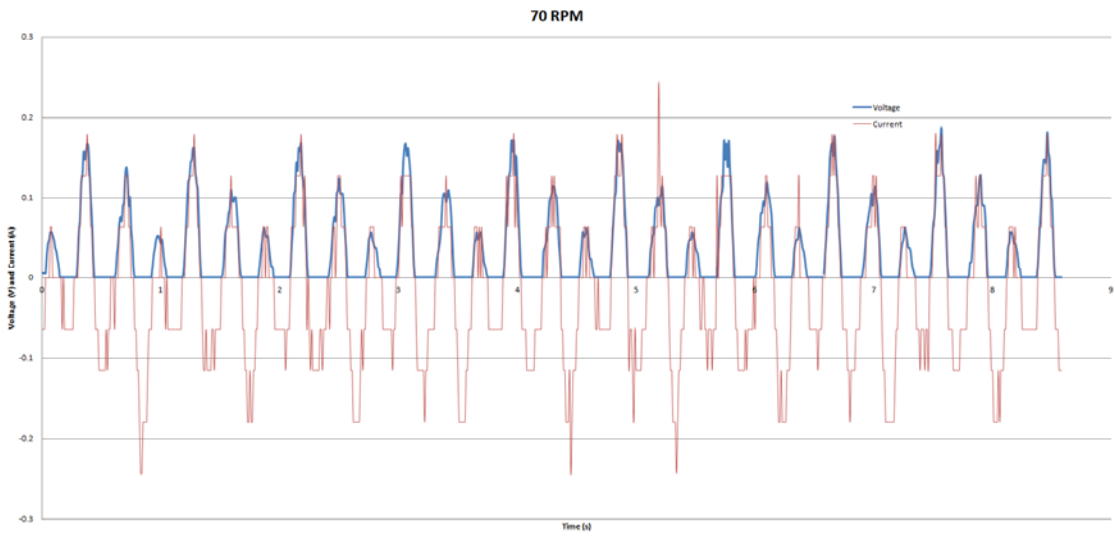
Appendix 14: Ansys Magnetostatic Analysis Linear Plot Data (Without Inner Magnet)

Distance (mm)	Magnetic Field Intensity (mT)
0	454.68
0.66146	624.02
1.3229	656.02
1.9844	622.25
2.6458	592.31
3.3073	491.65
3.9688	427.26
4.6302	396.86
5.2917	403.2
5.9531	397.73
6.6146	411.1
7.276	440.7
7.9375	507.99
8.599	696.95
9.2604	927.25
9.9219	1127.9
10.583	1242.6
11.245	1259.4
11.906	1210.5
12.568	1045.2
13.229	773.61
13.891	586.75
14.552	488.62
15.214	455.14
15.875	451.69
16.536	464.9
17.198	492.4
17.859	606.41
18.521	815.84
19.182	1072.5
19.844	1208.5
20.505	1256.8
21.167	1239.5
21.828	1141.5
22.49	912.54
23.151	664.29
23.813	513.31
24.474	449.01
25.135	417.58
25.797	401.84
26.458	403.43
27.12	409.96
27.781	431.58
28.443	492.48
29.104	578.62
29.766	608.94
30.427	657.65
31.089	677.54
31.75	482.88
Average	1088.12

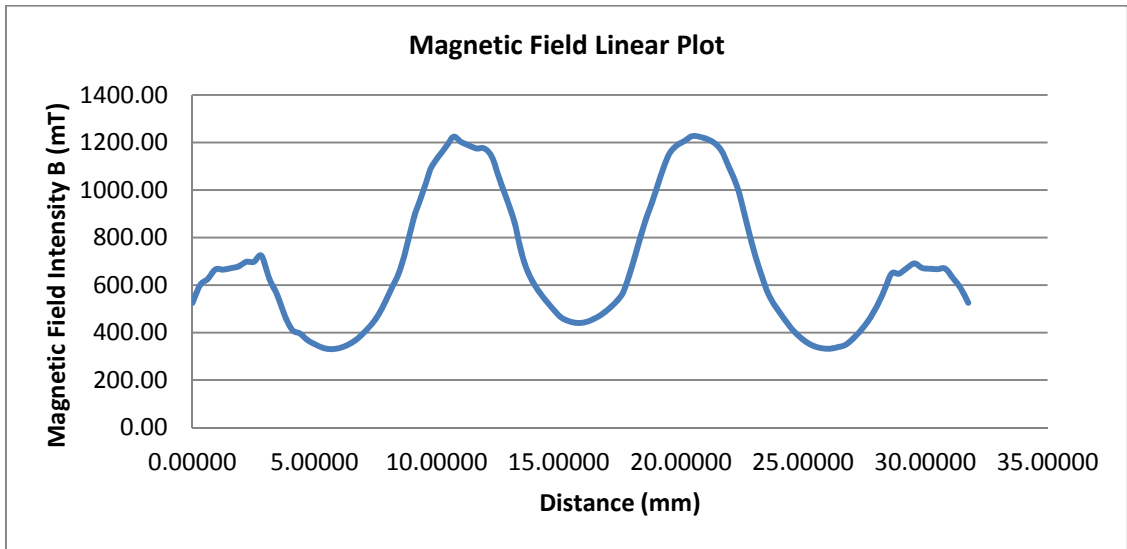
Appendix 15: Test Data







Appendix 16: Magnetic Field Plot for Outside Coils



Appendix 17: Ansys Magnetostatic Analysis for Varying Diameter Inner Magnet

Original		Inner Magnet 14.05		Inner Magnet 24.05		Inner Magnet 29.05		Inner Magnet 34.05	
Distance	B Field	Distance	B Field	Distance	B Field	Distance	B Field	Distance	B Field
0.00	738	0.00	796	0.00	637	0.00	557	0.00	476
0.66	992	0.66	1003	0.66	888	0.66	781	0.66	660
1.32	1071	1.32	1043	1.32	942	1.32	803	1.32	690
1.98	1053	1.98	1035	1.98	924	1.98	781	1.98	681
2.65	982	2.65	960	2.65	871	2.65	746	2.65	637
3.31	858	3.31	781	3.31	732	3.31	602	3.31	534
3.97	618	3.97	548	3.97	546	3.97	431	3.97	375
4.63	381	4.63	396	4.63	357	4.63	271	4.63	227
5.29	197	5.29	285	5.29	196	5.29	143	5.29	100
5.95	168	5.95	277	5.95	161	5.95	133	5.95	109
6.61	317	6.61	354	6.61	303	6.61	257	6.61	214
7.28	536	7.28	533	7.28	486	7.28	420	7.28	339
7.94	743	7.94	781	7.94	709	7.94	609	7.94	483
8.60	1057	8.60	1102	8.60	958	8.60	837	8.60	684
9.26	1369	9.26	1389	9.26	1249	9.26	1092	9.26	896
9.92	1609	9.92	1674	9.92	1494	9.92	1315	9.92	1092
10.58	1704	10.58	1781	10.58	1605	10.58	1416	10.58	1178
11.25	1724	11.25	1801	11.25	1606	11.25	1431	11.25	1198
11.91	1621	11.91	1728	11.91	1548	11.91	1393	11.91	1134
12.57	1461	12.57	1566	12.57	1367	12.57	1237	12.57	1015
13.23	1155	13.23	1237	13.23	1101	13.23	959	13.23	810
13.89	877	13.89	914	13.89	785	13.89	668	13.89	577
14.55	568	14.55	621	14.55	507	14.55	470	14.55	373
15.21	297	15.21	359	15.21	286	15.21	278	15.21	192
15.88	200	15.88	224	15.88	186	15.88	160	15.88	133
16.54	329	16.54	350	16.54	293	16.54	251	16.54	210
17.20	576	17.20	582	17.20	527	17.20	462	17.20	370
17.86	856	17.86	919	17.86	802	17.86	720	17.86	574
18.52	1166	18.52	1250	18.52	1086	18.52	987	18.52	786
19.18	1470	19.18	1567	19.18	1364	19.18	1230	19.18	1032
19.84	1663	19.84	1746	19.84	1560	19.84	1391	19.84	1159
20.51	1717	20.51	1804	20.51	1609	20.51	1433	20.51	1188
21.17	1717	21.17	1780	21.17	1608	21.17	1423	21.17	1172
21.83	1585	21.83	1665	21.83	1486	21.83	1302	21.83	1068
22.49	1321	22.49	1392	22.49	1244	22.49	1100	22.49	849
23.15	1038	23.15	1066	23.15	945	23.15	839	23.15	684
23.81	764	23.81	772	23.81	697	23.81	625	23.81	516
24.47	527	24.47	536	24.47	457	24.47	438	24.47	346
25.14	341	25.14	367	25.14	287	25.14	256	25.14	209
25.80	175	25.80	274	25.80	171	25.80	123	25.80	82
26.46	203	26.46	281	26.46	172	26.46	127	26.46	85
27.12	377	27.12	387	27.12	328	27.12	281	27.12	208
27.78	602	27.78	567	27.78	537	27.78	441	27.78	360
28.44	807	28.44	781	28.44	754	28.44	620	28.44	522
29.10	961	29.10	984	29.10	880	29.10	740	29.10	629
29.77	1043	29.77	1018	29.77	929	29.77	795	29.77	679
30.43	1073	30.43	1033	30.43	944	30.43	808	30.43	690
31.09	1017	31.09	1009	31.09	908	31.09	779	31.09	655
31.75	779	31.75	698	31.75	642	31.75	584	31.75	468
Average	1520	Average	1599	Average	1423	Average	1265	Average	1041

Appendix 18: Ansys Magnetostatic Analysis for Varying Thickness Magnet

Half Height		25% Thicker		50% Thicker		75% Thicker		100% Thicker	
Distance	B Field	Distance	B Field	Distance	B Field	Distance	B Field	Distance	B Field
0.00	489	0.00	792	0.00	706	0.00	733	0.00	657
0.33	569	0.83	1061	0.99	1052	1.16	1031	1.32	963
0.66	638	1.65	1082	1.98	1055	2.32	1018	2.65	959
0.99	654	2.48	1079	2.98	1052	3.47	1010	3.97	960
1.32	564	3.31	1019	3.97	1019	4.63	992	5.29	923
1.65	507	4.13	816	4.96	802	5.79	769	6.61	707
1.98	408	4.96	559	5.95	522	6.95	489	7.94	424
2.32	316	5.79	333	6.95	338	8.10	315	9.26	315
2.65	256	6.61	198	7.94	243	9.26	276	10.58	289
2.98	247	7.44	196	8.93	236	10.42	266	11.91	284
3.31	334	8.27	295	9.92	296	11.58	295	13.23	298
3.64	443	9.10	499	10.91	419	12.73	364	14.55	341
3.97	542	9.92	746	11.91	635	13.89	529	15.88	444
4.30	678	10.75	1071	12.90	989	15.05	843	17.20	741
4.63	787	11.58	1447	13.89	1445	16.21	1364	18.52	1257
4.96	888	12.40	1789	14.88	1842	17.36	1770	19.84	1702
5.29	928	13.23	1897	15.88	1928	18.52	1892	21.17	1798
5.62	951	14.06	1916	16.87	1936	19.68	1893	22.49	1802
5.95	934	14.88	1863	17.86	1905	20.84	1866	23.81	1774
6.28	795	15.71	1626	18.85	1667	21.99	1650	25.14	1572
6.61	667	16.54	1252	19.84	1241	23.15	1131	26.46	1029
6.95	551	17.36	863	20.84	798	24.31	717	27.78	584
7.28	425	18.19	559	21.83	502	25.47	417	29.10	392
7.61	323	19.02	295	22.82	294	26.62	318	30.43	332
7.94	259	19.84	160	23.81	234	27.78	289	31.75	315
8.27	334	20.67	279	24.81	287	28.94	319	33.07	331
8.60	449	21.50	561	25.80	469	30.10	414	34.40	392
8.93	574	22.32	883	26.79	787	31.25	682	35.72	573
9.26	710	23.15	1290	27.78	1224	32.41	1135	37.04	998
9.59	835	23.98	1645	28.77	1664	33.57	1663	38.37	1573
9.92	950	24.81	1857	29.77	1896	34.73	1857	39.69	1781
10.25	993	25.63	1926	30.76	1929	35.88	1890	41.01	1803
10.58	974	26.46	1898	31.75	1921	37.04	1885	42.33	1797
10.91	909	27.29	1780	32.74	1819	38.20	1769	43.66	1700
11.25	801	28.11	1479	33.73	1429	39.36	1349	44.98	1248
11.58	690	28.94	1061	34.73	993	40.51	849	46.30	720
11.91	551	29.77	737	35.72	623	41.67	517	47.63	448
12.24	430	30.59	490	36.71	401	42.83	358	48.95	342
12.57	325	31.42	302	37.70	290	43.99	295	50.27	298
12.90	245	32.25	194	38.70	244	45.15	268	51.59	286
13.23	246	33.07	199	39.69	246	46.30	273	52.92	290
13.56	327	33.90	365	40.68	326	47.46	337	54.24	316
13.89	418	34.73	578	41.67	515	48.62	473	55.56	434
14.22	518	35.55	833	42.66	799	49.78	757	56.89	727
14.55	604	36.38	1017	43.66	1021	50.93	982	58.21	922
14.88	673	37.21	1076	44.65	1055	52.09	1018	59.53	959
15.21	650	38.03	1091	45.64	1055	53.25	1018	60.85	958
15.54	572	38.86	1078	46.63	1062	54.41	1025	62.18	961
15.88	488	39.69	733	47.63	706	55.56	746	63.50	628
Average	866	Average	1690	Average	1703	Average	1651	Average	1560